Supersonic jet noise from launch vehicles: 50 years since NASA SP-8072

Caroline P. Lubert, Kent L. Gee and Seiji Tsutsumi

Citation: The Journal of the Acoustical Society of America **151**, 752 (2022); doi: 10.1121/10.0009160
View online: https://doi.org/10.1121/10.0009160
View Table of Contents: https://asa.scitation.org/toc/jas/151/2
Published by the Acoustical Society of America

JASA REVIEW

Supersonic jet noise from launch vehicles: 50 years since NASA SP-8072[a)]

Caroline P. Lubert,[1,b)] Kent L. Gee,[2,c)] and Seiji Tsutsumi[3]
[1]Department of Mathematics and Statistics, James Madison University, Harrisonburg, Virginia 22807, USA
[2]Department of Physics and Astronomy, Brigham Young University, Provo, Utah 84602, USA
[3]Research and Development Directorate, Japan Aerospace Exploration Agency, Sagamihara, Kanagawa, 252-5210, Japan

ABSTRACT:
In 1971, the U.S. National Aeronautics and Space Administration (NASA) published a seminal report—NASA SP-8072—which compiled the results of the early supersonic jet noise studies and provided methods to calculate the noise produced from launch vehicles. Fifty years later and despite known limitations, SP-8072 remains the foundation for much of the launch vehicle noise modeling today. This article reviews what has been learned about the physics of noise generation and radiation from free and impinging rocket plumes since the completion of SP-8072. State-of-the-art methods for the mitigation of launch vehicle noise are also reviewed. A discussion of launch vehicle noise modeling, from empirical to numerical and including reduced-order models of supersonic jets, points to promising approaches that can describe rocket noise characteristics not captured by SP-8072.
 https://doi.org/10.1121/10.0009160
(Received 26 March 2021; revised 17 November 2021; accepted 19 November 2021; published online 4 February 2022)
[Editor: James F. Lynch] Pages: 752–791

NOMENCLATURE

c_a	Ambient speed of sound (m/s)
c_e	Plume exit speed of sound (m/s)
D_e	Nozzle exit diameter (m)
D_j	Jet diameter for fully expanded condition (m)
D_t	Throat diameter (m)
f	Frequency (Hz)
h	Vehicle elevation, measured from nozzle exit (m)
He	Helmholtz number; $\mathrm{He} = fD_e/c_a$
L_C	Potential or laminar core tip length (m)
L_S	Supersonic core tip length (m)
M	Local Mach number
M_a	Ambient Mach number; $M_a = U_e/c_a$
M_e	Plume exit Mach number; $M_e = U_e/c_e$
M_j	Mach number for fully expanded condition
M_C	Convective Mach number; $M_C = \kappa U_e/c_a$, κ is an empirical constant
M_{CO}	Oertel convective Mach number; see Eq. (6), Sec. III D 1
N	Number of nozzles
OASPL	Overall sound pressure level (dB re 20 μPa)
OAPWL	Overall sound power level (dB re 1 pW $= 10^{-12}$ W)
p	Acoustic pressure (Pa)
p_a	Ambient pressure (Pa)
p_0	Chamber pressure (Pa)
φ	Azimuthal angle about vehicle or plume body (deg)
R	Radial distance from nozzle exit or impingement point (m)
Sr	Strouhal number; $\mathrm{Sr} = fD_e/U_e$
Sr*	Eldred *et al.* (1961) Strouhal number; see Eq. (3)
T	Thrust (N)
U_e	Plume exit velocity (m/s)
W	Acoustic power (W)
W_m	Mechanical power (W)
x	Free jet axis distance coordinate (m)
y	Offset distance from jet axis coordinate (m)
z	Height coordinate (m)
θ	Polar angle, referenced to plume centerline (deg)
γ	Ratio of specific heats
η	Radiation efficiency
ρ	Density (kg/m^3)
ρ_a	Ambient density (kg/m^3)

Subscripts

t	Throat
rms	Root mean square

I. INTRODUCTION

In spaceflight—commonly defined as any flight that crosses the Kármán line (100 km above mean sea level)—a launch vehicle is defined as a rocket, or group of rockets, which is used to carry a payload from the Earth's surface

[a)]This paper is part of a special issue on Supersonic Jet Noise.
[b)]Some of the work was done while the author was at the University of Plymouth, Devon, UK. Electronic mail: caroline.lubert@plymouth.ac.uk
[c)]ORCID: 0000-0002-5768-6483.

https://doi.org/10.1121/10.0009160

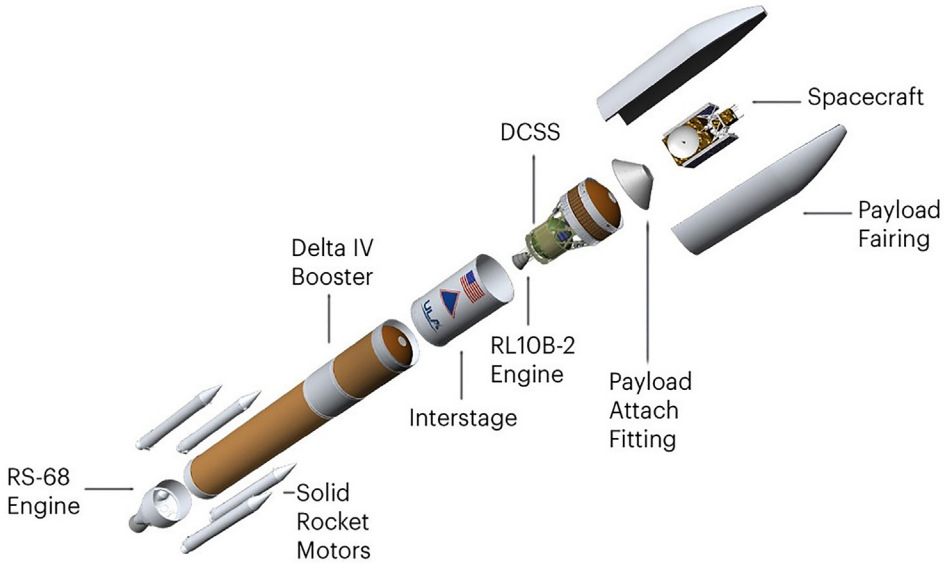

FIG. 1. (Color online) Diagram of the Delta IV M+ launch vehicle components. Illustration graciously provided by ULA.

into space. "Rocket" is a general term used broadly to describe anything whose forward motion is the result of its reaction to the rearward ejection of matter—typically, a jet of hot gases, which are the combustion products of the solid or liquid fuel—at high velocity. In this article, we focus primarily on the acoustic environment created by individual rockets, which are often configured with other rockets to form a launch vehicle.

Although a launch vehicle's payload is often an artificial satellite to be placed into orbit, some spaceflights, such as sounding rockets, are suborbital, whereas others enable a spacecraft to entirely escape the Earth's orbit. Most Earth orbital launch vehicles are multistage. The anatomy of a recently retired U.S. orbital launch vehicle, the Delta IV Medium+ rocket, is shown in Fig. 1. The vehicle's first-stage liquid engine, strap-on solid rocket boosters (SRBs), which provide additional liftoff thrust and are subsequently jettisoned in flight, and second-stage engine are designed to place the payload into orbit.

Rocket launch generates significant acoustic energy. For example, the overall sound pressure level (OASPL), measured outside and inside the payload fairing of the 3700-kN thrust Japanese M-V solid launcher, reached 158 and 144 dB, respectively (Onoda and Minesugi, 1997). Because liftoff is typically the most severe dynamic environment that a spacecraft will endure during its normal life, accurate prediction of noise generated by rockets at this moment is of the utmost importance. Figure 2 shows the Space Shuttle's root mean square (rms) vibration as a function of time relative to the SRB ignition. The initial vibration spike is caused by the main engines' ignition, after which the maximum vibration occurs at ∼5 s into liftoff when the Shuttle is approximately 90 m above the launch pad (Himelblau *et al.*, 2001; Arenas and Margasahayam, 2006). Note that liftoff vibroacoustic loading (VAL) on the vehicle induces greater vibration than during the transonic and Max-Q phases when the aerodynamic buffeting is the greatest. Although these phases also lead to structural vibrations during flight (Rainey, 1965; Cockburn and Robertson, 1974), it is the liftoff phase of a rocket launch that generates the potentially damaging VAL.

The VAL uncertainty on a launch vehicle, its payload, and supporting structures is large, making design optimization difficult. In the case of a satellite whose components can be excited by intense broadband waves, excessive noise levels inside the payload bays are responsible for up to 60% of the first-day failures (Griffin *et al.*, 2000), and up to 40% of a satellite's mass is required merely to enable it to survive the VAL environment (Henderson *et al.*, 2003). During liftoff, several parameters impact VAL, including nozzle exit flow parameters, pad and launch structure geometry, noise mitigation practices, near-pad vehicle drift, and vehicle design. An understanding of each of these and the roles they play in noise generation and transmission has evolved since the dawn of modern rocketry in the early 20th century.

Lubert (2018)'s review of rocketry developments began with the description by Goddard (1920) of a system for reaching high altitudes, progressed through World War II,

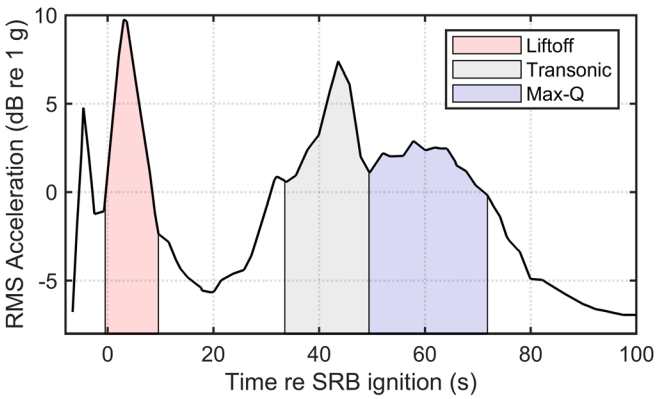

FIG. 2. (Color online) Space Shuttle vibration data from Fig. 7.6 of Himelblau *et al.* (2001), relative to the SRB ignition.

and culminated in the U.S.-Soviet Space Race that motivated the Apollo Program. This program, which ran from 1961 to 1972, resulted in numerous milestones in human space exploration, including the first lunar landing (Apollo 11) in 1969 and five subsequent U.S. moon landings. It also contributed greatly to advancements in rocket-related science and technology. Concern about the acoustic environment that the Saturn family of rockets (developed for the Apollo program) would produce resulted in research that was aimed at understanding the liftoff noise from launch vehicles, and Saturn-era measurements remain an important source of launch noise data. The eventual ground launch of the U.S. National Aeronautics and Space Administration's (NASA's) Saturn V rocket—whose first-stage rocket engines produced an overall sound power level (OAPWL) of 204 dB during the static-fire tests (Allgood, 2012)—generated one of the loudest sounds ever recorded. To determine the impact of the Apollo missions on buildings, personnel, etc., from launch-generated noise, the work of Guest and Jones (1967) applied an early model (Wilhold *et al.*, 1963) to predict the far-field Saturn V noise. Findings from Apollo and related research programs were compiled into NASA SP-8072: *Acoustic Loads Generated by the Propulsion System*, a report by Eldred (1971) that took existing data and 1960s understanding of jet and rocket noise and described empirical methodologies for predicting noise around launch vehicles. Its two distributed-source methods (DSM-1 and DSM-2) employ sound power level distribution curves together with directivity indices to predict the sound levels radiated by a rocket plume as a function of distance and angle while empirically accounting for plume deflection and impingement.

The foreword of SP-8072, as the report is colloquially known, says "*NASA plans to update this monograph when need is established.*" Although understanding of heated, supersonic jets has increased dramatically since its publication and researchers have attempted to improve on model limitations for specific situations, SP-8072 has remained the foundation for and, perhaps, the cornerstone of global launch vehicle noise research for the past 50 years. One reason for the lack of coordinated research progress is simply its dearth; after the Apollo-era research ended, relatively little new launch vehicle noise research was published from 1970 into the 1990s, effectively forcing researchers and engineers to return to the culminating document of the Space Race and begin anew. The NASA Shuttle program, which followed Apollo, assumed an SP-8072 framework for noise generation (Himelblau *et al.*, 2001), thereby limiting the perceived need and opportunity for additional research into the physics of noise generation and radiation. However, based on Fig. 3 (from McInerny, 1992b), the considerable disagreement between SP-8072-predicted and measurement-derived sound power level spectra from the first three Shuttle launches suggests that this assumption should have been revisited.

The kind of disagreement seen by McInerny (1990, 1992b) for the source power level characteristics is usually

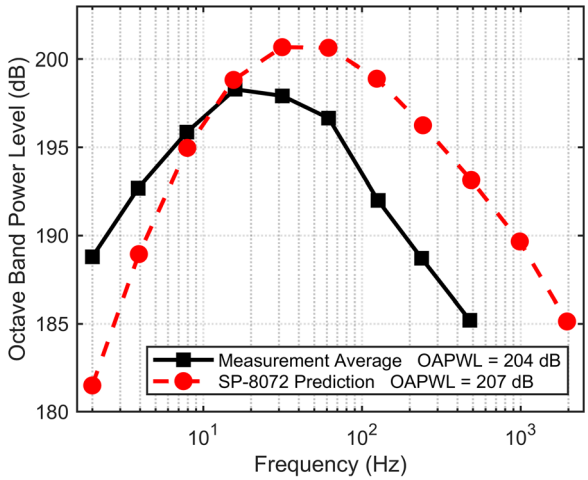

FIG. 3. (Color online) Shuttle launch octave-band power level spectra, as obtained from Fig. 15 of McInerny (1992b). The measurement average is the mean of the three power level spectra in McInerny's figure.

amplified when obtaining sound pressure level (SPL) spectra at different locations. For example, Fukuda *et al.* (2009) describe SP-8072-derived OASPL errors of more than 10 dB at some angles around a solid rocket motor after making model parameter adjustments to improve the model match at others. In the literature, *ad hoc* adjustments to SP-8072 are fairly common. However, in addition to demonstrating a lack of model generalizability, such modifications often still yield poor agreement between the SP-8072 predictions and experimental data, including OASPL underestimation at high frequencies (Park, 2019).

Five decades removed from SP-8072, we have entered a new age of global spaceflight. As shown in Fig. 4, much of the U.S. Space Shuttle era (1981–2011) occurred during a relative lull in global space-related activity, but numerous recent national and international initiatives related to human exploration, science, and leisure travel—together with the significant technological advances that make them possible—mean that the number of orbital launches globally per year has been increasing steadily over the past 10–15 years. The total

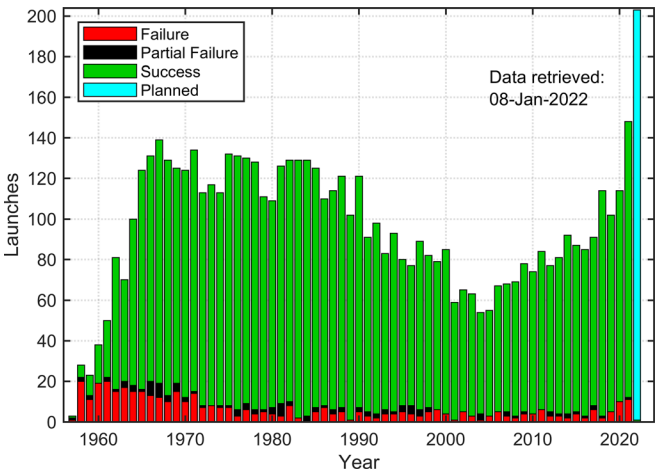

FIG. 4. (Color online) The number of orbital launches per year (footnote 7).

https://doi.org/10.1121/10.0009160

number of launches planned for 2022 is well over 200. Japan, South Korea, India, China, Russia, and the USA are just some of the many countries worldwide that are currently developing launch vehicles.[1] For a review of India's launch vehicle development, see Gupta *et al.* (2007), whereas Lipnitskiy and Safronov (2014) provide a summary of the ground acoustic testing for Russia's launch vehicle program.

Not only is today's space vehicle community becoming more global, it is also expanding in terms of the size and diversity of purpose. An important factor in this growth has been the expansion in the number, scope, and capability of commercial launch systems, which has significantly decreased launch costs. For example, low Earth orbit (LEO) launches have been reduced to 1/20 of their cost, and those to the International Space Station (ISS) are now about 1/4 of their cost, compared to a decade ago (Jones, 2018). While providing launch capability to government organizations, such as NASA, these systems are also responsible for the emerging industry of space tourism with the July 2021 spaceflights of Blue Origin and Virgin Galactic (billing itself as the "world's first commercial spaceline") attracting worldwide interest. Although such flights are suborbital, mankind is also turning its attention farther afield. For example, after a 12-year lull between 1978 and 1990, unmanned and manned lunar missions (e.g., the NASA Artemis program) are once more being planned and carried out by multiple countries.[2] Whereas Russia and the USA both began deep space exploration as early as 1960 and experienced a significant decline in interest in the intervening years, the last decade has seen a renewed enthusiasm for such missions.[3]

This article is intended to serve as a timely review of the current state-of-the-art in rocket and launch vehicle noise research to both complement and augment other reviews, including those by McInerny (1990, 1992b) and Lubert (2018). Although it is intended to be as thorough as possible and some principles may apply to other rocket-powered vehicles, its scope is limited to vertical launch vehicles. Appendix A briefly describes other limitations in the scope, including VAL, ignition overpressure (IOP), environmental concerns, measurement techniques, infrasound, and buffet loading.

This review article is structured as follows. Section II is intended to provide background material in the form of a discussion of supersonic jets and how highly heated, supersonic rocket plumes differ from other jets. This is followed by detailed descriptions of the origin and nature of the radiated sounds from both free (Sec. III) and impinging (Sec. IV) rocket plumes. Techniques for pad noise mitigation during rocket launches are summarized in Sec. V. Finally, Sec. VI presents different types of existing and candidate methods for modeling launch noise such as NASA SP-8072, subscale testing, and numerical simulation. The review concludes with a recommendation that an entirely new approach to rocket plume noise modeling be pursued, one that incorporates the underlying physics of the associated noise generation mechanisms.

II. SUPERSONIC JET AND ROCKET FUNDAMENTALS

This section provides some foundational knowledge regarding supersonic jets. We briefly review early research related to supersonic jets and describe the various regimes in the plume and turbulence characteristics and the differences between rockets and jets. These differences include not only the plume characteristics but also the launch considerations that are important to the noise.

A. Supersonic jets

A jet is referred to as "supersonic" when the Mach number at the nozzle exit is greater than one. Figure 5, based on a schematic by Nagamatsu *et al.* (1969), shows the anatomy of a supersonic jet with a nozzle exit diameter, D_e, and exit Mach number, M_e. Within the potential core, the supersonic jet velocity is relatively constant, although modulated by shock cells for a nonideal expansion. The turbulent mixing layer begins at the nozzle lip and grows in width with downstream distance until it is fully developed beyond the potential core length, L_c. Beyond the potential core tip, the flow remains supersonic across a part of the plume cross section until the supersonic core length, L_s, is reached. Beyond the supersonic core tip, $M < 1$, the jet is subsonic everywhere. These characteristic aerodynamic lengths, particularly L_c, have been important in identifying different regimes for the turbulence and noise generation. For $x < L_c$, turbulent mixing noise generation is primarily constrained to the shear layer, whereas noise is radiated from across the jet cross section once the turbulence is fully developed (Panda *et al.*, 2005). Both fine-scale turbulence, which is believed to radiate as uncorrelated, omnidirectional sources, and large-scale coherent structures, which radiate preferentially in the downstream direction, contribute to the mixing noise generation (Tam *et al.*, 2008; Viswanathan, 2009).

A second type of Mach number is important in connecting turbulence to supersonic jet noise radiation. The convective Mach number, M_C, refers to the characteristic velocity of turbulent eddies near the shear layer and their relationship to the quiescent medium. For regions in the plume where $M_C > 1$, Mach wave radiation occurs. Supersonic instability waves (e.g., Tam and Burton, 1984a,b) and families of Mach waves with different characteristic velocities have been studied (e.g., Oertel, 1982; Tam and Hu, 1989; Seiner *et al.*, 1992). Although the differences between large-scale radiation and Mach wave radiation are not completely clear,

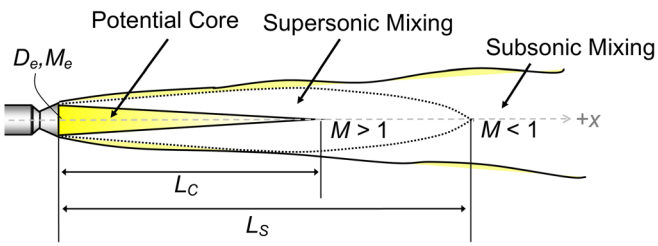

FIG. 5. (Color online) The anatomy of a supersonic jet. L_c refers to the potential core length and L_S refers to the supersonic core length.

TABLE I. The representative comparison of variables for a turbojet, an afterburning turbojet, and a typical rocket, based on McInerny (1992b, 2010). Note that some values may not be representative of fifth-generation afterburning military aircraft.

	Static temperature	Exhaust density	Exhaust velocity	Speed of sound in exhaust	$M_e = U_e/c_e$	$M_a = U_e/c_a$
Turbojet at military power	600–700K	0.3–0.5 kg/m^3	700–800 m/s	450–500 m/s	~1.5–1.8	~2.0–2.4
Afterburning turbojet	1200–1600K		1000–1200 m/s	700–800 m/s	~2.0–2.3	~2.9–3.5
Rocket	1350–2200K	0.14 kg/m^3	2400–4000 m/s	780–960 m/s	~3.2–4.7	~7–11.8

Mach wave radiation is described as coming from the convectively supersonic regions (i.e., Tam, 2009), whereas large-scale radiation appears to be important for both supersonic and subsonic jets (i.e., Viswanathan, 2002, 2009).

In describing a supersonic jet, the jet exit pressure is also an important parameter. Jets for which $p_e = p_a$ are described as pressure matched or ideally expanded. However, many jets are nonideally expanded in practice. For jets where $p_e < p_a$, the jet is described as overexpanded, and the flow is pinched by the greater atmospheric pressure as it exits the nozzle. On the other hand, if $p_e > p_a$, the jet is underexpanded and the flow cross-sectional area rapidly expands just beyond the nozzle. In both cases, shock cells form within the potential core. Compressible fluid relations can be used to calculate the equivalent fully (or ideally) expanded jet conditions from a knowledge of the flow parameters within the nozzle. For an overexpanded jet, $D_j < D_e$ and $M_j < M_e$ because the full expansion occurs within the nozzle. For an underexpanded jet, the opposite is true.

B. How do rockets differ from other jets?

Rocket plumes are supersonic jet flows with greater temperatures and velocities than other jets, including afterburning jet engine exhausts. Table I shows a comparison of several key variable values (such as temperature, density, and sound speed) for a turbojet, an afterburning turbojet, and a rocket plume. The extreme conditions at which rockets operate play a key role in making acoustic generation from their plumes different from that of other jets. For example, the ambient Mach number, M_a, is typically between 2.0 and 2.4 in a jet, whereas for a rocket, it is almost four times larger—typically between 7 and 8—as a result of the high temperatures and exit velocities in rocket plumes. Even more important in rocket noise radiation is the convective Mach number, M_C, which describes the characteristic speed of the turbulent eddies at the shear layer and dictates the angle of the primary radiation lobe. The convective Mach number is discussed further in Sec. III D.

Regarding pressure-matching conditions, most rockets are designed such that the plume is overexpanded at sea level. This is to help optimize performance at altitude where the atmospheric pressures are lower. Whereas military aircraft engines are also overexpanded at takeoff, rockets have to be designed to operate over a much greater altitude range. As an example, Fig. 6 shows a photograph of a 2020 Atlas V launch, where the overexpansion of the center liquid engines' flow is shown by its being pinched downstream of the nozzle exit. Note that burning aluminum particles obscure the plume structure of the strap-on SRBs. One exception to the rockets being overexpanded at the launch is the Shuttle reusable solid rocket motor (RSRM), which is understood to have operated at a slightly underexpanded condition at sea level. Figure 7 shows a still frame of a NASA video of the Space Shuttle launch where the RSRM plumes expand immediately outside of the nozzle exit, suggesting underexpansion. The RS-25 Shuttle main engine plumes, on the other hand, can be seen in Fig. 7 to have a classical Mach disk, additional shock cell, and plume width contraction, which are indicative of overexpansion.

FIG. 6. (Color online) The Atlas V-541 launch of the Mars Perseverance Rover in March 2020. The liquid core-stage engine plumes show clear signs of overexpansion, whereas the structure of the outer solid booster plumes is obscured by burning aluminum particles. Photo courtesy of NASA.

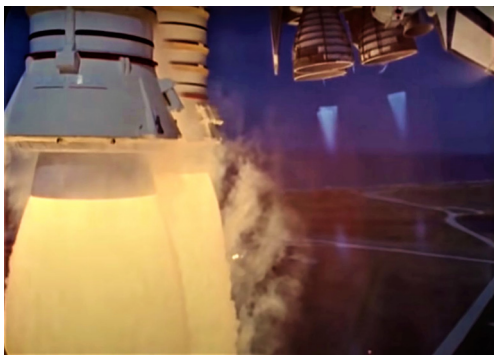

FIG. 7. (Color online) A still (at time 24:33) from a NASA video (footnote 8) of a Space Shuttle launch, which shows the slightly underexpanded RSRM (left) and overexpanded RS-25 main engine (right) plumes.

https://doi.org/10.1121/10.0009160

Videos of Shuttle launches show an eventual underexpansion of the plumes at a significant altitude, evidenced by a considerably larger plume diameter immediately outside of the nozzle. Appendix B discusses the use of fully expanded versus exit Mach numbers and diameters for a few rockets.

Another feature distinguishing typical rocket plumes from other jets is in their real-world application. Military aircraft operations include jet blast deflectors and, sometimes, short takeoff and vertical landings (STOVL), but space vehicle launches are more complicated. Rockets are launched from a pad composed of a deflector and flame duct for safely guiding high-speed and high-temperature exhaust jets downstream, a launch platform for supporting and transporting the vehicle, and an umbilical tower for supplying dry air, fuel, and power to launch the vehicles. The launch platforms are located above the deflector and have an exhaust hole to funnel exhaust jets from the rocket engines to the deflector and flame duct. The launch configuration, with its complex structures and plume impingement and deflection, has the potential to greatly change the associated noise generation.

A schematic of the acoustic generation mechanisms for launch vehicles at liftoff is shown in Fig. 8 for different vehicle elevations. The gradual ascent of a launch vehicle from the pad changes the primary noise source from that generated inside the flame duct, as a result of plume impingement onto the deflector and the wall plume, to that appearing above the launch platform due to Mach waves from the free plume and plume interaction with the launch platform. The noise sources appearing during liftoff are a consequence of free and impinging plume phenomena, and both need to be understood if they are to be properly modeled. The noise from free and impinging plumes is discussed in Secs. III and IV, respectively.

III. FREE ROCKET PLUME NOISE PHENOMENA

Highly heated, supersonic jets from solid rocket motors and liquid engines generate high-amplitude, broadband acoustic environments. This discussion of free (i.e., undeflected) rocket plumes covers both historical research, which was the foundation of SP-8072, as well as modern understanding of supersonic jet noise. To provide context and a more complete conceptual framework, comparisons with heated supersonic jets and military jet engine exhausts are made where appropriate. The free-plume noise discussion flows from four topics essential to the development of a rocket noise model, whether SP-8072 or another: the amount of sound radiated, its characteristics, its origin, and its directivity.

A. How much sound is generated?

Along with supporting experiments (e.g., Westley and Lilley, 1952), the acoustic analogy by Lighthill (1952, 1954) laid the foundation for the field of jet aeroacoustics by connecting the fluid mechanics of compressible, viscous fluid flow with the radiated sound. His work produced the widely accepted U_e^8 law for subsonic jets, in which the radiated sound power is proportional to the eighth power of the stream velocity, U_e. This foundational work quickly led to an interest in supersonic jet acoustics and developing scaling laws for radiated sound from jets of different scales and conditions.

1. Sound power

An early attempt to scale radiated sound power from subsonic and supersonic air jets, turbojets, and rockets showed, clearly, that afterburning turbojets and rocket data do not follow the U_e^8 scaling law. Figure 9 recreates the graph by Chobotov and Powell (1957), updated here to include an additional data point for the Space Shuttle RSRM). Although Fig. 9 shows more of a clustering of rocket data than a clear trend, rockets—and other highly supersonic jets—are believed to follow a U_e^3 scaling law for the radiated power, W (Chobotov and Powell, 1957; Ffowcs Williams, 1963; Tam, 1972).

NASA SP-8072 and other early literature justify the $W \propto U_e^3$ dependence via an acoustic efficiency argument. The acoustic power generated by a rocket should correlate with the physical parameters of the corresponding gas flow,

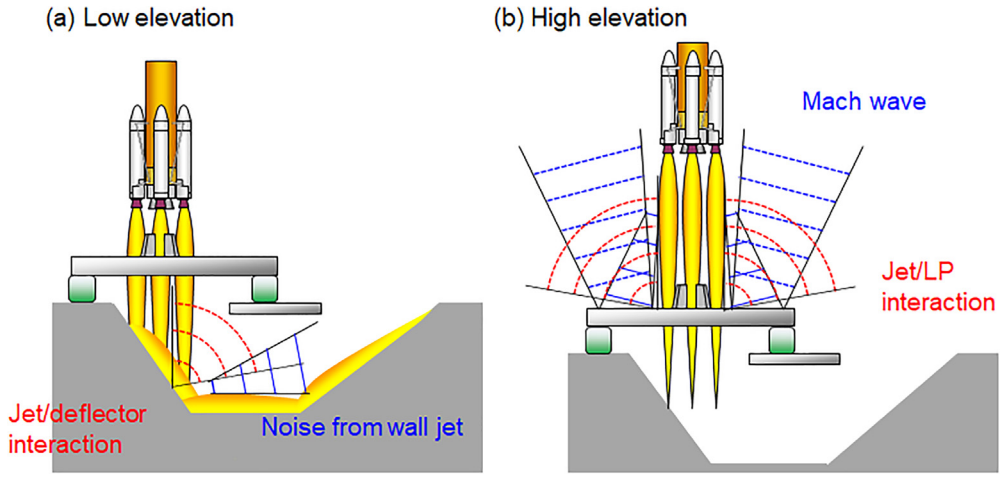

FIG. 8. (Color online) The schematic of the acoustic generation mechanisms for the launch vehicles at liftoff.

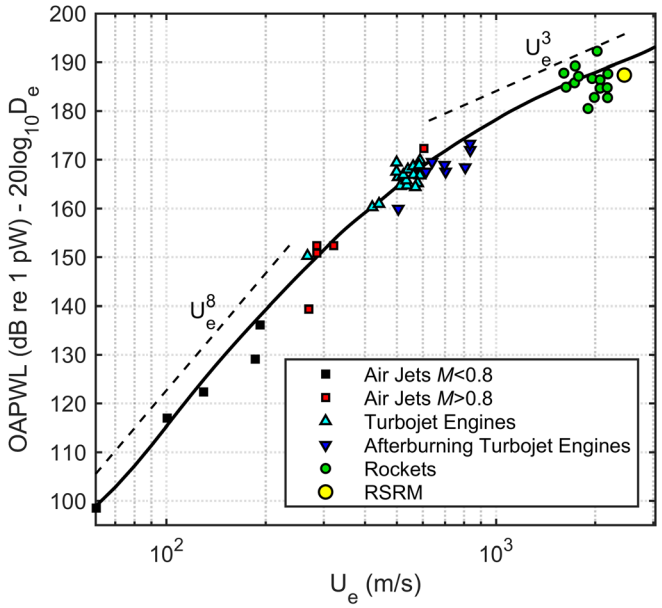

FIG. 9. (Color online) The overall sound power as a function of the jet velocity, adapted from Chobotov and Powell, Rama-Wooldridge Corp. Rept. E.M.-7–7 (1957) and Ffowcs Williams, Philos. Trans. R. Soc., A **255**(1061), 469–503 (1963). Note that improperly scaled versions of the original graph have appeared in the literature.

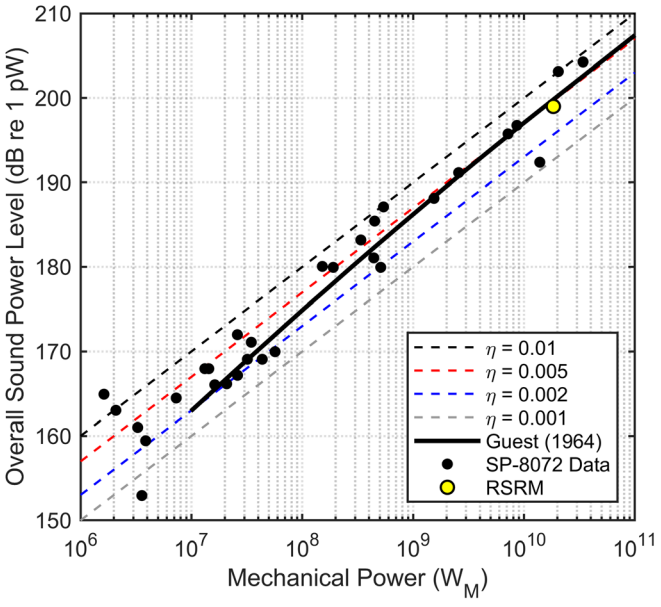

FIG. 10. (Color online) The OAPWL versus W_m, updated from Fig. 3 of SP-8072 to include the curve by Guest (1964) and the RSRM datapoint.

and Mayes *et al.* (1959) asserted that W is related to the engine mechanical power, W_m, by

$$W = \eta W_m, \tag{1}$$

where η is the acoustic radiation efficiency. The engine mechanical power is related to the engine thrust and plume exit velocity by $W_m = 0.5\,T\,U_e$ and because $T \propto U_e^2$ (ignoring a relatively small pressure-related contribution for non-ideal flow expansion[4]), then $W_m \propto U_e^3$ and $W \propto U_e^3$. The fact that Allgood (2012) shows a good scaling of W (or OAPWL, in decibels) with engine thrust, and not mechanical power, is likely a consequence of the relatively small range of plume exit velocities for most liquid engines.

The historical SP-8072 relationship between W and W_m is shown in Fig. 10 for various solid and liquid-fueled chemical rockets with T = 1.56–31 100 kN (350–7 000 000 lb). For reference, constant acoustic efficiency lines of $\eta = 0.1\%$, 0.2%, 0.5%, and 1.0% are shown, along with the variable acoustic efficiency model by Guest (1964). Guest's model suggested that $\eta \leq 0.5\%$, which was supported by a theoretical upper bound of $\eta = 0.6\%$ by Lighthill (1963). Although Sutherland (1993) proposed a plume parameter-dependent relation for η, which has been carried forward by others (e.g., Plotkin *et al.*, 2009; Casalino *et al.*, 2009; Requena-Plens, 2020), the expression is developed from a likely incorrect assumption that the dominant noise is generated in the subsonic portion of the plume (see Sec. III C 2). Ultimately, it has been traditionally accepted or assumed (Guest, 1964; Potter and Crocker, 1966; Eldred, 1971; Pearsons *et al.*, 1980; McInerny, 1990; Sutherland, 1993; Casalino *et al.*, 2009) that $\eta \approx 0.5\%$. This empirical radiation efficiency is mostly validated by more recent measurements. For example, the RSRM datapoint in Fig. 10 corresponds to $\eta = 0.43\%$. James *et al.* (2014a) found $\eta \approx 0.4\%$ for an Orion 50s XLG solid motor, and from far-field Falcon-9 launch measurements, Mathews *et al.* (2021) calculated $\eta = 0.34\%$. These modern assessments of η, thus far, suggest that the $\eta = 1\%$ assumed in SP-8072 (see Sec. VI A 1) was overly conservative. However, one source of uncertainty in historical and modern sound power assessments is the role of ground reflections. Despite improvements in ground-reflection modeling (see Gee *et al.*, 2014), their impact on sound power and radiation efficiency calculations from different measurement scenarios is uncertain.

2. Maximum far-field OASPL

The preceding discussion has covered the overall acoustic power radiated by rockets and its tie to plume parameters. Also of importance is the maximum radiated SPL, $\mathrm{OASPL_{max}}$. Related to the calculations by McInerny (1990, 1992b) of the octave-band power level spectra as estimated from far-field pressure levels during launch, McInerny (1996a) proposed a simple formula for predicting the maximum OASPL at a given distance based on an estimate of the OAPWL, which can be obtained from Eq. (1) as

$$\mathrm{OASPL_{max}} = \mathrm{OAPWL} - 10\,\log_{10}(4\pi R^2) + 8, \tag{2}$$

where the 8 dB is the peak directivity factor estimated from the data of Cole *et al.* (1957). Note that McInerny (1992b) had previously used a form of Eq. (2) but with a directivity factor of 5 dB when averaging over a 6 dB-down interval. An alternative, graphical formulation for $\mathrm{OASPL_{max}}$ has been given by Greska *et al.* (2008) for a wide range of jet conditions, including rockets. Kang *et al.* (2020) showed a good agreement between the curve by Greska *et al.* (2008)

https://doi.org/10.1121/10.0009160

and their data for a small supersonic jet, and Mathews *et al.* (2021) have compared both of these approaches with the recent Falcon 9 launch data. They show that both approaches agree with the measured maximum OASPL 8 km from the launch site within about 2 dB. Further study of these simple level-scaling methodologies is merited.

B. What is the nature of the radiated sound?

1. Relevant rocket noise phenomena

Whereas understanding of the noise from laboratory-scale nozzles and jet engines has steadily progressed since the days of Lighthill, much of the rocket-related work was related to the Apollo program and has mostly seen progress associated with major, recent space vehicle development programs. It is, thus, instructive to describe what is believed to be known about rocket noise in the context of other supersonic jets. In a nonideally expanded supersonic jet, noise is generated by the turbulent mixing of the jet with the ambient fluid and the sound generated by the presence of shock cells (Tam, 1995; Morris and Lilley, 2007; Bailly and Fujii, 2016). Turbulent mixing noise has been described in the literature as being of three types: noise from large-scale structures, noise from fine-scale turbulence, and Mach wave radiation. Although large-scale noise and Mach wave radiation in the supersonic jet noise literature have sometimes been used synonymously, Liu *et al.* (2016), Schmidt *et al.* (2018), and Leete *et al.* (2020) have recently described differences.

Shock-associated noise is both broadband and tonal with broadband shock-associated noise generated by the interaction of stability waves with the shock cell structure and the tonal screech being caused by a feedback loop. Whereas mixing noise and broadband shock-associated noise are evident in the noise spectra radiated by jets from low-bypass military engines (Tam *et al.*, 2018; Vaughn *et al.*, 2018; and Neilsen *et al.*, 2019a), rocket plumes seem to be dominated by mixing noise alone in that spectra at the sideline and forward directions do not resemble archetypal noise data from nonideally expanded supersonic jets. The mixing noise dominance could be caused by the combination of the saturation of the broadband shock-associated noise intensity with the stagnation temperature (Miller, 2015; Kuo *et al.*, 2015) and relative efficiency of the Mach wave generation. Consequently, despite the nonideal plume expansion at rocket launch (see Appendix B), the remainder of the discussion focuses on mixing noise characteristics.

2. Spectral characteristics

In radiated jet mixing noise, the downstream (aft) spectrum tends to be more peaked with a greater characteristic timescale and lower spectral peak frequency, whereas spectra toward the sideline and in the forward direction tend to be broader with a shorter characteristic timescale and corresponding greater spectral peak frequency (Tam *et al.*, 2008; Viswanathan *et al.*, 2011; Harker *et al.*, 2013). These general characteristics in the sound radiation from a rocket are shown in Fig. 11, using a short waveform segment and

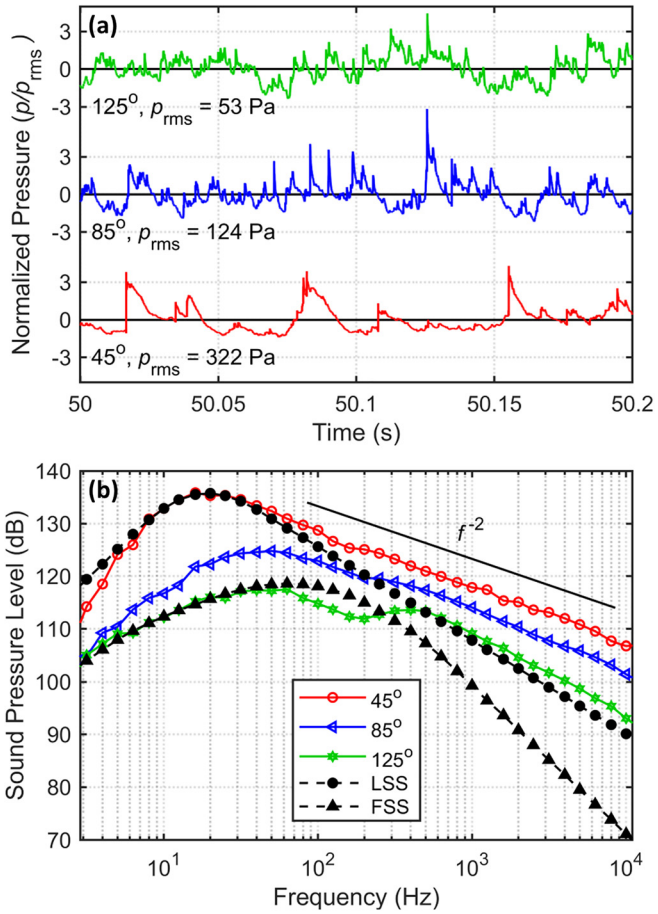

FIG. 11. (Color online) The (a) waveform segment and (b) one-third octave spectra from a Shuttle RSRM static firing. The measurements were made at a distance of 80 D_e with exhaust angles measured from the nozzle exit.

calculated noise spectrum from a test firing of the RSRM motor at a distance of 80 D_e. The one-third octave-band peak frequency is 16 Hz at 45° (re the plume axis) and increases to ∼100 Hz at 125°. (At 125°, the spectral peak frequency determination is complicated by ground-related interference.) Spectral broadening, particularly below the peak frequencies, is also apparent.

Also shown in Fig. 11(b) are the large-scale similarity and fine-scale similarity (LSS and FSS) spectral fits using the empirical spectra developed by Tam *et al.* (1996) with laboratory-scale jet data at a variety of Mach numbers and temperature ratios. The fine-scale noise is believed to be largely omnidirectional, broadband, and of short correlation lengths, whereas the large-scale structure noise, originating from the growth and decay of the instability waves, is more correlated, directional, and of greater amplitude. Tam *et al.* (2008) found that for a jet, the far-field noise at different angles could be described as a superposition of these two spectra. Because of their simplicity and explanatory power, these spectra have been widely applied to experiments from laboratory jets (e.g., Viswanathan, 2002; Karabasov, 2010; Vaughn *et al.*, 2016) to full-scale tactical engines (Schlinker *et al.*, 2007) and aircraft (Neilsen *et al.*, 2013, 2019a) to a small rocket (Tam *et al.*, 2017).

The applicability of similarity spectra analysis to rocket noise remains an open topic of research. A comparison shown in Fig. 11(b) between the similarity spectra and measured 45° RSRM spectra, where large-scale noise should dominate, and 125°, where fine-scale noise should dominate, is instructive. Whereas the LSS spectrum fits the 45° data in the peak region, it does not fit the low- or high-frequency trends. And although the FSS spectrum matches the low-frequency trends at 125° fairly well, the measured spectrum has a significantly shallower slope. Others have discovered problems with the similarity spectra fits— particularly for supersonic jets along the peak noise radiation angles. Schlinker *et al.* (2007) and Neilsen *et al.* (2019a) reported similar discrepancies in the similarity spectra fits to those seen for the RSRM at 45°. Giacomoni (2013) found the LSS/FSS spectra to be inappropriate for rockets and pursued different empirical fits entirely (Giacomoni and Kenny, 2014). Other spectral shapes, meant to improve the fits around the peak radiation region (Tam and Parrish, 2015; Greska *et al.*, 2008) and at other angles (Kandula, 2008b), have been proposed.

3. Acoustical nonlinearities

The time waveform segments in Fig. 11(a) reveal the reason for the shallower slopes in the rocket noise spectra—the presence of acoustic shocks at all three angles. (The term "acoustic" shock is used to clearly distinguish from the shock cells present in a nonideally expanded plume.) A noise waveform with a significant shock content produces a spectrum with a f^{-2} slope (Gurbatov and Rudenko, 1998), which is very close to what is seen at 45° and 85°. At 125°, the slope rolls off a little more quickly, which appears to be caused by the lesser prevalence of steep shocks. Nonlinearity and shock formation in supersonic jet noise have been investigated in recent years (e.g., Gee *et al.*, 2008; Gee *et al.*, 2016a; Petitjean *et al.*, 2006; Baars *et al.*, 2014; Mora *et al.*, 2015; Fiévet *et al.*, 2016)—including the subjective impression of jet "crackle" (Gee *et al.*, 2018)—but has not been treated as extensively for rocket noise. Morfey (1984) described the apparent absence of high-frequency absorption in the Atlas launch noise spectra, and a seminal work by McInerny (1996b) revealed the presence of large derivatives (acoustic shocks) in recorded noise from launch data. McInerny *et al.* (1997) and McInerny and Ölçmen (2005) followed this study with more detailed nonlinearity analyses of the noise propagation, which examined the waveform and spectral characteristics. Xu (2004, 2005) examined the acoustic shock properties using joint time-frequency analyses. More recently, nonlinearity has been considered in analyses of solid rocket motor data (Gee *et al.*, 2013a; Bassett *et al.*, 2021; Reichman *et al.*, 2016) and its propagation has been modeled near the peak directivity angle (Muhlestein *et al.*, 2012). Whether the shocks that exist in the far field radiate from the plume as shocks or as steepened waves, which become more shock-like during the propagation, is not a question that has been fully resolved, but shocks (and the f^{-2} spectral slope) are present in the near-field GEM-60 data (Gee *et al.*, 2009). Recent numerical studies by Langenais *et al.* (2019) and Pineau and Bogey (2021a), which describe acoustical nonlinearities for high-speed jets, could offer insight into rocket noise nonlinear propagation and transition from near- to far-field behavior.

4. Frequency scaling

An additional important characteristic of jet noise is an appropriate frequency scaling, which, ideally, would allow a collapse of noise spectra produced by jets of different diameters, velocities, and temperatures. The majority of the jet and rocket noise data are scaled by the Strouhal number, Sr. For example, SP-8072 shows Sr-scaled SPL and sound power level spectra. McInerny (1990, 1992b) notes that whereas the spectral peak frequencies in the maximum radiation direction for a supersonic jet are around Sr = 0.2 (Tam, 1995; Schlinker *et al.*, 2007; Greska *et al.*, 2008), the sound power spectrum for a rocket peaks at around Sr = 0.02–0.025. For the RSRM example in Fig. 11 at 45°, where $D_e = 3.80$ m and $U_e \approx 2500$ m/s, a one-third octave spectral peak of 16 Hz translates into Sr = 0.025. Although McInerny (1992b) associates the downward shift in the scaled peak frequency with the stretching of the supersonic core in a rocket plume relative to other jets, the physical reasons for this large discrepancy are still unclear.

Beginning with Cole *et al.* (1957), alternate frequency scalings have been proposed in jet and rocket noise research. For example, Cole *et al.* suggested a Helmholtz number-like scaling for the rocket plume noise, turbojet, and laboratory jets, fD_e/c_e. Applied to the 45° RSRM spectrum, the scaling by Cole *et al.* (1957) is approximately 0.08, which is in line with the overall power level spectrum peak that is shown by Cole *et al.* for other rockets, but which is lower than the other jets. Although less common than the Sr scaling, Long and Arndt (1984), Michel and Ahuja (2014), and Bogey *et al.* (2007) have discussed the traditional Helmholtz number scaling (He $= fD_e/c_a$) of jet noise. The Helmholtz scaling of the 45° RSRM spectral peak with the ambient sound speed results in He = 0.18. Sutherland (1993) proposed one additional alternative Helmholtz-type scaling with c_t, where $M = 1$, instead of c_a or c_e. For rockets (Greska *et al.*, 2008), the idea that the peak frequency is independent of the flow variables may be justified by Ffowcs Williams (1963), who observed that highly supersonic jets produce a frequency spectrum that is independent of the jet velocity.

Several Strouhal and Helmholtz-type scalings, using nozzle exit, nozzle throat, and ambient variables, were compared by Potter and Crocker (1966) with the goal of collapsing laboratory-scale, turbojet engine, and rocket noise spectra. Of these, the proposed scaling by Eldred (1959) appears the most promising; it may be reduced[5] to

$$\mathrm{Sr}^* = \frac{fD_t}{c_a}\left[\left(\frac{2}{\gamma+1}\right)^{\gamma/\gamma-1}\left(\frac{p_0}{p_a}\right)\right]^{1/2}. \tag{3}$$

https://doi.org/10.1121/10.0009160

Using the characteristic scaling in Eq. (3), Fig. 12 shows an annotated version of Fig. 8 from Potter and Crocker (1966). Figure 12 also includes the original scaling by Eldred (1959), which was adopted by McInerny (1990),[6] and a line corresponding to 16 Hz for the RSRM. According to Eldred *et al.* (1961), the sound power spectrum from supersonic jets peaks at $\mathrm{Sr}^* \sim 0.3$, using this characteristic scaling. Although its possible universality is inconclusive based on the limited data, Eq. (3) should be investigated for identifying self-similarity across rocket plumes and other jets.

5. Clustered nozzles

To this point, the discussion about noise characteristics has been limited to the flow from a single nozzle. The noise generation from clustered nozzles is more complex. Historically, a remarkable measurement campaign, reported by Tedrick (1964), compared the noise radiation from the full-scale Saturn S-1 to a single F-1 engine. The eight-engine cluster in the S-1—where engines were only separated by about 1 D_e—and the single F-1 engine had nearly the same total thrust at 6.7 MN (1.5×10^6 lb). Using a polar array of far-field microphones, Tedrick (1964) showed that the engines, which were fired vertically downward into identical flame deflectors, produced nearly identical overall power levels and sound power spectra with only minor differences in the directivity patterns. Whereas other work by Potter and Crocker (1966) provided more complex calculation methods for clustered nozzles, the work of Tedrick (1964) provided the justification for NASA SP-8072 to treat closely clustered nozzles as a single nozzle having an equal exit area as for the clustered nozzles. This approach was used for the Shuttle acoustic load calculations in Himelblau *et al.* (2001) and predicting far-field spectra for different vehicles by McInerny (1992b).

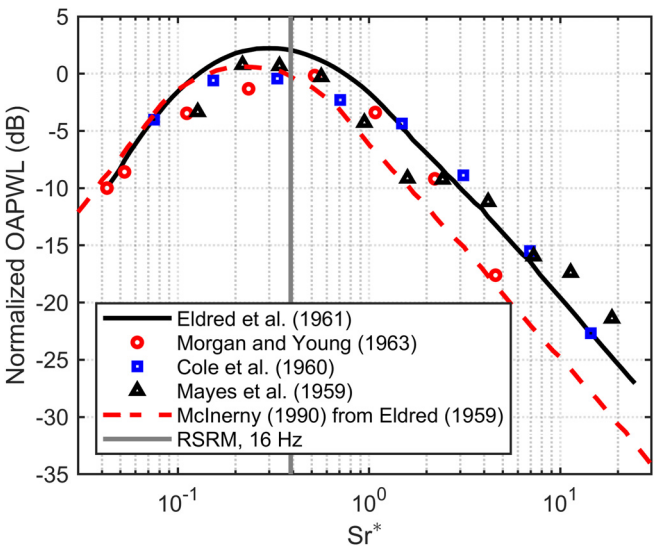

FIG. 12. (Color online) The historical scaling of the laboratory-scale, turbojet, and rocket plume sound power spectra based on Eq. (3). Adapted from Potter and Crocker, NASA-CR-566 (1966) and McInerny, AIAA Paper 90–3981 (1990), and includes a RSRM-based scaling at 16 Hz.

The simple scaling for closely spaced nozzles suggests that the individual plumes create one larger, equivalent plume. However, as the nozzle spacing increases, the noise generation changes and the radiated spectrum can have at least two peaks, a low-frequency peak corresponding to the downstream merging of the flow and a high-frequency peak corresponding to the noise generation near the nozzle where the flows can be considered independent. This effect, although minor in the scenario studied by Tedrick (1964), can be more significant in other cases, depending on the pressure ratio and the relative separation distance between the nozzles (e.g., see Coltrin *et al.*, 2013, for laboratory-scale jet arrays). Using a "two-zone" model for jet interaction by Eldred *et al.* (1963), Kandula (2008a) developed an empirical method for calculating the dual-peaked spectral shape depending on the clustered-nozzle characteristics. Apart from incorporation into an SP-8072-based model for launch pad noise by Vu and Plotkin (2010), the method has not yet seen adoption elsewhere in calculating the noise radiation from multiple engines.

Aside from Kandula's method, much of the recent jet noise literature on dual supersonic jet interactions has focused on mode coupling, screech tones, and related phenomena (e.g., see the review article by Raman *et al.*, 2012). However, because screech is not observed in launch vehicle measurements, the relevance of this body of work to the launch vehicle problem is unclear.

One final aspect of clustered nozzles is multiple-engine vehicle designs, where the potential for significant azimuthal asymmetry in noise generation exists. Examples include the Delta IV Heavy (three RS-68A engines, one per booster) and the Falcon Heavy (27 Merlin-1D engines, nine per booster) with their three side-by-side first-stage boosters. In one orientation ($\varphi = 0°$), all three boosters are seen but with a quarter-rotation about the vehicle axis ($\varphi = 90°$), only one booster is visible—suggesting the possibility of plume shielding effects. A review of the launch vehicle noise literature does not uncover much information about the plume shielding and azimuthal asymmetry, although McInerny (1990, 1992b) does mention the possibility of motor/engine asymmetry as the cause of the lower-than-expected noise levels from the Space Shuttle launches. Instead, twin-jet studies from the supersonic jet noise literature are useful to at least bound the possible significance of plume shielding, causing azimuthal asymmetry in noise radiation. A study by Kantola (1981) indicated that nozzle spacing was key: if the nozzles were separated such that the turbulence interaction was minimal, the acoustic shielding dominated. For different spacings and jet conditions, he found the in-plane OAPWL shielding approached 2–4 dB as $\varphi \to 90°$. For three different nozzle configurations, Bozak (2014) found the polar and azimuthally averaged twin-jet shielding effect on the OASPL to be 1.0–1.4 dB. Likely, of greatest relevance to the rocket noise problem, Pineau and Bogey (2021b) recently investigated twin Mach-3.1, highly heated jets with different nozzle spacings and found a maximum shielding effect of 2 dB. Combined, these studies suggest

azimuthal asymmetry for overall level of 2–3 dB for twin jets, which effectively suggests that the visible plume contributes "nearly" all of the radiation for $\varphi = 0^\circ$ and moderately separated nozzles.

C. Where does the sound originate?

1. Maximum SPL

The origin of noise within a turbulent jet is a complex subject. Determining the noise origin in a rocket exhaust plume is made more difficult because direct measurements of the flow parameters typically used to localize noise sources within subsonic or moderately heated supersonic jets, such as particle image velocimetry (PIV) and hot-wire anemometry, are not applicable to high-speed, high-temperature, turbulent rocket flows. However, the principal ideas associated with the mixing noise generation of other supersonic jets are believed to hold here, although the overall diameter-scaled noise source region is appreciably longer because of the greater plume velocity. This makes the region over which the plume is convectively supersonic (and a relatively efficient radiator) longer.

Acoustic field measurements (historical and modern) of rockets spanning a wide range of thrust/sizes have indicated that the maximum OASPL originates between 17 and 20 D_e downstream of the nozzle (Mayes *et al.*, 1959; Potter and Crocker, 1966; Gee *et al.*, 2013b). Contrast that with advanced fighter aircraft at full afterburner, for which acoustical holography indicates that the dominant frequencies originate from ∼6–15 D_e (Wall *et al.*, 2016; Leete, 2021a), and near-field measurements suggest that the maximum OASPL originates from around 8 D_e (Gee *et al.*, 2016b; James *et al.*, 2015). Although rocket noise originates significantly farther downstream than afterburning military jet engine noise, it is also well upstream of the 25–30 D_e maximum location suggested previously by McInerny (1996a).

2. Length-scaled power distributions

Because early launch vehicle acoustics work focused on connecting plume parameters to the radiated power, other research focused on determining the origin of this power within the plume. The classic experiment by Potter (1968) with a Mach 2.5, unheated nitrogen jet resulted in the sound power distribution per unit length and its relation to the jet potential and supersonic core lengths, L_c and L_s. Potter described the maximum sound power as coming slightly upstream of L_s and approximately 1.5 L_c downstream of the nozzle. Eldred (1971) extrapolated this result as the sound power per unit length for a "standard chemical rocket" in SP-8072. However, the comparison of SP-8072 by Gee (2021) with the use of the Potter result in the supersonic jet noise model development by Nagamatsu *et al.* (1969) and Nagamatsu and Horvay (1970) showed that Potter's report contained a plotting error, which has propagated from SP-8072 into many subsequent rocket noise publications. Figure 13, which contains both the Eldred (1971) and Nagamatsu *et al.* (1969) versions of the Potter result for

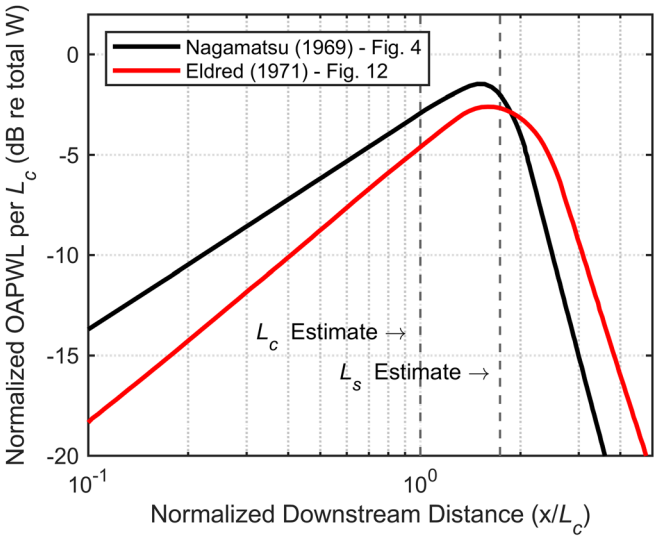

FIG. 13. (Color online) Potter's normalized overall power level per unit length result as adopted by Nagamatsu *et al.*, NASA SP-207 (1969) and Eldred, NASA SP-8072 (1971) and Gee, J. Acoust. Soc. Am. **149**, 2159 (2021).

relative sound power level per unit length, means that rocket and supersonic jet noise source models differ regarding the relative importance of the three noise-producing regions demarcated by L_c and L_s. Whereas the result of Potter (and Nagamatsu *et al.*) indicates that most of the sound power is radiated upstream of L_s, NASA SP-8072 and much of the subsequent research (literally, every study that has repeated the Eldred curve in Fig. 13) have been based on an erroneous assumption that the subsonic part of the plume is the dominant sound power-producing region.

This idea of using core lengths to quantify the scaled source locations is a convenient simplification in principle. However, the complexity of determining the peak sound power location increases when one learns that core lengths for real rocket motors and engines have not been well defined (McInerny, 1992b). This is true despite work by Eldred (1971), Varnier (2001), Nagamatsu and Horvay (1970), James *et al.* (2016), and others; various definitions of L_c, which rely on extrapolation of the laboratory-scale data (sometimes from unheated jets), vary drastically. For example, McInerny (1996a) provides two definitions from the literature for L_s and suggests that for rockets, L_c ranges from 16 to 25 D_e and L_s ranges from 25 to 35 D_e. For the approximate RSRM parameters, L_c ranges from 7 to 15 D_e and L_s ranges from 31 to 37 D_e. Given that the maximum OASPL region appears to be ∼17 D_e (Gee *et al.*, 2013b), these are large ranges with significant implications for the source location and physical interpretation of Fig. 13. Ultimately, the uncertainty around core lengths, both potential and supersonic, suggests that their use to conclusively describe the scaled source locations is problematic at the present. It should be noted that none of the previous models for potential core length have included the jet temperature as a parameter. Thus, Koudriavtsev *et al.* (2004) proposed a core length that was related to the jet temperature and

https://doi.org/10.1121/10.0009160

various other jet thermodynamic data, whereas Greska proposed an alternative model for the normalized core length in which the effect of the jet temperature is represented by inclusion of the convective Mach number [see Eq. (6), Greska *et al.*, 2008, for details].

3. Acoustic source location measurements

With an inability to rely on established core length source definitions, acoustical arrays are the best present means to reconstruct the acoustic source field. However, although acoustical holography and beamforming and associated reduced-order models (ROMs; see Sec. VI D) are becoming increasingly used for laboratory-scale jets and even jet engines, they have not been applied to the detailed characterization of the rocket plume. Beamforming has, however, been applied to launch pad environments (Casalino *et al.*, 2012; Panda and Mosher, 2011, 2013; Panda *et al.*, 2014; Ishii *et al.*, 2012; Ishii *et al.*, 2016; Palmieri *et al.*, 2017; Malbequi *et al.*, 2017; Mortain *et al.*, 2019).

To date, the only acoustic array processing method that has been applied to full-plume noise source characterization is near-field vector intensity. Early efforts to use intensity to characterize laboratory-scale subsonic jets (Roth, 1984; Jaeger and Allen, 1993) have been significantly expanded in the study of supersonic laboratory jets (Gee *et al.*, 2017), military aircraft (Stout *et al.*, 2015a,b), and large solid rockets (Gee *et al.*, 2009; James and Gee, 2012; Gee *et al.*, 2016b). An example intensity characterization of a horizontally fired GEM-60 solid rocket motor (880-kN thrust, 1.09-m D_e) is shown in Fig. 14. The near-field, frequency-dependent intensity measurement with several vector probes as a function of frequency [see Figs. 14(a) and 14(b) for examples] results in a ray-traced source region using the maximum-amplitude intensity vectors. The peak intensity source characterization over a broad range of frequencies (Gee *et al.*, 2016b) has been used to annotate a recreated frequency-dependent source location figure from SP-8072, which is shown in Fig. 15. The intensity results, which begin at Sr = 0.013 (30 Hz), most closely align with a study by Morgan and Young (1963), who positioned microphones along the plume boundary of a 5.91 cm diameter, 1.91 kN thrust solid rocket motor, as well as an additional multiple-nozzle industry study referenced in SP-8072, whose results may indicate a sharp transition from merged to individual jet behavior. The intensity results indicate a source location of ∼22 D_e for a frequency of Sr = 0.025, the historical spectral peak frequency for the sound power spectrum.

An additional important finding from the intensity study is that although source location does move downstream with decreasing frequency, there is little justification for source locations greater than 40 D_e at (scaled) frequencies of importance. Also included in Fig. 15 is a recent effort to characterize the RSRM source locations using a linear array of microphones, which are offset 18 D_e from the centerline (James *et al.*, 2014b). This study tried to adopt the approach of the measured spectral peak frequencies at different downstream distances but did not incorporate the source directivity and with the 18 D_e array offset likely resulted in the low-frequency sources being localized as too far downstream.

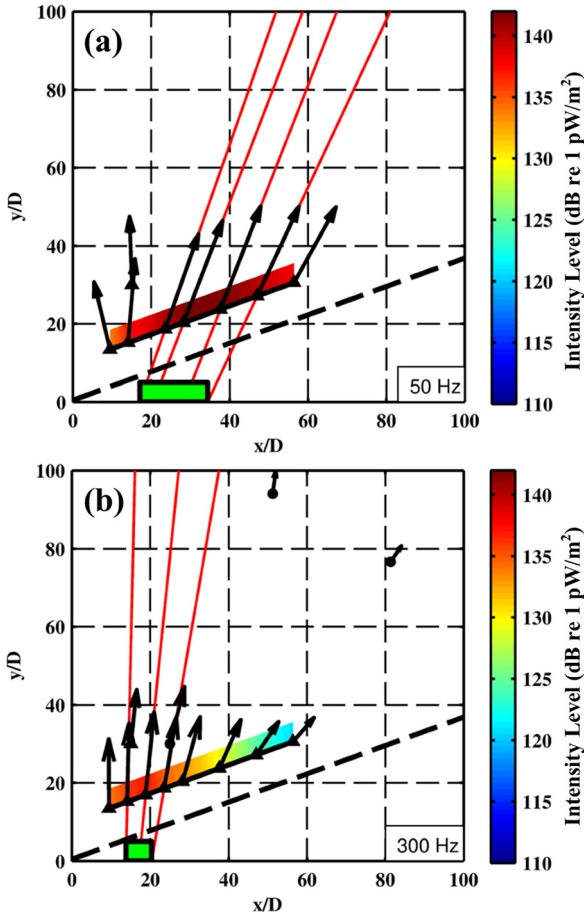

FIG. 14. (Color online) An example of the intensity characterization of a GEM-60 solid rocket motor.

D. Where does the sound radiate?

1. Peak directivity: The role of convective Mach number

From the commencement of jet noise studies, researchers have sought to understand the directionality of the noise radiation and how it changes as a function of jet parameters and frequency. Early work by Cole *et al.* (1957) and others was summarized by Eldred (1971) in SP-8072, which describes the maximum radiation of an undeflected rocket plume to be at ∼50° relative to the exhaust flow. Eldred asserted that the maximum radiation angle is governed by the exhaust flow parameters, such as exit velocity, exit Mach number (flow sound speed), exit density, and exit static pressure, but their ties to the noise radiation were unclear. Understanding of modern supersonic jet noise indicates that because a highly supersonic jet's noise radiation is dominated by the Mach wave radiation, the peak directivity

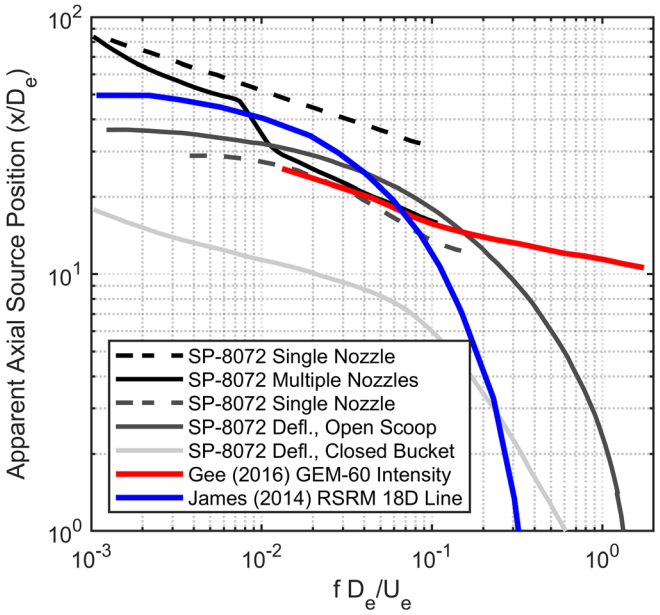

FIG. 15. (Color online) The apparent axial source location in nozzle diameters as a function of the Strouhal number. Adapted from Fig. 14 of SP-8072 and updated to include the GEM-60 intensity characterization; Gee *et al.*, Trans. Jpn. Soc. Aeronaut. Space Sci. Aerospace Technol. Jpn. **14**, Po_2_9–Po_2_15 (2016b), shown in Fig. 14, and a source location estimate by James *et al.*, Proc. Mtgs. Acoust. **18**, 04008 (2014b).

angle is controlled by the convective Mach number such that

$$\theta_{\mathrm{pk}} = \cos^{-1}\left(\frac{1}{M_c}\right). \tag{4}$$

Although not discussed by Eldred (1971), the increased convective Mach number may explain the increase in the directivity angle from chemical to nuclear rockets (see Manhart *et al.*, 1966), which is mentioned in SP-8072.

For supersonic jets, the convective Mach number is usually described empirically as

$$M_c = \frac{\kappa U_e}{c_a}, \tag{5}$$

although McInerny (1990, 1992a) uses c_e instead of U_e to justify an assumed radiation angle of 50°–60°. In Eq. (5), κ is a constant, which ranges from about 0.6 to 0.85 in the jet noise literature.

Although Eq. (5) has seen wide adoption in the jet noise interpretation, alternate analytical expressions for M_c have been used to describe the families of Mach waves. For example, the experimental work by Oertel (1982) with ideally expanded supersonic jets led to identification of three distinct convective Mach numbers, each depending only on M_j, c_a, and c_j. Subsequent work by Greska (2005) identified another Mach number, the arithmetic mean of two of Oertel's Mach numbers, which collapsed the far-field jet noise data from a variety of sources, representing a wide range of operating conditions. He referred to this mean as the Oertel convective Mach number, M_{CO}, where

$$M_{CO} = \frac{U_j + 0.5c_j}{c_a + c_j}. \tag{6}$$

Recently, Eq. (6) has been successfully used to describe the peak directivity angle for unheated (Baars, 2014) and heated (Greska *et al.*, 2008) laboratory-scale jets as well as a large-scale SRB (James *et al.*, 2014b) and a Falcon 9 launch (Mathews *et al.*, 2021).

This discussion of the convective Mach number reveals that early rocket noise research did not connect the directionality of the noise radiation with the flow physics. Plume velocities and sound speeds for the solid and liquid-fuel rockets, applied to Eq. (6), suggest peak directivity angles between 62° and 72°. Whereas Cole *et al.* (1957) and, later, Eldred (1971) described the peak directivity angle as being around 50°, Cole *et al.* also described the directivity patterns educed from the launch data, which had maxima between 70° and 80°, and McInerny later used this study to assume a peak radiation angle of 70° in an analysis of the Titan IV, Delta, Peacekeeper, and Scout launch data (McInerny, 1996a,b). Because neither historical angular range appears to match the relevant physics, the recent static and launch measurements are examined.

2. Directivity measurements

The peak radiation angle described in historical documents is less than that obtained through convective Mach number estimates. One possible explanation for this discrepancy is the use of polar microphone arrays with an origin at the nozzle exit and an insufficient radius to be fully in the geometric far field of an extended turbulent noise source. As described by James *et al.* (2014b), this shifts the directivity angle aft because of the downstream origins of the dominant low-frequency noise sources. Despite the use of polar arrays in most of the historical work, a near-field sound level mapping by Potter and Crocker (1966) clearly shows a peak noise source origin between 15 and 20 D_e and a peak radiation angle of 60°–65°.

The importance of selecting an appropriate noise source origin when using polar arrays and the impact on the historical data and decades' worth of subsequent modeling can be summarized using the RSRM data described previously. The goal of the RSRM measurements (Kenny *et al.*, 2009; Haynes and Kenny, 2009) was to update the frequency-dependent directivity indices, which are critical to SP-8072-based models. However, the 80 D_e polar array was centered at the nozzle exit, not at the ~17 D_e apparent OASPL maximum source origin suggested by a subsequent RSRM data analysis (Gee *et al.*, 2013b). Consequently, the raw OASPL measurements at 80 D_e have been corrected for the angles and levels based on a new origin. As shown in Fig. 16, the peak directivity shifts significantly from 53°, similar to that predicted by SP-8072, to 65°. Based on the RSRM plume parameters, this new angle is described almost perfectly by the Oertel convective Mach number. Furthermore, the expected ~65° peak radiation angle has

https://doi.org/10.1121/10.0009160

been confirmed by Bassett *et al.* (2021) with far-field measurements of a GEM-63 solid rocket motor. It also suggests an appropriate value of $\kappa \approx 0.32$ in Eq. (5), which is much smaller than anything described in the supersonic jet noise literature outside of $\kappa \approx 0.31$, recently predicted by Mathews *et al.* (2021) from Falcon-9 launch data. Although the results illustrate a marked disconnect between rocket plumes and other supersonic jets, the 3 dB-down OASPL lobewidth in Fig. 16 is approximately 35°, which is similar to that in SP-8072 and for military aircraft (see James *et al.*, 2015).

Regarding the historical observation of 70°–80° by Cole *et al.* (1957) for launch-derived peak radiation angle, there is no satisfactory physical explanation. Whereas the exit conditions of some liquid-fuel engines (e.g., the RS-25) are sufficient for a predicted static peak directivity angle that slightly exceeds 70° when using Eq. (6), directivity estimates educed from far-field launch measurements can be influenced by forward-flight effects, which will reduce the effective convective Mach number and reduce the peak radiation angle. Although forward-flight models exist for jet noise, their application to launch data has been sparse and tenuous (Sutherland, 1993). However, a recent study by Mathews *et al.* (2021) sheds new light on this historical paradox. Drawing from three recent Falcon-9 launch measurements (Mathews *et al.*, 2020), estimates of the directivity function are obtained by correcting for the vehicle trajectory and distance. Whereas static conditions predict a directivity of 69° for the Merlin-1D engines, the measured peak directivity angle of 63°–64° in Fig. 17 is in good agreement with an effective Oertel convective Mach number that has been reduced to account for flight effects. Ultimately, although the Cole *et al.* historical directivity paradox cannot be fully resolved, the overall directivity angles from modern measurements can be tied to Mach wave radiation physics.

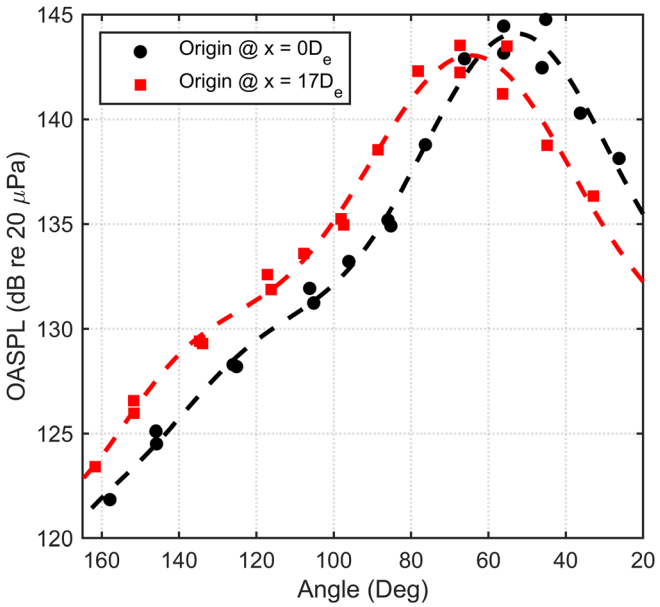

FIG. 16. (Color online) The RSRM OASPL directivity at 80 D_e with the array as measured (Gee *et al.*, 2013b) and adjusted here for an estimated source location at 17 D_e.

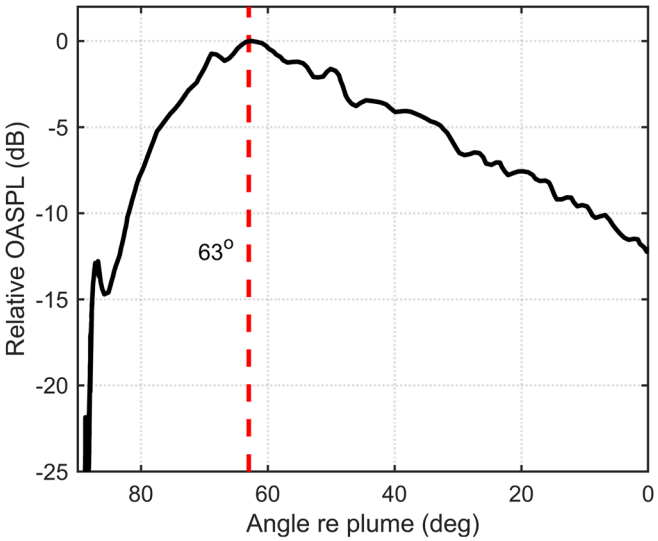

FIG. 17. (Color online) The relative OASPL (normalized to maximum) as a function of the plume angle for the Falcon 9, based on Mathews *et al.* (2021).

3. Frequency-dependent directivity

All of the radiation characteristics, thus far, have been for overall levels. How do radiation patterns change with frequency? Although the frequency-dependent directivity patterns in SP-8072 are problematic and have since been updated (Haynes and Kenny, 2009; James *et al.*, 2014b), they show that the rocket plume peak radiation angle increases with frequency and the directivity pattern broadens. Phenomenologically, these are consistent with expected supersonic jet behavior. Low frequencies are generated by larger-scale turbulent structures, which reach maximum intensity farther downstream with a lower convective Mach number and, therefore, radiate with a lesser angle. Higher frequencies are generated by smaller-scale turbulence with shorter coherence lengths closer to the nozzle where the convective Mach number is greater, resulting in a broader directivity pattern with a larger angle.

The greater convective Mach number causes the maximum radiation angles for rockets to be larger than those for military aircraft or heated laboratory-scale jets for all frequencies. Near-field intensity measurements of solid rocket motors (Gee *et al.*, 2016b; James and Gee, 2012) and spatial maps of the RSRM radiation (Gee *et al.*, 2013b) for different frequencies show that the high-frequency radiation angle shifts to angles greater than 80°. These shifts are not well accounted for in the historical or updated directivity patterns, where the peak radiation angle seems to be limited to a maximum of around 65°. One cause is a mismatch of the assumed and actual noise source origin as a function of frequency. However, another possible cause are the competing effects of the atmospheric absorption, which will tend to reduce the high-frequency energy, and nonlinear propagation, which will tend to enhance it. Because the nonlinear propagation and shock content are likely to be most prevalent around the θ_{pk} angle (as observed by Bassett *et al.*, 2021), high-frequency

energy may persist along those angles even when it begins to decrease elsewhere—thus, narrowing the directivity pattern. Some possible evidence of this nonlinear narrowing is observed in the high-frequency patterns published by Haynes and Kenny (2009) and updated by James *et al.* (2014b) and for military aircraft as observed in James *et al.* (2015).

4. Absence of spatiospectral lobes

A topic of recent interest in the supersonic jet engine research community has been the observation of the multiple radiation lobes. These so-called "spatiospectral lobes," which result in the splitting of the overall directivity pattern at different frequencies, vary with frequency and engine condition (e.g., see Wall *et al.*, 2015; Leete *et al.*, 2021a; Leete *et al.*, 2021b). The lobes, which appear mutually incoherent (Swift *et al.*, 2018), overlap across frequency and space to form the overall broad radiation pattern (Leete *et al.*, 2021a). The lobes are mentioned in this article because the analyses of full-scale rocket noise have not revealed clear evidence of their presence. This could be because rocket measurement arrays have been spatially coarser than recent tactical jet noise measurements, which revealed their presence and permitted their study. Another possible explanation, however, is that the relative importance of the phenomena, which result in their appearance in high-power, military jet engine noise but not in laboratory measurements, may shift again, going from military jet engines to rockets. Different lobe explanations—Mach waves versus subsonic, large-scale structure noise (Liu *et al.*, 2015), large-scale structure versus indirect combustion noise (Tam and Parrish, 2015), and scattering of supersonically convected structures by shock cells (Long, 2008; Wall *et al.*, 2017)—have been proposed with no quantitatively satisfactory explanation appearing in the literature. Understanding the reasons for the conspicuous absence of broadband shock-associated noise and spatiospectral lobes in rocket noise, in contrast to their obvious presence in military jet noise measurements, could result in an overall improved understanding of heated, supersonic jet noise phenomena.

IV. IMPINGING ROCKET PLUME NOISE PHENOMENA

This section builds on the previous discussion of the essential noise characteristics of free rocket plumes. However, prediction of launch vehicle noise during liftoff also requires an understanding of impinging plumes. Clearly, the physical processes associated with impinging jets are very different from those present in free jets. However, it is extremely difficult to conduct experiments on such jets, particularly at the impingement point where the flow is very hot and fast flowing. In this section, the differences between free and impinging jets are described by focusing on the nature, origin, and directionality of the radiated noise.

A. What is the nature of the radiated sound?

As expected, impingement alters the nature of the radiated noise. Like the free rocket plume, there are major differences between the results of laboratory-scale and full-scale experiments. In the case of laboratory-scale supersonic jets impinging onto flat plates and inclined plates, a strong impingement tone has been observed in the spectrum in several studies (e.g., Krothapalli *et al.*, 1999; Henderson, 2002; Henderson *et al.*, 2005; Worden *et al.*, 2017; Edgington-Mitchell, 2019). However, like screech, laboratory-scale impingement tones are not observed in static tests of sub- and full-scale rocket engines or launch data. For example, acoustic data from the Epsilon launch vehicle (Tsutsumi *et al.*, 2015b) are shown in Fig. 18. The microphone, located at the top of the boom appearing in Fig. 18(a), was used to record the acoustic pressure from 0.5 s until 1.5 s after liftoff, at which point the nozzle exit was 8.7 D_e above the pad. The resulting power spectral density in Fig. 18(b) shows no evidence of an impingement tone. Analyses of the STOVL aircraft have also shown no evidence of the laboratory-like impinging tones (Soderman,1990; Reichman *et al.*, 2016). One potential explanation is that in high-temperature supersonic jets, the broadband turbulent mixing noise is so intense that the tonal noise is overwhelmed by the turbulent mixing noise. The shape of

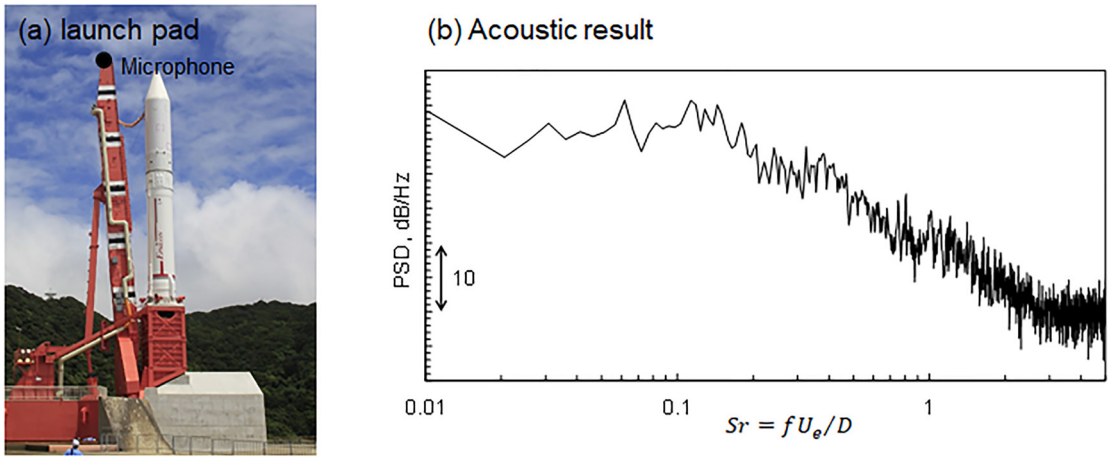

FIG. 18. (Color online) The (a) Epsilon vehicle launch pad with a microphone located atop the boom and (b) relative SPL spectrum at the boom microphone during early launch before flow impingement on the microphone are shown.

https://doi.org/10.1121/10.0009160

the launch vehicle base and components of the launch pad, such as the deflectors and launch platform, may also affect the formation of the tonal noise. Therefore, in this section, a discussion of impingement tones is omitted.

In the empirical prediction method described in SP-8072 (Eldred, 1971), deflected impinging rocket plumes are assumed to be monopole sources located along the centerline of free and wall plumes. Although a reduced acoustic efficiency was assumed in the case of the impinging plume, the source power distribution, frequency distribution, and directivity were left unchanged from that used for a free plume. In the empirical prediction method proposed by Potter and Crocker (1966), the plume before and after impingement at the deflector was theoretically obtained. The two acoustic fields generated from the plume before and after impingement were calculated separately and then superimposed on one another. Because the plume spreads along the deflector and the flame duct, the acoustic field was empirically modeled based on the experimental results of the acoustic fields generated from the rectangular nozzles.

An example of the different noise generation mechanisms observed in free and impinging jets is shown in Fig. 19, using numerical results for a cold, ideally expanded, $M_e = 1.8$ jet. For the free jet depicted in Fig. 19(a), the fine-scale turbulent mixing noise propagating laterally is observed. Mach wave radiation due to the large-scale vortex structure propagating 30° from the jet axis is also observed. The acoustic field for a jet impinging onto a 45° inclined flat plate located $5D_e$ downstream from the nozzle exit is shown in Fig. 19(b). In this case, there is a prominent wave field that radiates from the vicinity of the impingement region.

B. Where does the sound originate?

Because of the difficulty associated with performing detailed analyses of the acoustic generation of high-speed and high-temperature impinging plumes, our best physical understanding is currently obtained from laboratory-scale jet experiments and computational work. Many of the recent studies were conducted for a $M_e = 1.8$ or 2.0 ideally expanded unheated jet impinging on a 45° inclined flat plate located $5D_e$ downstream from the nozzle exit. Numerical study using large-eddy simulation (LES) was conducted by Nonomura and Fujii (2010), Nonomura *et al.* (2011), Nonomura *et al.* (2016), Tsutsumi *et al.* (2014), and Brehm *et al.* (2016). A detailed analysis using a two-dimensional Euler solver was conducted by Kurokawa *et al.* (2020) and experimental studies were performed by Akamine *et al.* (2015), Akamine *et al.* (2018), and Akamine *et al.* (2021). Jiang *et al.* (2019) have recently reviewed much of the literature in this field, but more work is needed on deflected, heated, supersonic plumes to identify the quantitative and qualitative differences.

Before discussing the origin of the acoustic waves associated with impingement on a deflector, the mean hydrodynamic field generated under these conditions is described. A schematic of the flow field is shown in Fig. 20. When the distance between the nozzle exit and the plate is shorter than the length of the supersonic core, L_S, a plate shock wave is generated at the impingement point, generating expansion fans, compression waves, and tail shock waves in the supersonic wall jet, which is deflected along the plate. As the launch vehicle ascends, the velocity of the free jet at the impingement point gradually decreases, and the plate shock wave and the tail shock wave finally disappear when the flow becomes subsonic. The deflectors employed in practical launch pads deflect the jet toward the ground (i.e., change the jet direction by 90°). Some deflectors use curvature to smoothly change the direction of the plume flow, whereas other deflectors are composed of multiple flat plates with slightly different inclination angles. If the change in angle is large, a separation bubble followed by a separation shock wave appears as shown in the downstream side of Fig. 20.

The acoustic waves generated as a result of impingement are summarized in Fig. 20. They are classified into five

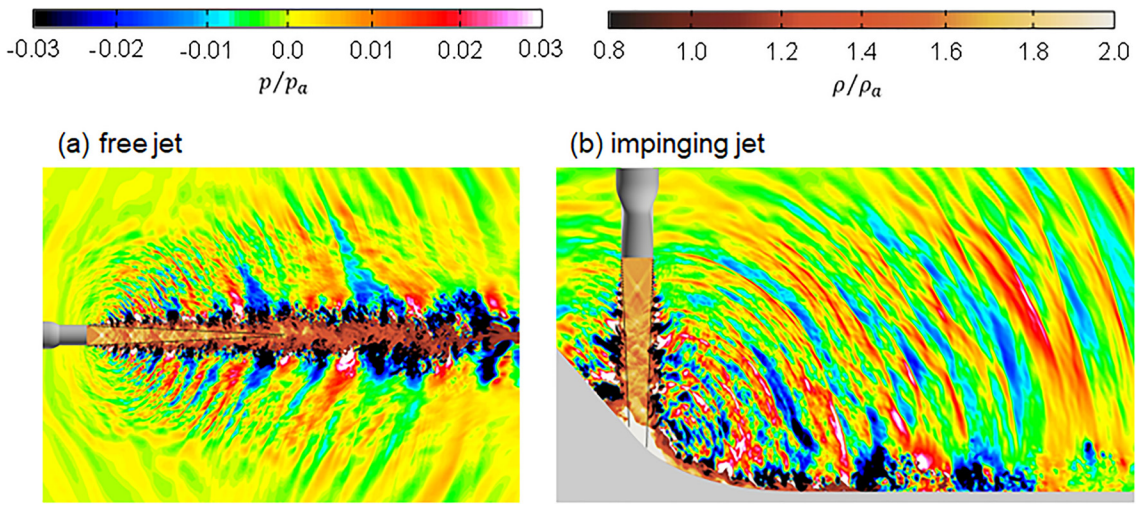

FIG. 19. (Color online) Computational fluid dynamics (CFD) results for a supersonic jet cold jet with $M_e = 1.8$ for the (a) free case and (b) impinging case. Hydrodynamic field, density; acoustic field, acoustic pressure (based on Tsutsumi *et al.*, 2014).

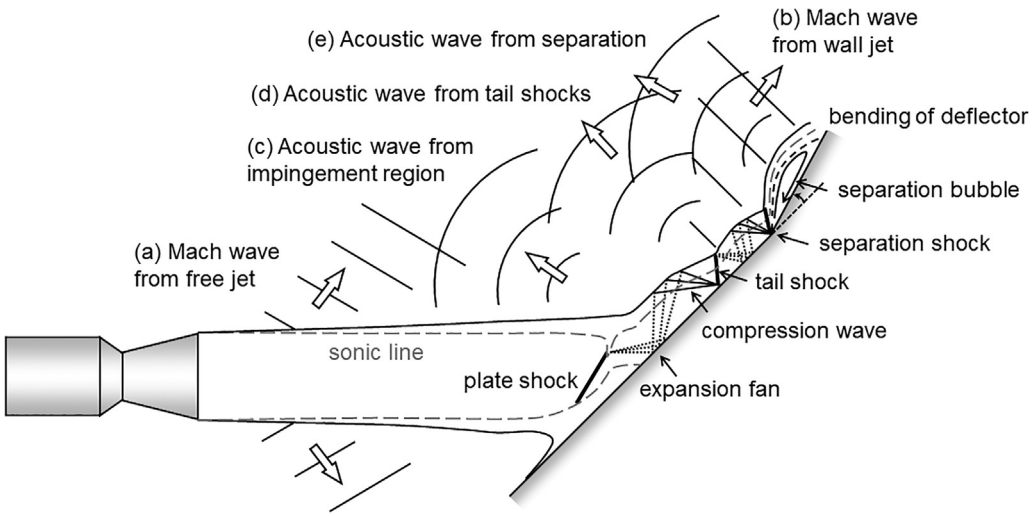

FIG. 20. Schematic of the hydrodynamic and acoustic fields for supersonic jet impingement on the deflector.

types. Mach waves are radiated from the undeflected jet before impingement [represented as (a) in Fig. 20]. Other Mach waves radiate from the large-scale structure of the supersonic wall jet [represented as (b) in Fig. 20]. These Mach waves were observed in all prior studies (Nonomura and Fujii, 2010; Nonomura *et al.*, 2011; Akamine *et al.*, 2015; Akamine *et al.*, 2018; Tsutsumi *et al.*, 2014; Brehm *et al.*, 2016). However, there is a debate about the acoustic waves radiated from the vicinity of the impingement region. Based on the work of Nonomura and Fujii (2010), Nonomura *et al.* (2011), Akamine *et al.* (2015), Akamine *et al.* (2018), Tsutsumi *et al.* (2014), and Brehm *et al.* (2016), these waves are classified into (c), (d), and (e), as shown in Fig. 20. From these studies, it was deduced that acoustic wave (c) from the impingement region is generated because of the interaction of the vortices in the jet shear layer with the plate shock wave, and Brehm *et al.* (2016) pointed out that distortion of the shear-layer vortices (such as stretching and tearing) caused by the plate impingement could be a mechanism for the formation of this acoustic wave (c). Comparing the location of the tail shock waves and acoustic field, it was observed that the acoustic wave represented as (d) in Fig. 20 is generated from the tail shock wave. Thus, it was inferred that interaction between the vortices in the wall jet shear layer and tail shock wave (a mechanism similar to that responsible for the broadband shock-associated noise) is the origin of these waves. Note that the tail shock wave appears in the wall jet as a shock train, similar to the barrel shock wave in an undeflected jet. In the experiments conducted by Akamine *et al.* (2015) and Akamine *et al.* (2018), it was observed that an acoustic wave (d) is generated at each tail shock wave. In the numerical studies conducted by Nonomura and Fujii (2010) and Nonomura *et al.* (2011), a separation bubble followed by a separation shock wave was generated instead of the tail shock waves, even for the inclined flat plate. They observed that the acoustic wave represented as (e) in Fig. 20 is radiated from the separation bubble and concluded that the interaction between the vortices in the wall jet shear layer with the separation shock wave is one of the acoustic generation mechanisms for this wave.

In the studies discussed previously, the acoustic waves resulting from impingement were investigated through various analysis techniques, such as the causality method, based on Lighthill's acoustic analogy, to reveal the causal relationship between the hydrodynamics and acoustics (Brehm *et al.*, 2016), proper orthogonal decomposition (POD; Nonomura and Fujii, 2010; Brehm *et al.*, 2016), and the acoustic-triggered conditional sampling method (Akamine *et al.*, 2018; Akamine *et al.*, 2021), after which possible generation mechanisms were discussed. However, the impinging supersonic jet originates in a complicated turbulent flowfield, involving multiple spatial and temporal scales; therefore, the causes of the acoustic waves (c)–(e), shown in Fig. 20, were conjectures. Consequently, Kurokawa *et al.* (2020) conducted a two-dimensional simulation based on the Euler equations for an ideally expanded cold planar jet with $M_e = 1.8$ impinging on a 45° inclined flat plate located $5D_e$ downstream from the nozzle exit. As discussed above, through previous work it was already known that the coherent structure in the shear layer is related to the generation of acoustical waves (c)–(e) in Fig. 20. In the study by Kurokawa *et al.* (2020), a short and controlled periodic disturbance, representing the coherent structure, was supplied to the shear layer of the free jet, and then the correlation between the flowfield (including the plate and tail shock waves) and vortex was investigated in detail. It was found that the acoustic waves generated due to impingement could be classified into four types, which are not necessarily identical to those in Fig. 20. Two types are generated synchronously from the impingement region and propagate upward to the nozzle. When the vortex passes through the two-dimensional plate shock wave, the plate shock wave deforms, resulting in the generation of these acoustic waves from both ends of the plate shock wave. The third acoustic wave, propagating omnidirectionally, is found to be generated from the tail shock when the vortex structure passes the tail shock. This acoustic wave is formed when the first tail

https://doi.org/10.1121/10.0009160

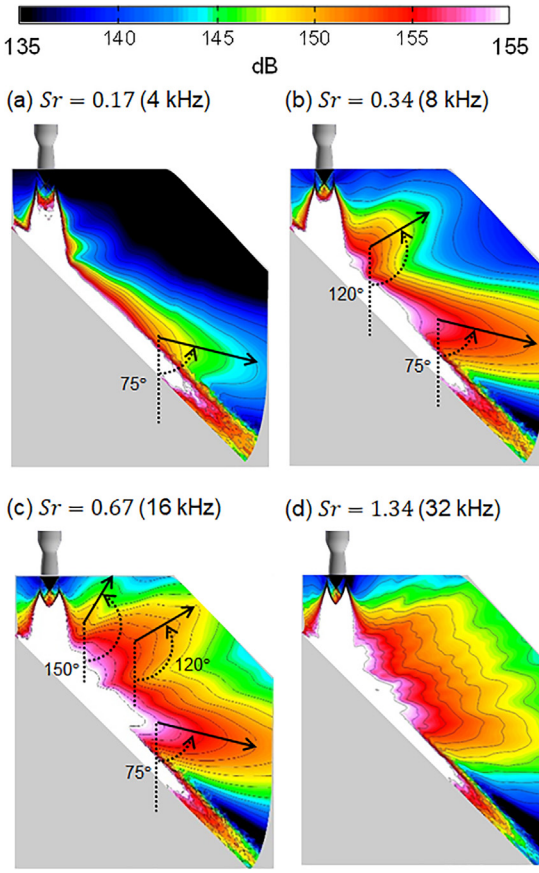

FIG. 21. (Color online) The octave-band filtered SPLs based on Tsutsumi *et al.* (2014). The conditions for the analysis correspond to Fig. 5 in Akamine *et al.* (2015).

shock wave is deformed from normal reflection to Mach reflection by the vortex passing through the tail shock wave. The fourth acoustic wave is generated by a sudden increase in the pressure amplitude of the input disturbance downstream of the plate shock and propagates normal to the inclined plate.

C. Where does the sound radiate?

Tsutsumi *et al.* (2014) conducted a numerical analysis corresponding to the experiments of Akamine *et al.* (2015). Figure 21 shows the 1/1 octave-band-filtered SPLs for the near field. At 4 kHz (Sr = 0.17), the acoustic waves propagating from the downstream side of the wall jet at a direction of $\theta = 75°$ (30° from the plate) are observed as shown in Fig. 21(a). Considering their origin and directivity, these correspond to the Mach wave from the wall jet. At 8 kHz (Sr = 0.34), acoustic waves with a directivity of $\theta = 120°$ are generated from the vicinity of the impingement region in addition to the Mach wave radiated from the wall jet [see Fig. 21(b)]. In addition to the two acoustic waves observed in the 8 kHz result, acoustic waves also propagate from the impingement region in the direction $\theta = 150°$ at 16 kHz (Sr = 0.67) as shown in Fig. 21(c). At 32 kHz (Sr = 1.34), no acoustic waves with the characteristic directivities are observed, but acoustic waves appear over the whole region of the jet [Fig. 21(d)]. The acoustic waves (c)–(e) identified in Fig. 20 are superimposed on the results appearing in Fig. 21, so it is difficult to extract their individual contributions. To develop an empirical model similar to that for the undeflected plumes described in SP-8072 (Eldred, 1971), it is desirable to clarify the source power, frequency, and directivity characteristics for each acoustic wave.

In the previous discussion, the distance between the nozzle exit and the plate (h) is $5D_e$, but the effect of the vehicle elevation on the acoustic field should be considered. Using the same jet as in previous work, Akamine *et al.* (2015) and Akamine *et al.* (2018) conducted experiments in which h was changed from $5D_e$ to $25D_e$. Comparing the OASPL measured by the upstream microphone, $R/D_e = 40$ and $\theta = 120°$, the maximum OASPL was observed to occur at $h = 15D_e$. In Fig. 22, the ray tracing lines of the acoustic intensity vectors of the Mach waves that are generated from the undeflected jet region and reflected by the plate are compared for the cases $h = 5D_e$ and $15D_e$. The acoustic intensity vectors at 13 kHz (Sr = 0.54) are shown in Fig. 22.

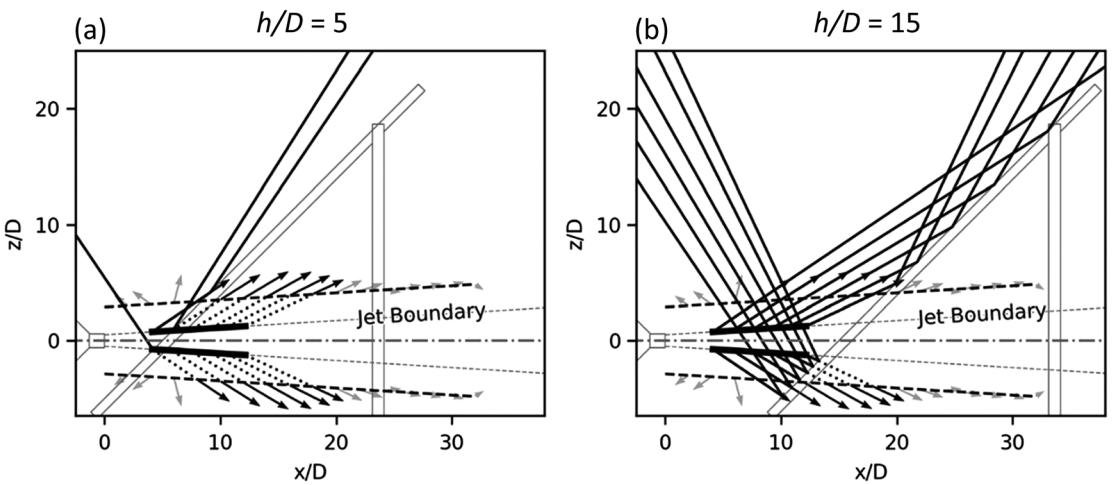

FIG. 22. The ray tracing lines of the acoustic intensity vectors at 13 kHz (Sr = 0.54) of $M_e = 1.8$ jet impinging onto 45° inclined flat plate. Reproduced with permission from Akamine *et al.*, AIAA J. **56**(5), 1943–1952 (2018).

In the case of $h = 5D_e$, it was found that the effect of the Mach wave radiation from the free jet is negligible. As discussed above, the acoustic waves (c)–(e) (shown in Fig. 20) affect the upstream location. On the other hand, in the case of $h = 15D_e$, the Mach wave radiated from the free jet appears. As depicted in Fig. 22(b), the Mach waves radiated from the lower part of the free jet shear layer propagate obliquely to the plate and then are reflected upstream by the plate. An increase in the acoustic level at the upstream location was, therefore, found to be caused by the Mach wave from the free jet. In practical launch pads, the situation may be different because the launch platform is located above the deflector. However, these results suggest that the Mach wave generated from the free plume is more influential than the acoustic wave generated by the plume impingement, and that it is important to reduce the Mach wave reflections from the launch pad structures. Measurements of the acoustic intensity of the free plume and analysis of the ray tracing lines of the acoustic intensity vectors will also be an effective method for understanding the acoustic generation and propagation in actual launch pad configurations.

V. ROCKET NOISE MITIGATION

Because launch vehicles are exposed to intense acoustic environments at liftoff (as described previously), reducing the acoustic load on the launch vehicle is essential. The modifications of the nozzle shape—a technique often employed for jet noise reduction (e.g., Samimy *et al.*, 1993; Callender *et al.*, 2005; Meyer *et al.*, 2013)—is difficult to apply to rocket engine nozzles. Thus, in the case of rocket launch noise, mitigation of the acoustic load is generally achieved through revisions to the launch pad itself, such as changes to the shape of the flame deflector (e.g., altering the deflector angle), the development of movable launch platforms (where the size of the exhaust exit and number of exhaust exit perforations is variable), or the use of water injection onto the pad and into the rocket exhaust trench. A review of some of these mitigation techniques follows.

A. Modifications to the launch pad structure

1. Deflector

Most of the deflectors used in actual launch pads consist of a straight section, where the jet impinges, and a curved section, which smoothly connects the straight section to the ground (Evans and Sparks, 1963). Thus, there are two major deflector design parameters: the inclination angle of the straight section and the curvature of the curved section.

The effect of the inclination angle on the launch pad acoustics is discussed by Tsutsumi *et al.* (2009), Tsutsumi *et al.* (2014), Brehm *et al.* (2013), Kurbatskii *et al.* (2014), Nonomura *et al.* (2016), and Akamine *et al.* (2021) in terms of numerical and experimental results, for the case of an ideally expanded supersonic jet impinging on an inclined flat plate located $4D_e$ or $5D_e$ downstream from the nozzle exit of numerical and experimental results. The acoustic fields generated when a supersonic jet with $M_e = 1.8$ impinges on a flat plate inclined at 45° and a plate at 14° are compared in Fig. 23 (Tsutsumi *et al.*, 2014). Acoustic waves of types (c) and (d) (see Fig. 20) propagate spherically from the vicinity of the impingement region in the 45° plate case [Fig. 23(a)]. However, for the 14° plate, it was observed that the majority of the acoustic waves are Mach waves from the free and wall jets with less from the impingement region [Fig. 23(b)]. As discussed in Sec. IV, acoustic waves generated from the impingement region are attributed to the plate and tail shock waves. These shock waves are weakened by reducing the inclination angle of the deflector. Tatsukawa *et al.* (2016) explored the role of the flame deflector shape in minimizing acoustic emission in the direction of the launch vehicle using a LES and genetic algorithm. Park *et al.* (2018) also applied a genetic algorithm to conduct shape optimization of the flame deflector using an augmented SP-8072 based method. As expected, the optimized shape has a steep inclination only around the impingement region.

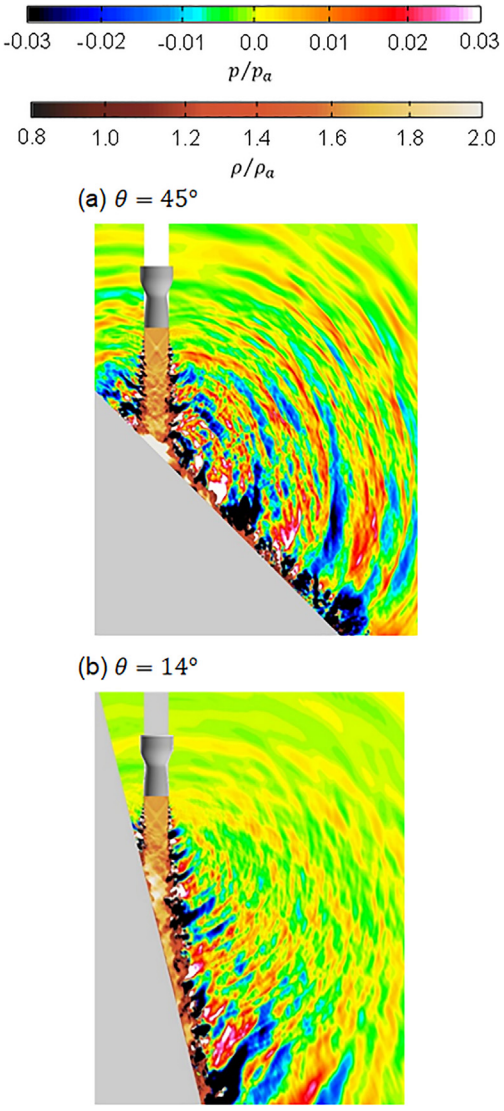

FIG. 23. (Color online) The comparison of the acoustic fields based on Tsutsumi *et al.* (2014) for an ideally expanded cold jet with $M_e = 1.8$, impinging on inclined flat plates located $5D_e$ downstream from the nozzle exit.

https://doi.org/10.1121/10.0009160

According to a numerical study by Tsutsumi *et al.* (2009), the acoustic level near the launch vehicle is significant for deflectors where the inclined straight section is directly connected to the ground. On the contrary, the acoustic level is mitigated for a deflector having a large curvature. It should be noted that if the flow direction of a supersonic wall jet is rapidly changed, strong tail shock waves are generated and an excessive change of flow direction leads to flow separation followed by separation shock waves. In such deflectors, the acoustic waves (d) and (e) (see Fig. 20) increase the acoustic level near the launch vehicle. Thus, the curved section should change slowly enough to prevent the separation and tail shock waves from forming to ensure a reduced acoustic environment. As tail shock waves are formed due to reflection of the expansion fan generated at the downstream end of the plate shock wave, wall jets without tail shocks can be obtained with a deflector whose contour suppresses the reflection of the expansion fan. Tsutsumi *et al.* (2014) employed the gradient-based shape optimization method to obtain a tail-shock-free deflector, and the acoustic field was numerically studied. Although the idea is only applicable to small and medium-sized launch vehicles having just one first-stage engine, an improvement of the acoustic environment is expected. In the design of a deflector, reduction of the heat load is also an important issue to be considered. Because the plate, tail, and separation shock waves increase the heat load, any design criteria for acoustic reduction also leads to heat load mitigation.

2. Flame duct

Almost all launch pads have a flame duct in which the high-speed and high-temperature plumes are channeled downstream safely. The flame duct is installed not only to ensure safety but also to shield the launch vehicle from the acoustic waves generated as a result of impingement of the rocket plume on the deflector and the Mach wave from the wall plume. There are four key parameters to consider in flame duct design: the duct length, whether the duct is covered or uncovered, the number of ducts, and the duct shape. Each of these are now considered in more detail.

Gely *et al.* (2000) conducted 1/47-scale model tests for the Ariane 5 launch vehicle. It was observed that the 1/1 octave-band SPL decreased by 4 dB at 31.5 Hz (full scale) if the flame duct is extended by 10 m. Additionally, when the flame duct was extended by 15 and 30 m, the acoustic level was reduced by 5 and 8 dB at the 31.5 Hz octave band, respectively. The effectiveness of the flame duct extension in noise reduction was confirmed by flight measurements. Malbequi *et al.* (2017) conducted 1/40-scale model tests for the Ariane 6 and also observed that the acoustic levels could be reduced by extending the flame duct. The acoustic waves, generated due to the impingement of the rocket plume on the deflector and the wall plume Mach wave, are ejected through the exit of the flame duct. By extending the flame duct, the propagation distance to the launch vehicle is increased, resulting in a reduction of the acoustic level there. In a 1/33-scale model test of a 120-in. solid booster for the Titan III, the effect of flame duct extension from $10D_e$ to $24.5D_e$ was investigated (Bond, 1964). It was discovered that beyond a certain duct length (i.e., $15D_e$), the acoustic level does not continue to decrease even if the flame duct is extended. It is suggested that at this point, the acoustic waves coming from the duct exit become smaller than the acoustic waves propagating upward through the launch platform and the fine-scale turbulent mixing noise from the undeflected plumes.

The effect of covering the flame duct was examined by Kandula and Vu (2003) and Kandula (2006, 2011), using a cold jet with $M_e = 2.5$, and also by Gely *et al.* (2005), using a 1/33-scale model test of the VEGA launch vehicle. Not surprisingly, these studies found that covering the flame duct is effective in mitigating the acoustic level. It is assumed that the acoustic waves propagating toward the launch vehicle—especially acoustic waves generated as a result of impingement of the plumes on the deflector—are reduced. However, according to Gely *et al.* (2005), only a 1–2 dB reduction was observed at the frequencies lower than 150 Hz (full-scale). The effect of covering the flame duct may depend on the configuration of the flame duct, launch platform, and deflector, and it is, therefore, necessary to examine the effectiveness at each specific launch pad.

The number of flame ducts used is different for different launch vehicles. For example, the H-IIA has only one flame duct, but the Ariane 5 has three flame ducts, one corresponding to each engine. In the 1/33-scale model test of the VEGA launch vehicle, Gely *et al.* (2005) compared the acoustic results of a single flame duct and double flame ducts facing in opposite directions. It was observed that there was no significant difference in the acoustic levels for the two scenarios. On the other hand, Xing *et al.* (2020) investigated this effect numerically and found that the single flame duct configuration showed higher acoustic levels than the double flame duct. Indeed, a 6.4–8.9 dB difference was observed in the OASPL at $h/D_e = 0$. Clearly, this result is not consistent with the conclusions of Gely *et al.* (2005); further studies are required to understand the effect of the number of flame ducts on the acoustic field.

In a 1/33-scale model test of the Epsilon launch vehicle, Ishii *et al.* (2012) compared the acoustic level at the launch vehicle for the three flame duct configurations shown in Fig. 24. The launch vehicle is located at the shroud ring on the upper part of the launch pad. Config. 1 has no flame duct, and the deflected plume is ejected directly outside. Config. 2 and Config. 3 have the same length, and their cross-sectional areas are the same as the exit area of Config. 1. The cross section of Config. 2 is gradually widened in the lateral direction, whereas the cross section of Config. 3 is constant. An image of the Epsilon launch vehicle and its launch pad based on Config. 3 is shown in Fig. 18(a). The acoustic measurements at several fairing locations were taken at $h/D_e = 8$ for all three of the configurations. It was

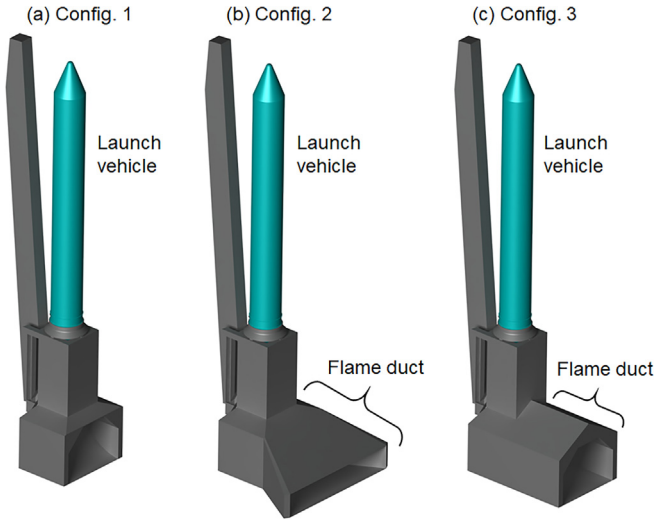

FIG. 24. (Color online) The flame duct configurations studied in the development of the Epsilon vehicle launch pad.

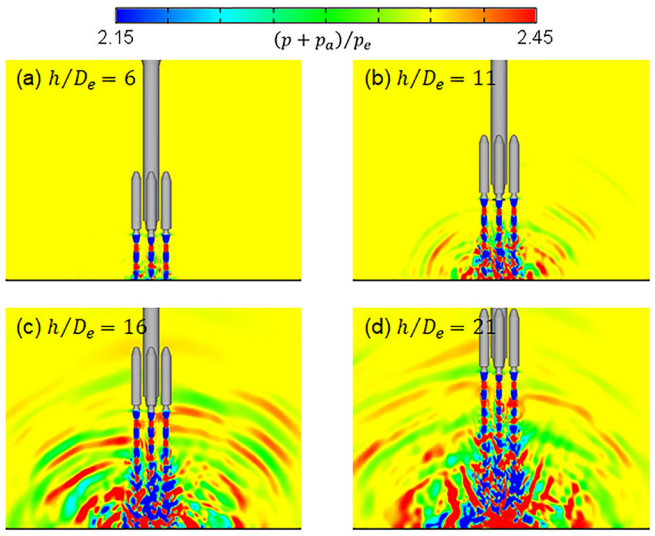

FIG. 25. (Color online) The numerical prediction for the acoustic waves above the H-IIA launch vehicle platform. Here, p_e represents the pressure at the nozzle exit (Tsutsumi *et al.*, 2008a).

observed that Config. 2 shows the highest OASPL level of the three configurations. Based on the discussion above, it should be possible to reduce the acoustic level by extending the flame duct. However, while the acoustic level of Config. 2 was higher than that of Config. 1 (without a flame duct), the acoustic level of Config. 3 was 2.9 dB lower (OASPL) than that of Config. 1. Through acoustic source localization using a beamforming technique, it was found that the area of acoustic emission, appearing at the exit of the flame duct, is wider in Config. 2 than in Config. 3. The difference in the acoustic emission area is deduced to be related to the difference in the acoustic level at the fairing. This study shows that the flame duct may adversely affect the acoustic environment, and the shape of the flame duct should be designed after careful consideration.

Almost all of the previous studies on flame ducts were conducted in the development of specific launch pads. A fundamental study on generic configurations is, thus, necessary to fully understand the effect of the four flame duct design parameters, discussed above, on the associated hydrodynamic and acoustic fields.

3. Launch platform

The launch platform's role is to transport the launch vehicle from the vehicle assembly building to the launch pad and attach it to the pad until liftoff. The launch platform is located at the flame duct entrance and has an exhaust hole for the rocket plume to enter the duct. Because there is a deflector directly underneath the launch platform, the launch platform plays a role in shielding the vehicle from the acoustic waves generated as a result of the plume impingement on the deflector. It should be noted that the platform also screens the vehicle from the IOP. Figure 25 shows the results of a numerical study to investigate the acoustic waves appearing above the launch platform of the H-IIA launch vehicle for different rocket elevations (Tsutsumi *et al.*, 2008a). It was shown that the most intense sound at the vehicle occurred at $h/D_e = 16$ [Fig. 25(c)] and was due to a combination of free-plume Mach waves and the interaction of the plume with the launch platform. This finding has been strengthened by subscale model tests conducted by Dumnov *et al.* (2000), Ignatius *et al.* (2015), and Malbequi *et al.* (2017). As mitigating various sources of acoustic waves is considered, the design of the launch platform is not straightforward.

The launch platform for the VEGA launch vehicle had openings around the exhaust hole when it was developed. Through acoustic source localization using beamforming and numerical simulation, it was revealed that the acoustic wave generated by the plume impinging on the deflector propagated upward to the launch vehicle through these launch platform openings. By covering the platform—except for the exhaust hole—the 1/3 octave-band SPLs were found to decrease by 1.5–2 dB at most frequency bands (Palmieri *et al.*, 2017; Mortain *et al.*, 2019).

It is known that the rocket plume interacts with the rim of the exhaust hole due to the jet shear-layer growth and this interaction generates an additional source of noise (Panda and Mosher, 2013; Panda *et al.*, 2014; Malbequi *et al.*, 2017). In addition, the free jet Mach wave, propagating obliquely downstream, is reflected by the launch platform or launch pad structures back to the launch vehicle. This reflected Mach wave is known to be one of the causes of deterioration of the launch vehicle's acoustic environment (Dumnov *et al.*, 2000; Tsutsumi *et al.*, 2008a). To analyze the effect of exhaust hole size, Tsutsumi *et al.* (2015c) numerically investigated the acoustic field generated by interaction between a subscale solid booster and four types of infinite plates with different exhaust holes. The distance between the nozzle exit and the infinite plate was $20D_e$. It was found that the acoustic level of the launch vehicle is almost the same for the cases with $2D_e$ and $3D_e$ exhaust holes and about 2 dB lower for the $4D_e$ case. But at higher altitudes, such as $h/D_e = 24$ (investigated by Varnier and Raguenet, 2002), the effect of the exhaust hole

size on the acoustic field becomes smaller. As stated previously, the launch platform shields the launch vehicle from the acoustic waves that arise due to the plume impingement. If the size of the exhaust hole is large, these waves may propagate through it and deteriorate the launch vehicle's acoustic environment. In a subscale model test conducted by Dumnov *et al.* (2000), two types of launch platforms, having $1.58D_j$ and $2.46D_j$ exhaust holes, were compared. At $h/D_j < 10$, the acoustic environment for the launch platform with a $2.46D_j$ exhaust hole was worse than that with a $1.58D_j$ exhaust hole. In an experiment conducted by Koudriavtsev (2000) at $h/D_e = 4.3$, the acoustic environment obtained with a launch platform having a $3D_e$ exhaust hole was almost the same as that without the launch platform. The shielding effect was also investigated by Yenigelen and Morris (2020). Based on the aforementioned studies, it is suggested that there is an optimum exhaust hole size, but research to find this optimum—which should also take into account the effects of IOP—is yet to be conducted.

A launch vehicle can drift during ascent because of the effects of wind, maneuvers, etc. When the position of the launch vehicle deviates during liftoff, the plume does not enter the exhaust hole but impinges onto the upper surface of the launch platform, resulting in an additional acoustic source (Panda and Mosher, 2013). Giacomoni and Kenny (2016) conducted scale model tests to define the relationship between launch vehicle drift and the associated acoustic levels. Following this work, the development of a model for predicting the increase in acoustic level relative to vehicle drift at launch is highly recommended.

B. Water injection

Water-based suppression systems are commonly used on launch pads for two purposes: to mitigate heat and noise. In the case of the Space Shuttle, Himelblau *et al.* (2001) reported a 4 dB OASPL decrease when water was injected at 200% of the propellant mass flow rate and an 8 dB reduction when water was injected at 500% of the propellant mass flow rate. Studies on the launch pad water injection system are conducted—usually through subscale tests—as an integral part of the development of most launch vehicles. Details of work related to Ares I and the Space Launch System (SLS) are provided by Counter and Houston (2012), Panda and Mosher (2013), and Houston *et al.* (2015). European launch vehicles are discussed by Gely *et al.* (2000), Lambaré (2016), and Malbequi *et al.* (2017). The research related to the H3 launch vehicle is presented by Sarae *et al.* (2016), whereas Ignatius *et al.* (2008) and Ignatius *et al.* (2015) give an overview of the Indian launch vehicle development. The investigations have also been conducted to understand the mechanisms of acoustic mitigation, optimize the water injection system, and develop prediction models (e.g., Zoppellari and Juve, 1998; Kandula, 2008c; Sankaran *et al.*, 2009; Shimizu *et al.*, 2009; Salehian and Mankbadi, 2020). Water injection is also used for rocket engine test stand noise suppression (Allgood *et al.*, 2014).

As reviewed by Henderson (2010), the use of water injection for aircraft jet engine noise mitigation also has a long history and studies in the laboratory (e.g., Krothapalli *et al.*, 2003; Norum, 2004; Ragaller *et al.*, 2011) and on engines (Greska, 2005) have been performed. The major difference between water injection for jet noise reduction and rocket plume noise reduction is the water flow rate. For supersonic jet engines, additional water for noise reduction translates into greater aircraft weight and reduced performance; thus, there is a greater need to minimize the water used. Krothapalli *et al.* (2003) injected water with a 17% mass flow rate relative to that of the jet $0.1D_e$ downstream from the nozzle exit at an angle of 60°, and a 2–6 dB reduction in the OASPL was obtained through a reduction in the turbulent structures that radiate the acoustic waves. The concept was later validated on an F404 engine (Greska *et al.*, 2005).

Figure 26 shows the H-IIA launch vehicle at liftoff. The white-colored plume (enclosed by red dotted lines) appearing on the top of the launch platform and emitted from the flame duct consists of the solid booster's plume (including Al_2O_3 particles) and the vapor generated due to the water injection. Based on the studies cited above, water injection reduces the noise by the following mechanisms:

(1) decrease of plume mean velocity, velocity fluctuations, and turbulent shear stresses due to momentum and heat transfer between the water and the plume and evaporation of water; and
(2) scattering and absorption of the acoustic wave by water vapor consisting of droplets and acoustic insulation by a water curtain.

For launch pads, there are two primary types of water-based acoustic suppression systems, as shown in Fig. 27: a below-deck system, where water is injected into the exhaust plume to reduce the far-field noise by more rapid dispersion of the rocket exhaust (Allgood *et al.*, 2014) and an above-deck system, where water is injected around the pad. The below-deck systems are generally used to suppress the noise during the hold-down phase of the rocket immediately before launch and, also, the noise emitted from the flame duct. The above-deck suppression systems, such as the "rainbirds" employed at Space Shuttle launches, generally provide a 2–3 dB reduction in the sound (Counter and Houston, 2011, 2012; Panda and Mosher, 2013; Houston *et al.*, 2015). However, it is not clearly understood which of the acoustic reduction mechanisms described previously is responsible for the rainbirds' effectiveness.

The design of below- and above-deck water injection systems includes parameters such as mass flow rate, water flow velocity (injection pressure or momentum flux ratio), water injection angle, and droplet size (type of water nozzle), injection location, and timing (Zoppellari and Juve, 1998; Kandula, 2008c; Sankaran *et al.*, 2009; Lambaré, 2016). Although constrained by the launch platform design, it has been observed that injecting water near the nozzle exit is effective for acoustic reduction because it enhances the

FIG. 26. (Color online) An image of the H-IIA launcher at liftoff.

overall mixing and the resulting evaporation of the water. Regarding water injection velocity and angle, Zoppellari and Juve (1998) and Ignatius *et al.* (2015) showed that it is optimal if the water jet only enters the plume shear layer; deep penetration into the plume creates a new acoustic source and the effect of the water injection decreases. The mass flow rate is an important parameter. For example, based on the SLS scale model test, Houston *et al.* (2015) recommended that it was generally desirable for the mass flow rate of the rainbirds to be ~350% of the propellant mass flow rate. It should be noted that the acoustic suppression effectiveness diminishes beyond a certain mass flow rate (Counter and Houston, 2011; Ignatius *et al.*, 2015). The system timing is also critical. The below-deck water is usually turned on before liftoff, but the above-deck water is generally turned on after the launch vehicle has elevated to prevent the water from splashing on the vehicle. However, recent work indicated that a slightly earlier start of the

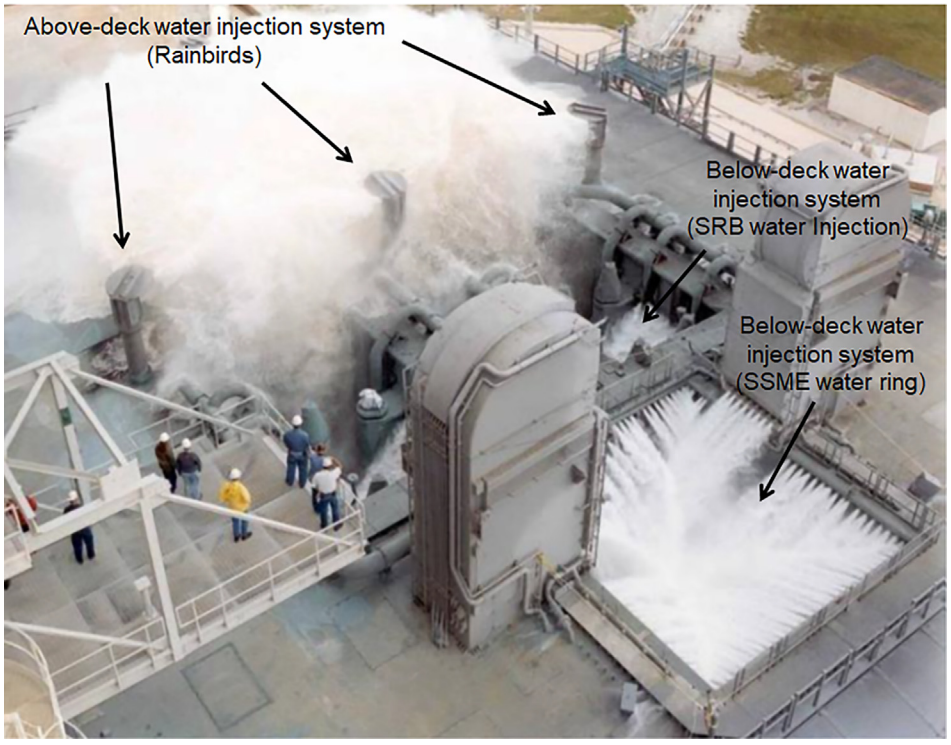

FIG. 27. (Color online) The above- and below-deck water injection systems for the Space Shuttle.

https://doi.org/10.1121/10.0009160

above-deck water system would provide even greater noise mitigation (Panda *et al.*, 2014).

As stated previously, launch pad noise suppression system design and optimization are mainly performed using subscale tests. If Strouhal number is used for comparing the acoustic results obtained in a subscale test and a full-scale launch, the subscale acoustic spectrum is centered at higher frequencies. Because of the relationship to the acoustic wavelength, the effects of the scattering and absorption of the water droplets are larger in a subscale test environment. Consequently, subscale test results should be treated carefully.

C. Other methods

In addition to the techniques for acoustic mitigation described in Secs. V A and V B, various other methods have been studied. Karthikeyan and Venkatakrishnan (2017) conducted laboratory-scale experiments using a cold jet with $M_e = 2$ to compare a conventional launch platform composed of a solid plate with a launch platform composed of a perforated plate. It was observed in the latter case that the acoustic level around the launch vehicle was reduced at all of the elevations measured in this study, namely, $h/D_e = 4$, 8, and 12. However, before using a perforated launch pad in an actual flight, it is necessary to examine the effect of the heat load from the exhaust plumes on such a plate as well as the maintainability issues associated with perforated plates. In addition, for heavy launch vehicles, several launch pad design issues must be considered when using a perforated plate, such as the arrangement of the propellant feed lines. Thus, further study is recommended prior to the practical application of this technique.

Ahuja *et al.* (2014) conducted laboratory-scale experiments using a cold jet with $M_e = 1.3$ and an acoustic liner, and it was found that the acoustic waves caused by jet impingement on the ground plate located $3D_e$ downstream can be reduced by 10 dB by the installation of such a liner. A similar acoustic reduction technique was also proposed for impinging jets by Dhamanekar and Srinivasan (2014). According to work by Malbequi *et al.* (2017), the acoustic waves reflected from the upper part of a flame duct are observed at high elevations. Thus, it may be possible to reduce acoustic waves by spreading an acoustic absorption material on the launch pad components from which the acoustic waves are reflected, although the frequency range of interest—from 31.5 to 500 Hz in an actual flight—may make the size of the liner required an issue. As in the discussion of the perforated launch platform, it is necessary to examine maintainability issues, etc., prior to implementing these acoustic mitigation techniques for an actual launch.

As stated previously, jet noise reduction often focuses on modifications of the nozzle shape, but this is difficult to apply to rocket engine nozzles. In a rocket engine that has a thrust-optimized nozzle contour for its exhaust nozzle, three types of flow structures appear inside of the exhaust nozzle during the transient engine startup and shutdown: free-shock separation, restricted-shock separation (RSS), and end-effects regime (EER; Nguyen *et al.*, 2003). In the EER regime particularly—just before the full flow is achieved—sawtooth separation lines, which oscillate in the circumferential direction, appear near the nozzle lip. It was observed by Canchero *et al.* (2016) that in the case of clustered rocket engines, acoustic waves were generated by the flapping of the exhaust jet due to the EER separation line oscillation, resulting in acoustic loading on the base of the launch vehicle. A significant reduction of the acoustic loading at the EER can be realized when the engine start-ups are staggered (Rojo *et al.*, 2016).

VI. ROCKET NOISE MODELING

The existing supersonic jet noise models cannot be extrapolated to rockets because of inherent differences in the underlying sound generation mechanisms (Sec. II B). Wilby (2007) discusses existing empirical methods for noise level prediction on a launch vehicle at liftoff, including modifications that attempt to deal with the discrepancies between the predictions and measurements. As described previously in this review, NASA SP-8072 and its derivatives have hitherto been used extensively to predict the sound field emitted by a rocket. This methodology is summarized here along with other approaches. As these models often arise from the results of subscale tests, these tests will also be discussed, as will the use of numerical methods in rocket launch noise modeling.

A. Empirical methods

1. NASA SP-8072

Despite having been created 50 years ago by Eldred (1971), NASA's SP-8072 empirical acoustic load prediction model is still one of only a few approaches that relate the rocket flow parameters to the radiated SPLs. Thus, it is still an active research area, spawning many derivatives. The method uses empirical curves from a variety of largely subscale measurements from the 1950s and 1960s to distribute the overall sound power from a given rocket exhaust along the plume axis via multiple acoustic subsources. This is then combined with the far-field directivity indices to predict the sound levels as a function of the frequency, distance, and direction from the plume. The overall acoustic loading is predicted as the sum of the radiated acoustic fields from each of these sources. Plume deflection and impingement are empirically accounted for in this model. The various elements of SP-8072 have previously been described in Secs. III and IV. Here, we will review the process of combining these elements to provide a prediction of the acoustic loading on the launch vehicle and suggest that after half a century, the moment has arrived for developing a new, physics-based rocket launch noise model.

a. Acoustic radiation efficiency. The physical parameters of the rocket plume are related to the resulting acoustic power, W, via the acoustic radiation efficiency, η. Accurate estimates of these plume parameters should lead to a

reasonable estimate of the overall sound power. As described in Sec. III A 1, our best estimate for the radiation efficiency has been empirically derived to be ~0.5%.

b. Sound power level distribution. The OAPWL is then distributed along the rocket plume. Two alternative empirical methods are used to perform this acoustic source allocation, which is central to NASA SP-8072. DSM-1 assumes that the source of rocket noise for each frequency band is restricted to a different, discrete section of the rocket plume and bases the unique sound power level emitted by a given source on the Strouhal number, Sr. Although it uses curves directly from observed historical data to estimate the source location, it is then fundamentally too simplistic in its assumption that rocket noise in a given frequency band is emitted from only one specific region of the rocket plume. Additionally, as was pointed out in Sec. III C, an erroneous plot was used in DSM-1 for obtaining the total power emitted by each slice of the plume. On the other hand, DSM-2 divides the jet exhaust into slices and assumes a distribution for W along the rocket plume as a function of an empirically determined characteristic reference length. Unlike DSM-1, each DSM-2 slice is assumed to generate sound across the entire range of the observed frequencies, and a sound power spectral shape is assigned empirically for each source. Although DSM-2 might seem more physically realistic, James *et al.* (2014a) reported (see their Fig. 10) that at $\mathrm{Sr} = 0.025$, the source of the rocket noise is estimated to be around 50 D_e, for which there is no experimental justification (see the discussion regarding Fig. 15 in Sec. III C 3).

c. Characteristic length. DSM-2 relies on the use of an aerodynamic reference dimension to distribute the sound power along the length of the flow. In SP-8072, this was defined as the length of the plume's potential core region, L_C, and obtained based on Lighthill's subsonic jet studies (Lighthill, 1962) and the supersonic work of Anderson and Johns (1955). The uncertainty around the rocket plume core lengths has already been noted in Sec. III C 2. In an attempt to improve the model predictions, Varnier (2001) proposed a modified core length, which has been used in later models (see Sec. VI A 2). For further discussion of the core lengths, including a comparison of the lengths from various models, see McInerny (1990, 1992b) and Baars *et al.* (2014).

d. Directivity index. The sound power level spectra previously obtained are used to calculate the associated SPL spectra. This calculation includes the use of an empirically determined, frequency-dependent directivity index, $\mathrm{DI}(f, \theta)$, which is used to adjust the shape of the sound pressure spectra to compensate for the incorrect assumption, inherent in NASA SP-8072, that the acoustic sources radiate incoherently. The OAPSL at any point on or around the launch vehicle is then calculated from the logarithmic summation of all of the contributions. As noted previously, any inaccuracies in the OAPWL spectra will be amplified in the OASPL spectra (Sec. III D 2).

In 2007, new directivity indices were produced by Plotkin and Sutherland for undeflected flow (Plotkin *et al.*, 2009). Although they followed the general trend of Eldred's data, they suggested even shallower radiation angles than those proposed by Eldred (Smith, 2013). Given the likely disconnect with the rocket plume convective Mach numbers, they are not discussed further. Alternative directivity indices were also considered by Smith (2013).

Far-field acoustic data collected on three horizontal static tests of the RSRM (Kenny *et al.*, 2009) were used to develop updated directivity indices (Haynes and Kenny, 2009), and these were improved upon by James *et al.* (2014b) as described in Sec. III D 2. Although these are probably the most appropriate directivity indices developed to date, in general, the accuracy of using $DI(f, \theta)$ is questionable due to the many unrealistic assumptions made, including linear propagation and neglect of ground-reflection effects. Ideally, the rocket plume directivity should be an integral part of any future model rather than an "add on" correction.

e. Impingement modeling. One of the biggest differences between the two SP-8072 source allocation methods is their treatment of the sound source distribution after the core impingement. Although Eldred provides empirical source distribution curves for plumes deflected through an open scoop and into a closed bucket, DSM-1 merely modifies the acoustic efficiency in the case of the plume impingement by relocating the sound sources much closer to the nozzle exit. In an alternative approach, DSM-2 ignores the effect of a deflector on the sound source location altogether, instead, merely redirecting them. However, this assumed smooth plume deflection described in Sec. IV A seems unlikely to be realistic in practice. Neither DSM-1 nor DSM-2 accurately captures the associated physics. Haynes and Kenny (2009) proposed an alternative impingement model in which a shortened potential core, which terminated on deflection, was used. In this approach, the acoustic sources were moved appreciably closer to the vehicle. Although Haynes and Kenny's modifications improved the agreement between their model and the experimental data, their physical meaning is unclear, and their methodology is neither systematic nor generalizable, which is a necessity for any proposed modeling framework. Section IV has indicated that correct modeling of the deflected plumes requires a thorough understanding of the frequency, source power, and directivity of each of the acoustic sources shown in Fig. 20.

2. NASA SP-8072 derivatives

Despite the shortcomings discussed in detail in this and previous sections (Secs. III C 1, III D 2, III D 3, IV A, VI A 1), the SP-8072 methodology has proved to be valuable in that it has been a common motivation for much of the subsequent work with multiple new datasets and corrections having been created to augment the SP-8072 modeling framework (Li, 2012). Revisions have focused on

https://doi.org/10.1121/10.0009160

identifying the dominant rocket plume noise source region, improving the estimate of the potential core length, updating the directivity indices, including the effects of core termination, and accounting for factors not included in the original model, such as the launch pad structure (e.g., Ranow, 2021). For example, Campos (2005) applied the methodology to assess the effects of a missile launch on the launcher and its environs, whereas Fukuda *et al.* (2009) developed a computational fluid dynamics (CFD) model and a model based on SP-8072 and used data obtained from two static firings of a solid rocket motor to compare the results. Although the CFD yielded the better of the two predictions, there were very large errors (>10 dB) in both cases. The scalar pressure measurements yield a reasonable agreement between the Orion-50S XLG data and both of the SP-8072 source allocation methods for the undeflected plumes (James *et al.*, 2014a). However, developing these comparisons prompted significant questions regarding the underlying physics of the two methods DSM-1 and DSM-2. Varnier (2001) compared results from an acoustic simulation model based on the characteristic length relationship suggested in SP-8072 with measured data from a static reduced-scale rocket and proposed a modified core length. Varnier's alternative length formed the basis of many subsequent models. For example, Casalino *et al.* (2009) used Varnier's core length to create an 8072-CFD/computational aeroacoustics (CAA) hybrid model to include reflections from the launch pad environment. Comparison of this model with data from a scale model of the VEGA launch vehicle yielded a reasonably good agreement. However, recent work by James *et al.* (2016) indicates that Varnier's rejection of Eldred's core length and suggestion of an amended definition was likely drawn from the limited extent of his measured data. Varnier may have been also influenced by adopting the erroneous sound power distribution curve described in Sec. III C 2 that places the acoustic sources farther downstream, in the subsonic flow.

To predict the launch noise on the support structures, Plotkin *et al.* (2009) employed a traditional NASA SP-8072 model, which was modified to include a reduced core length and an alternative plume parameter-dependent relation for η. They used more recent data and updated the model to take into account the launch pad and deflector geometry, including the shielding. Meanwhile, Kumar and Karthikeyan (2013) developed an amended empirical model, which included the water injection effects and the deflector's three-dimensional (3D) nature in the prediction of the noise levels on the entire launch vehicle. A more recent extension to SP-8072 (Park *et al.*, 2017; Park, 2019) developed novel methods for considering physical phenomena not included in the original model such as diffraction, reflection, and the addition of an impingement source. Effects that should be accounted for in the future models include vehicle drift and scattering. Although methods based on the modifications to NASA SP-8072 improve the agreement between modeling and experimental results for a given scenario, this is mostly the result of *ad hoc* empirical corrections, which are, generally, neither systematic nor easily transferable to other situations.

The preceding discussion clearly indicates that it is no longer appropriate to use NASA SP-8072 as the basis for predictions of the acoustic environment generated at launch and developing a new model is essential. This model should encapsulate the essential physics of the process, including the Mach waves, large-scale structure and fine-scale noise emission, and plume impingement. It must accurately capture the spectral levels, shapes, and spatial correlation properties and be able to incorporate the type of modifications necessary to realistically model an actual physical launch situation. Thorough and detailed experiments using cutting-edge technology (Sec. VI B) together with advanced numerical simulations using high-performance computing (Sec. VI C) can be used in the development of such models (Sec. VI D).

3. Other models

The traditional NASA SP-8072 distributed source models and their derivatives all make assumptions about the acoustic sources, and predictions based on these assumptions, with relatively little input regarding the rocket parameters. An alternative approach to rocket noise modeling is to predict the jet noise more directly from the design features of the rocket itself by first developing an aerodynamic model of the jet flow and then relating this model to the associated acoustic characteristics. For example, Koudriavtsev *et al.* (2004) attempted to develop a new core length that incorporated the jet temperature and other thermodynamic data for cold and heated supersonic jets. This physics-based core length was then plugged into the predictive approach of Varnier (2001). However, this substitution produced relatively poor agreement with experimental data (see Fig. 11, Koudriavtsev *et al.*, 2004), further supporting the assertion made in Sec. VI A 2 that *ad hoc*, piecemeal adjustments to NASA SP-8072 do not represent the future of rocket launch noise modeling.

An alternative model for predicting the far-field acoustic environment created by a rocket launch, which incorporates the concepts from Eldred (1971) and Tam *et al.* (1996), was developed by Kenny and Giacomoni (2014). They assumed a "directional" source, dominant at $\theta < 80°$, and a "broadband" source, which was dominant at $\theta \geq 80°$, and used five sets of horizontally fired rocket data (three solid and two liquid propellants) to fit the new similarity curves to Tam's two-source model with Strouhal number frequency scaling. Using the SP-8072 method of calculating the acoustic power, the sound power level was modified for the two sources based on the vehicle parameters and combined with the previously obtained similarity spectra to yield predicted spectra. Comparison of these with experimental results for the five rocket motors studied indicated a reasonable agreement between the two—generally, within 5% and 5 dB for $30° \leq \theta \leq 160°$. However, the authors note that the model, which is not obviously generalizable, has not yet been applied to other rockets and future models should

incorporate a combination of the CFD and propagation methods for modeling the far-field acoustics. They also state that "…*liquid and solid motors exhibit similar spectra at similar amplitudes*," although agreement between the predictions and actual data is not as good for rockets using a liquid propellant, indicating that the same model may not be appropriate for both types of rockets.

B. Subscale rocket testing

The early days of supersonic jet and rocket noise research—driven by the commencement of the Space Race (1955–1975), including the Apollo programs of the 1960s—were typified by a decade of significant experimental programs aimed at a better understanding and characterization of the aeroacoustic noise sources present in such flows. In particular, several sets of full-scale rocket noise experiments were conducted under static and launch conditions (Cole *et al.*, 1957; Humphrey, 1957; Mayes *et al.*, 1959; Tedrick, 1964), and these results formed the cornerstone of much of the subsequent empirical analysis (Potter and Crocker, 1966; Eldred, 1971). To facilitate this work, Sutherland (1968) provided an excellent and extremely comprehensive summary of the state of knowledge concerning the acoustic and vibration environment related to large launch vehicles. Although there have been a small number of full-scale experiments in the intervening decades—including on the Space Shuttle, Ariane 5, ATK's RSRM, Antares, and VEGA—most modern testing has been at subscale because of the difficulties inherent in conducting full-scale rocket launch noise experiments, together with the lack of economic viability of such tests.

Bies and Franken (1961) helped provide the foundation for subscale testing criteria. They asserted that a rocket engine and its small-scale model are examples of dynamically similar systems provided that the pressure fluctuation amplitudes at the scaled positions are the same and the spectra are the same when the frequency is scaled by a characteristic length (Giacomoni and Kenny, 2014). Significant progress in acoustical instrumentation capabilities over the last half-century—together with development of such advanced techniques as near-field vector intensity and acoustic beamforming—has meant that empirical results can sometimes outstrip modeling, especially if the latter is based on NASA SP-8072. In fact, SP-8072, itself, stated that full- or subscale test programs could give "…*a more accurate prediction* [of acoustic loading] *than that obtained through empirical analysis.*"

The time required to develop a full-scale prototype rocket engine and vehicle for testing means that launch vehicle design, in particular, is heavily reliant on scale model testing (Sarae *et al.*, 2016). In addition, subscale testing can be especially useful for examining nozzle configurations, deflectors, and/or shrouds, which are significantly different from normal practice. These types of tests can also be used to yield results that cannot be obtained by any other means, such as to simulate and understand the effects of atmospheric conditions that are which are significantly different from those existing on the Earth's surface (Eldred, 1971), or estimate the spatial correlation functions on a launch vehicle. Figure 28 shows a full-scale Ares I at the Kennedy Space Center, together with a 1/20 scale model of the Ares I undergoing tests to verify the predicted liftoff acoustic environment and evaluate the water suppression system (Counter and Houston, 2011, 2012).

Nesman (2017) provides an excellent chronological overview of the major subscale test campaigns conducted, including from the Apollo era. He clearly illustrates the different configurations tested and the associated knowledge obtained from the test. Although by no means exhaustive, Table II outlines some of the subscale experimental work conducted on different launch vehicles over the past two decades.

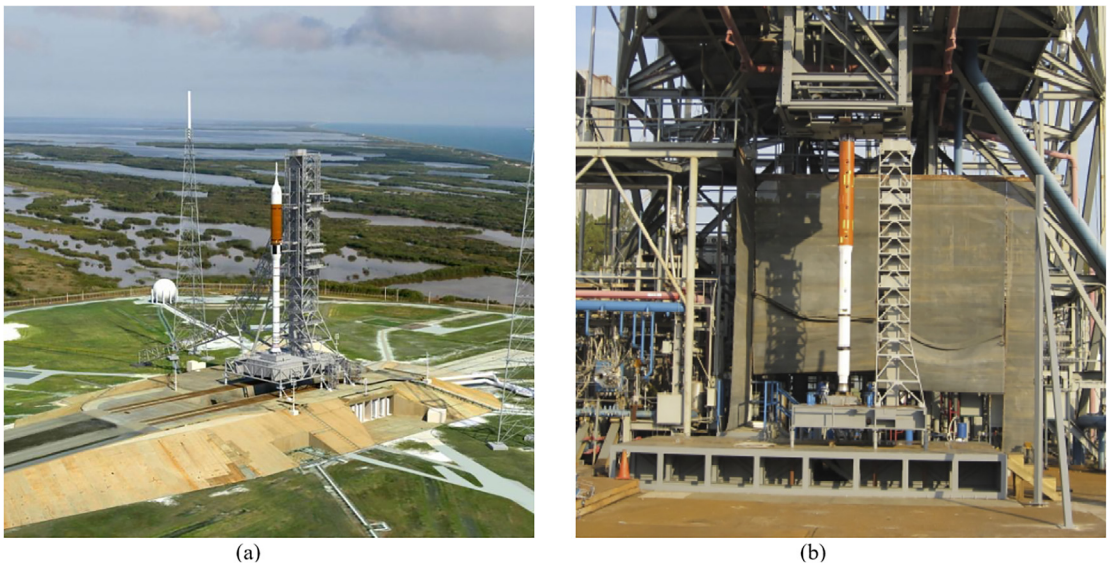

(a) (b)

FIG. 28. (Color online) The (a) full-scale Ares I on the launch pad at Kennedy Space Center and (b) 1/20 scale model Ares I undergoing subscale tests are shown.

https://doi.org/10.1121/10.0009160

TABLE II. Examples of recent subscale launch vehicle experimental work.

Launch vehicle	Scale	Aim (M = mitigation, Q = quantification)	Reference
VEGA	1/33	Optimize launch pad configuration (M)	Gely *et al.* (2005)
	1/20	Determine actual acoustic field induced on a launcher at liftoff by stage I engine (Q)	Gely *et al.* (2005)
	1/20	Analyse acoustic load on surface of launch vehicle (Q)	Casalino *et al.* (2012)
Orion		Quantify internal vibration response of vehicles and components to acoustic environment (Q)	Houston (2016)
Ariane 5	1/20	Characterize fairing acoustic loads at liftoff (Q)	Varnier *et al.* (1996)
	1/47	Optimize existing water injection devices (M)	Gely *et al.* (2000)
	1/47	Optimize launch pad geometry (M)	Gely *et al.* (2000)
	1/20	Characterize the acoustic environment at liftoff (Q)	Troclet *et al.* (1995)
	1/20	Check the efficiency of the water suppression system (M)	Troclet *et al.* (1995)
Ariane 6	1/40	Localization of noise sources on the launch pad (Q)	Malbequi *et al.* (2017)
Ares I	1/20	Verify the predicted liftoff acoustic environment (Q)	Counter and Houston (2012)
	1/20	Test the above-deck water supply system (M)	Counter and Houston (2012)
SLS	1/20	Verify the predicted liftoff acoustic environment (Q)	Houston *et al.* (2015)
	1/20	Test the above-deck water supply system (M)	Houston *et al.* (2015)
Space Shuttle	∼1/15	Optimize the launch pad noise suppression techniques (M)	Guest and Jones (1976)
	∼1/15	Correlate the 1970s scale model work with the actual Shuttle data (Q)	Dougherty and Guest (1984)
Indian launch system	1/100	Investigate aeroacoustic environment (Q)—hot jet	Ignatius *et al.* (2015)
	1/100	Test water supply techniques for the acoustic suppression system (M)—hot jet	Ignatius *et al.* (2015)
Epsilon	1/42	Launch pad design optimization (M)	Tsutsumi *et al.* (2015a,b)
H3	1/42	Launch pad design optimization (M) and characterize the acoustic environment at liftoff (Q)	Sarae *et al.* (2016)

As stated previously, scale models are often used to predict the acoustic environment associated with launch vehicles as a result of the obvious advantages they offer, including reduced cost and test times and fewer safety issues. To be able to be used to make predictions, however, the model experiments need to exhibit complete similarity with the full-scale tests in terms of the flow, noise generation, and noise propagation. However, many subscale model tests are not performed on high-speed hot jet flows that typify, which typify rockets, and, thus, their utility for deducing full-scale results from subscale model testing is called into question. To address this, Kandula (2008b) executed a detailed review of previous experimental and theoretical work on heated jets, which led him to develop refinements to the existing jet noise scaling laws. He proposed a single generalized semi-empirical similarity spectrum, which includes a factor representing the physical effects of convective Mach number, M_C, and the receiver angle, θ, on the directivity factor and similarity spectrum. This spectrum is entirely different from, but bounded by, the fine-scale and large-scale spectra of Tam *et al.* (1996). Predictions for the overall sound power levels, directivity, and similarity spectra agreed reasonably well with the data.

It should be noted that there is a large body of laboratory-scale experimental work on supersonic jets. However, most of these studies use cold jets because of the increased cost and complexity of heated jet experimental facilities. According to Kandula and Vu (2013), cold supersonic jets are useful for indicating order-of-magnitude changes in the noise radiated for different configurations. As the temperature plays such a significant role in the difference between behaviors observed for the supersonic jets and rocket plumes, such experiments are outside the scope of this review, aside from those related to the physics of plume impingement already described in Sec. IV.

C. Numerical methods

The empirical and experimental methods described in Secs. VI A and VI B have previously been used to design launch pads and predict acoustic environments. Recently, thanks to progress in the CFD technology represented by LES and the performance improvement of supercomputers, the acoustical design of launch pads has begun to be performed numerically. In this section, real-life examples of the use of numerical analyses for the development of launch pads, as well as related research issues, are discussed.

The use of a LES to solve the jet aeroacoustics problems began around the 2000s (Bodony and Lele, 2008) and is currently widely applied (Lyrintzis and Coderoni, 2020). Although most of the numerical studies on heated supersonic jet noise focus on aircraft engines, numerical analysis as part of practical launch vehicle research has also been performed recently, including on the VEGA launch vehicle by Casalino *et al.* (2009), Barbarino *et al.* (2017), and Palmieri *et al.* (2017), the SLS by Harris *et al.* (2015) and Harris *et al.* (2016), the Ares I by Liever *et al.* (2017), the H-IIA, M-V, Epsilon, and H-3 by Tsutsumi *et al.* (2008a), Tsutsumi *et al.* (2008b), Tsutsumi *et al.* (2015b), and Tsutsumi *et al.* (2019), and on a launch vehicle with 20 liquid-propellant rocket engines by Xing *et al.* (2020). However, numerical analyses of rocket noise are still limited in comparison with those on aircraft because there are major differences between the two (described below), which still present a significant challenge for numerical study of the latter.

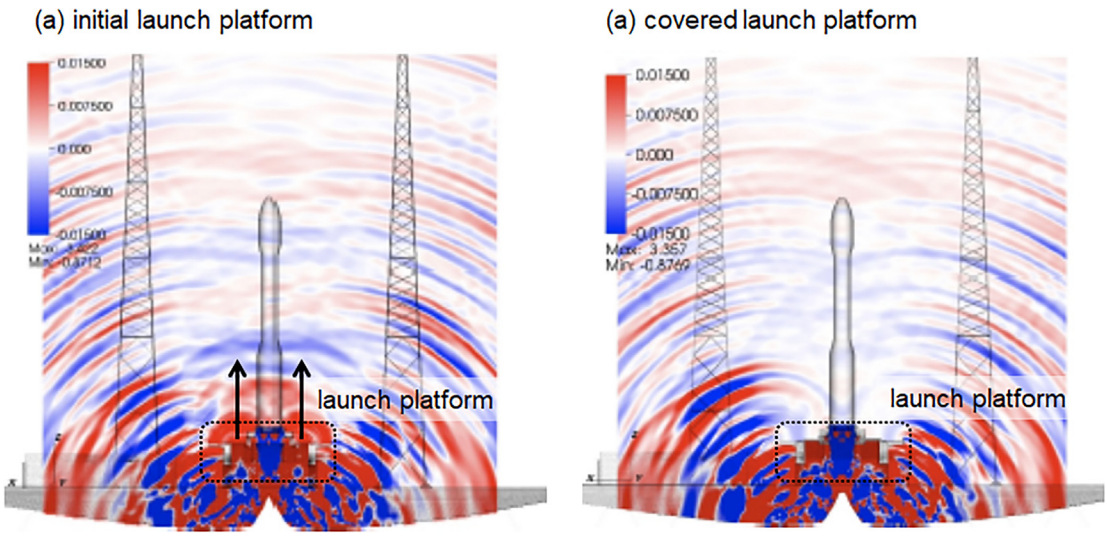

FIG. 29. (Color online) The numerical results from the VEGA launch vehicle CFD (Palmieri *et al.*, 2017).

As described in Sec. II B, the exhaust velocity and temperature of a rocket plume are much higher than those of an aircraft engine exhaust. A plume is in the overexpanded condition at liftoff and contains barrel shock waves. Additionally, plumes interact with the launch pad structures, resulting in more shock waves appearing, such as plate and tail shocks. A high-resolution numerical method is desirable to properly resolve the turbulent jet shear layer—a source of acoustics—but at the same time, it is also necessary to capture such shock waves (Fujii *et al.*, 2010). For example, the numerical method used in Palmieri *et al.* (2017) for the VEGA launch vehicle, shown in Fig. 29, employed a fifth-order accurate shock-capturing weighted essentially non-oscillatory scheme for the space discretization (Kiris *et al.*, 2016). For the Epsilon (Fig. 30) and H3 launch vehicles, Tsutsumi *et al.* (2015b) and Tsutsumi *et al.* (2019) employed a sixth-order compact difference scheme (Kobayashi, 1999) for the smooth region, which is replaced with a second-order scheme for the non-smooth region where the shock waves appear. Harris *et al.* (2015), Harris *et al.* (2016), and Liever *et al.* (2017), on the other hand, employed a high-order accurate unstructured mesh discontinuous Galerkin method for space discretization in the CAA research related to the SLS. Recently, Brès and Lele (2019) developed a compressible LES solver in which a low-dissipation numerical method was used with an unstructured mesh generated based on the Voronoi diagrams to perform computations for heated overexpanded supersonic jets at military conditions with afterburners. The turbulent boundary layer on the nozzle wall was accurately simulated with a realistic number of meshes by using the wall modeling approach. In this way, a jet noise prediction with high accuracy was possible. The study by Brès and Lele (2019) contains important information for analyzing launch vehicle acoustics with high accuracy. It should be noted that, resulting from the complexity of many real-world CFD problems, the empirical method described in Sec. VI A is sometimes still considered an attractive alternative. For example, Casalino *et al.* (2009) and Barbarino *et al.* (2017) used this approach to model the VEGA launch environment.

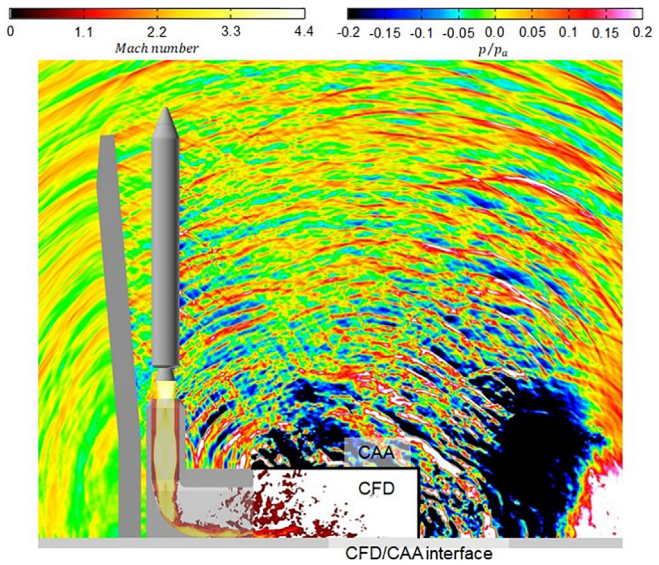

FIG. 30. (Color online) The numerical results from the Epsilon launch vehicle CFD and CAA (Tsutsumi *et al.*, 2015b).

Because gas compositions of plumes from liquid-propellant and solid-propellant rocket engines are different from the ambient air, high-fidelity numerical simulation method must consider the multi-gas compositions. Thus, Palmieri *et al.* (2017), Liever *et al.* (2017), Tsutsumi *et al.* (2019), and Xing *et al.* (2020) all employed the multi-species 3D Navier-Stokes equations, although chemical reactions were not taken into account. Instead, a frozen flow was assumed.

As discussed in Sec. IV, the interaction of the rocket plume with the launch pad structures, such as the deflectors, generates acoustic waves. As the flow structure formed on the deflector is related to the acoustic generation, numerical methods are required to analyze the turbulent boundary layer on the walls of the launch pad structures as well as in

the shear layer of the plume. However, application of wall-resolved LES is still impractical due to its computational cost. To simulate the turbulent boundary layer on the walls of the launch pad structures, Xing *et al.* (2020) employed a scale-adaptive simulation (Menter and Egorov, 2010), and Liever *et al.* (2017), Tsutsumi *et al.* (2015b), and Tsutsumi *et al.* (2019) employed a hybrid of the Reynolds-averaged Navier-Stokes (RANS) and LES methods. In an alternative approach, in the study by Palmieri *et al.* (2017), the immersed boundary method (Kiris *et al.*, 2016)—previously validated by Brehm *et al.* (2016)—was used.

For any analysis of the acoustic waves propagating into a large space containing a launch vehicle and launch pad, the effects of the reflection and diffraction should be taken into account. In particular, it is known that the acoustic waves from plumes undergo nonlinear propagation features (McInerny, 1996b; Muhlestein *et al.*, 2012). Thus, although CAA methods based on the linear assumptions are often used in jet noise simulation, the nonlinear propagation effects should be properly computed in the case of rockets (Cacqueray *et al.*, 2011; Langenais *et al.*, 2019). Consequently, Harris *et al.* (2015), Harris *et al.* (2016), Liever *et al.* (2017), Tsutsumi *et al.* (2015b), and Tsutsumi *et al.* (2019) employed the full Euler equations for the CAA, and the computation was conducted by one-way coupling between the CFD and CAA. In the results of the work on the Epsilon launch vehicle shown in Fig. 30, CFD was used to compute the plume deflected by the deflector and flowing downstream in the flame duct, and CAA was used to compute the acoustic wave propagating from the flame duct to the launch vehicle. The boundary between the CFD and CAA was located downstream of the flame duct. Palmieri *et al.* (2017), on the other hand, did not employ CAA but calculated the hydrodynamic and acoustic fields using CFD alone. In this study, the effect of the launch platform configuration on the acoustic level of the VEGA launch vehicle was investigated as shown in Fig. 29. Langenais *et al.*, 2018; 2019; 2021 have recently developed a two-way coupling method for rocket noise simulation to include the acoustic feedback on the flow field, and it is expected that this technique will soon be applied to practical rockets.

As discussed in Sec. V B, almost all of the launch pads used for heavy rockets employ water injection for acoustic mitigation. Because the effect of water injection on the acoustic field is significant, modeling of the water injection is essential for the quantitative prediction of rocket noise. West *et al.* (2012), Vu *et al.* (2014), Zhou *et al.* (2020), and Lu *et al.* (2021) performed numerical analyses for investigating the flow field emitted by the water injection systems, whereas Canabal and Frendi (2006) and Osipov *et al.* (2015) developed CFD techniques to analyze the effect of water injection on the mitigation of the IOP, which appears at the startup of the rocket engines. However, numerical simulations of the interaction between the broadband turbulent mixing noise and injected water have only been conducted to date by Salehian and Mankbadi (2020), and the computation of such an interaction is still an emerging technology with further study necessary.

D. ROMs

Because of the complexity of extracting the physics of the jet noise radiation from the turbulent plume, the development of ROMs has been pursued. These ROMs can be classified into data-driven and model-based ROMs. Data-driven ROMs are inductively developed based on experimental or numerical data. Model-based ROMs are deductively developed based on first principles or theory. Because the jet noise ROMs suggest a promising, computationally efficient modeling approach to rocket noise, some approaches in both categories are briefly reviewed here.

NASA SP-8072 is an example of a data-driven ROM developed from early measurements, but as discussed in this article, there are issues in the modeling of the acoustic generation mechanisms for free and impinging plumes, which result in inaccurate predictions. The recent data-driven ROMs have used acoustic arrays to extract the parameters for the assumed source or wave-field models, which are described in terms of wavepackets (see a review by Jordan and Colonius, 2013). In addition to acoustic field-derived ROMs for laboratory-scale jet noise developed using a variety of methods (e.g., Morris, 2009; Reba *et al.*, 2010; Suzuki, 2013; Sinha *et al.*, 2014; Neilsen *et al.*, 2019b; Pedersen *et al.*, 2020), ROMs based on advanced beamforming (Harker *et al.*, 2017; Harker, 2017) and holography (Wall *et al.*, 2018) have been applied to full-scale, installed tactical engines to obtain analytical equivalent acoustical wavepacket models as a function of frequency. An example from Wall *et al.* (2018) is shown in Fig. 31, where the acoustical holography-derived source partial fields were fit to analytical wavepacket functions. The fit is particularly good for the lower-order partial fields [PFs; see PF 1 and PF 2 versus PF 6 in Fig. 31(a)]. Figure 31(b) shows that because the data-derived axial source coherence lengths become much shorter than the source region for the pressure amplitude, an increasing number of wavepackets is required to represent the radiated field and its spatial coherence function. This modeling framework could be applied to the spatially dense measurements in the radiated rocket noise near field or numerical databases from high-fidelity LES.

Unsupervised techniques, such as dynamic mode decomposition (Taira *et al.*, 2017; Taira *et al.*, 2020) and spectral POD (e.g., Schmidt *et al.*, 2018, Towne *et al.*, 2018), are widely used to identify the physically relevant wavepackets from turbulent jets. These techniques are also promising candidates for developing data-driven ROMs.

Physics-based approaches to extracting features of turbulent jets are also being developed for model-based ROMs for supersonic jet noise. Two such ROMs are related to resolvent analysis and momentum potential theory (MPT). Recently, resolvent analysis has attracted attention for revealing the causal relationships in turbulent flow fields. In resolvent analysis (McKeon and Sharma, 2010; Yeh and Taira, 2019), a resolvent operator is obtained from the

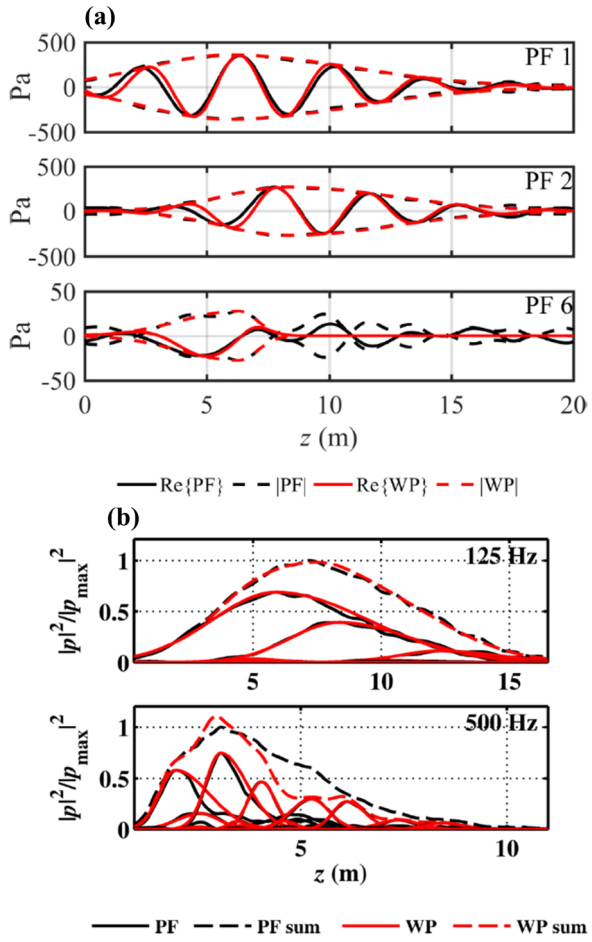

FIG. 31. (Color online) The (a) real part of three orthogonal source-related PFs and their analytical wavepacket (WP) fits for an installed tactical engine at a frequency of 125 Hz and military power and (b) normalized squared pressure amplitudes and intensity summation of the PFs and WPs as a function of the distance downstream of the nozzle. Adapted from Wall *et al.*, J. Acoust. Soc. Am. **144**, 1356 (2018).

linearized Navier-Stokes equations, and then singular value decomposition is used to decompose the resolvent operator. The eigenvectors (forcing and response modes) corresponding to the largest eigenvalue (resolvent gain) show the most dominant amplification mechanisms at each frequency. Because resolvent analysis identifies the most relevant flow features for generating jet noise in a turbulent jet, a great deal of research is currently being conducted in this area (Jeun *et al.*, 2016; Schmidt *et al.*, 2018; Towne *et al.*, 2018; Pickering *et al.*, 2021). The MPT of Doak (1989) is a physics-based decomposition in which the hydrodynamic, acoustic, and entropic components are identified through a Helmholtz decomposition of the "momentum density." Unnikrishnan and Gaitonde (2016) applied the MPT to a supersonic jet, and in 2020 [Unnikrishnan and Gaitonde (2020)], they extended the MPT to directly decompose the jet's pressure fluctuations into the turbulent jets into the three-momentum density components. Goparaju *et al.* (2018) have also used MPT to examine acoustic shielding by supersonic, twin jets, demonstrating the technique's versatility. Finally, recent developments based on the generalized acoustic analogy (Goldstein, 2011) are worth mentioning as candidate for a model-based ROM. Afsar *et al.* (2019) employed the generalized acoustic analogy based on RANS simulation, and successfully predicted and explained the temperature effect in heated supersonic jets at a fixed M_a. A similar approach is also employed for the prediction of supersonic jet noise (e.g., Morris and Farassat, 2002; Leib and Goldstein, 2011). These approaches have been demonstrated only in free jets, but the advantage in terms of computational cost is large, because these approaches employ mean flow results obtained from the RANS simulation. Further efforts to extend these approaches for model-based ROMs are expected in the future. It should be noted that before applying data-driven approaches, it is desirable to extract as many features (such as the hydrodynamic and acoustic components) as possible based on the physical laws (model-based approach). Although none of these methods—data-driven or model-based—have yet been applied to the rocket plume ROM, they represent the current state-of-the-art and are promising candidates for developing a more physical model of rocket noise.

VII. SUMMARY AND CONCLUSIONS

Fifty years have passed since the semi-empirical modeling framework to predict launch vehicle noise was developed and published as NASA SP-8072. SP-8072 approached rocket noise modeling in a way that was tractable in the 1960s and because of its relative simplicity and the lack of fully developed alternatives, remains the foundation for much of the launch vehicle noise modeling today. This article has reviewed what has been learned about highly heated, supersonic rocket plumes since SP-8072, including the physics of noise radiation from undeflected and deflected plumes, noise mitigation, and modeling. In the process, we have tried to illustrate the need for more physical models for rocket noise with greater transferability.

Despite the progress made by an increasingly global launch vehicle noise community in recent years, many fundamental, unresolved questions remain that are key to developing a more physics-guided modeling framework. For example, Sec. III has described how little we still know regarding the essential physics of the noise generation from free rocket plumes, including its sound power distribution, spectral characteristics, and spatial correlation properties, and their connection to other heated, supersonic jets. Additionally, whereas Sec. IV has described the evidence of several noise sources in laboratory-scale supersonic jets impinging on inclined flat plates, the sound power and spatiospectral characteristics of the noise from each source have not yet been clarified. And similarly to free rocket plumes and their connection to other jets, the correlation between laboratory-scale jets impinging on plates and highly heated, supersonic rocket plumes impinging on practical deflectors is not well established. Regarding launch pad noise mitigation, although viable methods have been developed for practical launch scenarios, it is unclear if a given mitigation technique developed for a specific launch vehicle

and pad configuration is applicable elsewhere. Fundamental research on generic flame deflectors, flame ducts, launch platforms, and water injection systems is necessary to derive a general understanding of noise mitigation that is relevant to all launch vehicles. State-of-the-art near-field measurements and high-fidelity CFD with data analysis techniques play an important role in resolving these outstanding questions and in the development of a reduced-order modeling framework that moves beyond SP-8072's limitations and inaccuracies.

This review article's publication coincides with an exciting period in the six-plus decades of the launch vehicle noise timeline. As numerous commercial and government-sponsored vehicles are being developed and launched around the world for myriad purposes, including satellite deployment, space tourism, the Artemis program, and eventual travel to Mars, a renewed focus on the study of launch vehicle noise will ensure payload and vehicle integrity and astronaut safety. More broadly and despite considerable 1950s and 1960s efforts in this area, an improved understanding of noise generation from rocket plumes will hopefully lead to scaling laws for heated jet noise across a greater range of velocities and temperatures and expansion ratios. The pursuit of more universal jet noise scaling models, which span laboratory, aircraft, and rocket scales and conditions, will result in a greater collaboration, coordination, and overall convergence across the supersonic jet noise-related communities with, at present, divergent thrusts.

ACKNOWLEDGMENTS

The idea for this review article stemmed from a decade's worth of special sessions on launch vehicle acoustics and supersonic jet noise at the Acoustical Society of America meetings and other conferences. We gratefully acknowledge those researchers from the global launch vehicle noise community who have supported and contributed new knowledge to these special sessions. Dr. Jeremy Kenny (NASA), Janice Houston (NASA), and Dr. Alan Wall (AFRL) helped organize and chair these sessions. We also thank Michael James (Blue Ridge Research and Consulting, LLC) and Dr. Hadrien Lambaré (CNES), who contributed to the review's initial development. We are extremely grateful to the reviewers, whose diligent, thorough review and thoughtful and insightful comments significantly improved this article. Finally, we are especially grateful to Dr. Sally Anne McInerny, whose measurements, analyses, and physical insights related to rocket noise constituted the bulk of new knowledge produced for the span of nearly two decades. For her willingness to pursue and perservere in a relatively solitary area of research, we thank her.

APPENDIX A

This appendix summarizes rocket noise-related topics that are not reviewed in depth. Although certainly not complete, several references spanning the early and recent literarature are provided.

1. VAL

Analysis of VAL is important during design to ensure that the vehicle and payload mechanical and electrical components function normally in the harsh acoustical environment (e.g., Himelblau *et al.*, 1970; Archer, 1970). VAL analysis is performed using acoustic tests (e.g., Gibson *et al.*, 2004; Lane *et al.*, 2007) or numerical simulations using finite-element (e.g., Hipol, 1989), boundary-element, or statistical energy analysis methods (e.g., Conlon and Hambric, 2003; Ferrara *et al.*, 2007) or some hybrid (e.g., Troclet *et al.*, 2009; Djojodihardjo, 2015; Pirk and Souto, 2015), depending on the frequency. Vibroacoustic analysis is not limited to the vehicle and payload (Yunis, 2013). To control vibration levels on launch pad structures, the dynamic characteristics of the structure need to be thoroughly understood, and experimental modal analysis and numerical methods have been employed (Margasahayam and Caimi, 1997; Margasahayam *et al.*, 2002; Caimi and Margasahayam, 1997; Caimi *et al.*, 2001).

2. IOP

The ignition of the rockets can create an intense blast-like wave, called the IOP, with an amplitude on the order of 10 kPa at the launch complex (e.g., Walsh and Hartt, 1982). The IOP analysis is conducted using analytical methods (Ikawa and Laspesat, 1985), subscale and full-scale measurements (Troclet *et al.*, 2007), and CFD techniques (e.g., Ravish *et al.*, 2000; Engblom *et al.*, 2001; Kiris *et al.*, 2008; Troyes *et al.*, 2009; West *et al.*, 2012; Dargaud *et al.*, 2014; Nance and Liever, 2015). On ignition, the plume expands rapidly, and a compression wave forms at the plume tip and propagates. Subsequently, a vortex ring forms in the plume, causing a propagating rarefaction and completion of the IOP blast wave. Due to its high intensity, the IOP is an important design issue in the development of a launch pad and launch vehicle. However, because the IOP generation mechanism is different from that of the broadband turbulent mixing noise, the IOP is only briefly discussed in this article.

3. Environmental issues

As the number of rocket launches increases and more spaceports are being developed (some as dual-use airports), urban encroachment, community-noise, and other environmental issues must be assessed. Launch noise, reentry noise and sonic boom, and static operations need to be considered. Tools are being developed to examine launch vehicle jet noise and reentry booms (e.g., James and Salton, 2017; Tran *et al.*, 2018; Bradley *et al.*, 2018; Lonzaga, 2019).

4. Advanced experimental techniques/measurement system design

Advanced experimental techniques, such as acoustic intensity measurements, acoustic holography, and acoustic beamforming (e.g., Gee *et al.*, 2016b; Wall *et al.*, 2016; Leete, 2021a; Panda *et al.*, 2014; Ishii *et al.*, 2016; Mortain

et al., 2019), are used in the acquisition of rocket launch noise data. However, this review focuses on the results of such experiments rather than the methods used to achieve these results. Measurement system design is also beyond the scope of this review, and examples of the measurement protocols used recently to collect data for Falcon 9, Falcon Heavy, Antares 230, and Delta IV Heavy, including the acoustic, operational, and meteorological measurements, can be found in James *et al.* (2020).

5. Infrasound

Rocket launches generate low-frequency infrasound (<20 Hz), and it is common to observe rocket launch infrasound tens or hundreds of kilometers away from the launch site. For example, a Saturn V launch on 9 November 1967 from Cape Kennedy, FL (now Cape Canaveral), generated low-frequency sound that was recorded nearly 1500 km away at the Lamont Geological Observatory in Palisades, NY. For further details on rocket noise infrasound, see Balachandran and Donn (1971a, 1971b), Donn *et al.* (1968), Kaschak *et al.* (1970), Olson (2012), and Blom *et al.* (2016).

6. Buffet loading

The buffet load on a launch vehicle arises from the pressure fluctuations caused by the shock wave/boundary layer interaction, the wake from the protuberances and/or the boattail of the vehicle, and the turbulent boundary layer (e.g., Rainey, 1965; Cole *et al.*, 1970; Cockburn and Robertson, 1974; Ericsson, 2001; Engblom, 2003; Camussi *et al.*, 2007; Piatak *et al.*, 2012; Piatak *et al.*, 2015; Pain *et al.*, 2014; Panda *et al.*, 2018).The low-frequency components of the buffet load—below 60 Hz—affect the bending modes of the launch vehicle, and the rest excites the launch vehicle and payload fairing as VAL (Piatak *et al.*, 2015).

APPENDIX B

In the rocket noise literature, there is some confusion related to whether the exit or fully expanded values are being used and/or should be used in models or in calculation of key quantities related to the noise radiation and characteristics. Additionally, it is sometimes hard to calculate the fully expanded values for a rocket plume because such calculations require inputs that are often not reported in the literature. Two fully expanded parameters of interest are M_j and D_j. What differences are there between these and the exit variables?

Because there are relatively few comparisons of the fully expanded versus exit variables in the rocket noise literature, outside of Varnier (2001), three examples are shown here: the Shuttle RSRM, a 1:42 scale model of the Epsilon solid fuel motor (Tsutsumi, 2015a; Ishii *et al.*, 2012), and the Shuttle RS-25 main engine. See Mathews *et al.* (2021) for an additional example from the Falcon 9's Merlin 1D engine. For the RSRM, $D_e = 3.80$ m and $M_e = 2.95$, based on an expansion ratio of 7.72 and $\gamma_e = 1.14$. Using the equations of Varnier (2001), $M_j/M_e = 1.04$ and $D_j/D_e = 1.10$, indicating a slight underexpansion at liftoff (see Fig. 7 and the accompanying discussion). For the overexpanded scale model Epsilon motor with $D_e = 42$ mm and $M_e = 3.7$, $M_j/M_e = 0.89$ and $D_j/D_e = 0.75$. The Shuttle and, now, SLS main engine (RS-25), which is notably overexpanded at sea level, have $D_e = 2.29$ m and $M_e = 4.7$, based on the parameters provided by McInerny (1992b). In terms of the fully expanded conditions, $D_j/D_e = 0.52$ and M_j/M_e=0.80. These latter two examples, for a solid motor and a liquid engine, illustrate appreciable differences between exit and fully expanded conditions. Care should be taken to understand which an author has used or intends to be used in the case of modeling. However, it should also be noted that there are multiple plume parameter estimation methods (e.g., equilibrium versus frozen flow; Sutton and Biblarz, 2000) and uncertainties associated with available rocket parameters, which further complicate the issue. There is not a satisfactory resolution at the present.

[1]See https://en.wikipedia.org/wiki/List_of_orbital_launch_systems (Last viewed 1/9/2022).
[2]See https://en.wikipedia.org/wiki/List_of_missions_to_the_Moon (Last viewed 1/9/2022).
[3]See https://en.wikipedia.org/wiki/List_of_missions_to_Mars (Last viewed 1/9/2022).
[4]Varnier (2001) makes essentially the same argument to arrive at a U^3 scaling but instead of neglecting the pressure difference term present in the thrust for non-ideally expanded plumes, he suggests using the fully expanded velocity, U_j. At present, it is unclear if one approach leads to a more accurate scaling for rockets.
[5]Potter and Crocker (1966) employed the total pressure at the throat instead of p_0 in the right-hand side of Eq. (3). However, assuming the flow is quasi-one-dimensional and frozen with a constant specific heat ratio (calorically perfect gas), the total pressure is the same at the throat and combustion chamber. Note that the total pressure varies along the nozzle, assuming a thermally perfect gas.
[6]McInerny (1992b) uses Potter and Crocker's version of the figure but repeats their error when discussing a simpler form of Eq. (3) by neglecting a square root symbol.
[7]See https://en.wikipedia.org/wiki/Timeline_of_spaceflight (Last viewed 1/9/2022).
[8]See https://www.youtube.com/watch?v=vFwqZ4qAUkE&list=RDCMUCLA_DiR1FfKNvjuUpBHmylQ&index=2 (Last viewed 1/9/2022).

Ahuja, K. K., Alvord, D., Mattingly, J., Mittelman, J., Schuttler, W., and Dickey, D. (**2014**). "Thoughts on use of university-scale rocket models to study launch acoustics," AIAA Paper 2014-3056.
Akamine, M., Nakanishi, Y., Okamoto, K., Teramoto, S., Okunuki, T., and Tsutsumi, S. (**2015**). "Acoustic phenomena from correctly expanded supersonic jet impinging on inclined plate," AIAA J. **53**(7), 2061–2067.
Akamine, M., Okamoto, K., Gee, K. L., Neilsen, B. T., Teramoto, S., Okunuki, T., and Tsutsumi, S. (**2018**). "Effect of nozzle–plate distance on acoustic phenomena from supersonic impinging jet," AIAA J. **56**(5), 1943–1952.
Akamine, M., Okamoto, K., Teramoto, S., and Tsutsumi, S. (**2021**). "Experimental study on effects of plate angle on acoustic waves from supersonic impinging jets," J. Acoust. Soc. Am. **150**, 1856–1865.
Allgood, D. C. (**2012**). "A brief historical survey of rocket testing induced acoustic environments at NASA SSC," Engineering Analysis Record 00294, NASA Doc. 20120003777, Washington, DC.
Allgood, D. C., Saunders, G. P., and Langford, L. A. (**2014**). "Reduction of altitude diffuser jet noise using water injection," NASA Technical Report SSTI-8080-0056, Washington, DC.
Anderson, A. R., and Johns, F. R. (**1955**). "Characteristics of free supersonic jet exhausting into quiescent air," Jet Propul. **25**(1), 13–15.
Archer, S. J. (**1970**). "Structural vibration prediction," NASA SP-8050, Washington, DC.

Arenas, J. P., and Margasahayam, R. (**2006**). "Noise and vibration of spacecraft structures," Ingenaire: Rev. Chil. Igenieria **14**(3), 251–328.
Afsar, M. Z., Sescu, A., and Sassanis, V. (**2019**). "Effect of non-parallel mean flow on the acoustic spectrum of heated supersonic jets: Explanation of 'jet quietening,' " Phys. Fluids **31**, 105107.
Baars, W. J., Tinney, C. E., Wochner, M. S., and Hamilton, M. F. (**2014**). "On cumulative nonlinear acoustic waveform distortions from high-speed jets," J. Fluid Mech. **749**, 331–366.
Bailly, C., and Fujii, K. (**2016**). "High-speed jet noise," Mech. Eng. Rev. **3**(1), 1–13.
Balachandran, N., and Donn, W. (**1971a**). "On the propagation of infrasound from rocket—Effect of the winds," J. Acoust. Soc. Am. **50**(2), 397–404.
Balachandran, N., and Donn, W. (**1971b**). "Characteristics of acoustic signals from rockets," Geophys. J. R. Astron. Soc. **26**, 135–148.
Barbarino, M., Adamo, F. P., Bianco, D., and Bartoccini, D. (**2017**). "Hybrid BEM/empirical approach for scattering of correlated sources in rocket noise prediction," J. Sound Vib. **403**, 90–103.
Bassett, M. S., Smith, J. R., Miller, C. O., Gee, K. L., Hart, G. W., Rasband, R. D., Mathews, L. T., Irarrazabal, F. J., Novakovich, D. J., Jithame, R., and Johnson, J. P. (**2021**). "Far-field acoustical measurements of multiple solid rocket booster static firings," Proc. Mtgs. Acoust. **39**, 040004.
Bies, D. A., and Franken, P. A. (**1961**). "Notes on scaling jet and rocket noise," J. Acoust. Soc. Am. **33**(9), 1171–1173.
Blom, P., Marcillo, O., and Arrowsmith, S. (**2016**). "Analysis and modeling of infrasound from a four-stage rocket launch," J. Acoust. Soc. Am. **139**, 3134–3138.
Bodony, D. J., and Lele, S. K. (**2008**). "Current status of jet noise predictions using large-eddy simulation," AIAA J. **46**(2), 364–380.
Bogey, C., Barré, S., Fleury, V., Bailly, C., and Juvé, D. (**2007**). "Experimental study of the spectral properties of near-field and far-field jet noise," Int. J. Aeroacoust. **6**, 73–92.
Bond, D., A. (**1964**). "A summary of model and full-scale acoustic data for prediction of missile lift-off noise environments," Report NOR-64-215, Northrop Corp., September.
Bozak, R. (**2014**). "Twin jet effects on noise of round and rectangular jets: Experiment and model," AIAA Paper 2014-2890.
Bradley, K. A., Wilmer, C., San Miguel, V., James, M. M., Salton, A. R., and Calton, M. F. (**2018**). "User guides for noise modeling of commercial space operations—RUMBLE and PCBoom," ACRP Research Report 183, Transportation Research Board, Washington, DC.
Brehm, C., Housman, J. A., and Kiris, C. C. (**2016**). "Noise generation mechanisms for a supersonic jet impinging on an inclined plate," J. Fluid Mech. **797**, 802–850.
Brehm, C., Sozer, E., Moini-Yekta, S., Housman, J. A., Barad, M. F., Kiris, C. C., Vu, B. T., and Parlier, C. R. (**2013**). "Computational prediction of pressure environment in the flame trench," AIAA Paper 2013-2538.
Brès, G. A., and Lele, S. K. (**2019**). "Modeling of jet noise: A perspective from large-eddy simulations," Philos. Trans. R. Soc. A **377**, 20190081.
Cacqueray, N., Bogey, C., and Bailly, C. (**2011**). "Investigation of a high-Mach-number overexpanded jet using large-eddy simulation," AIAA J. **49**(10), 2171–2182.
Caimi, R. E., and Margasahayam, R. (**1997**). "Validation of a deterministic vibroacoustic response prediction model," NASA TM-112649, April, Washington, DC.
Caimi, R. E., Margasahayam, R. N., and Nayfeh, F. (**2001**). "Rocket launch induced vibration and ignition overpressure response," NASA Technical Document, ID No. 20020002698, Washington, DC.
Callender, B., Gutmark, E., and Martens, S. (**2005**). "Far-field acoustic investigation into chevron nozzle mechanisms and trends," AIAA J. **43**(1), 87–95.
Campos, E. (**2005**). "Prediction of noise from rocket engines," AIAA Paper 2005-2837.
Camussi, R., Guj, G., Imperatore, B., Pizzicaroli, A., and Perigo, D. (**2007**). "Wall pressure fluctuations induced by transonic boundary layers on a launcher model," Aerosp. Sci. Technol. **11**(5), 349–359.
Canabal, F., and Frendi, A. (**2006**). "Study of the ignition overpressure suppression technique by water addition," J. Spacecr. Rockets **43**(4), 853–865.
Canchero, A., Tinney, C. E., Murray, N., and Ruf, J. H. (**2016**). "Acoustic imaging of clustered rocket nozzles undergoing end effects," AIAA J. **54**(12), 3778–3786.
Casalino, D., Barbarino, M., Genito, M., and Ferrara, V. (**2009**). "Hybrid empirical/computational aeroacoustics methodology for rocket noise modeling," AIAA J. **47**(6), 1445–1460.
Casalino, D., Santini, S., Genito, M., and Ferrara, V. (**2012**). "Rocket noise source localization through a tailored beamforming technique," AIAA J. **50**(10), 2146–2158.
Chobotov, V., and Powell, A. (**1957**). "On the prediction of acoustic environments from rockets," Rama-Wooldridge Corp. Report E.M.-7-7.
Cockburn, J. A., and Robertson, J. E. (**1974**). "Vibration response of spacecraft shrouds to in-flight fluctuating pressures," J. Sound Vib. **33**(4), 399–425.
Cole, H. A., Erickson, A. L., and Rainey, A. G. (**1970**). "Buffeting during atmospheric ascent," NASA Special Vehicle Design Criteria, NASA SP-8001, Washington, DC.
Cole, J. N., Von Gierke, H. E., Kyrazis, D. T., Eldred, K. M., and Humphrey, A. J. (**1957**). "Noise radiation from fourteen types of rockets in the 1,000 to 130,000 pounds thrust range," Wright Air Development Center Technical Report 57-354, AD 130794.
Coltrin, I. S., Blotter, J. D., Maynes, R. D., and Gee, K. L. (**2013**). "Shock-cell structures and corresponding sound pressure levels emitted from closely spaced supersonic jet arrays," Appl. Acoust. **74**, 1519–1526.
Conlon, S. C., and Hambric, S. A. (**2003**). "Predicting the vibroacoustic response of satellite equipment panels," J. Acoust. Soc. Am. **113**(3), 1455–1474.
Counter, D. D., and Houston, J. (**2011**). "Overview of the Ares I scale model acoustic test program," NASA Report No. M11-1210, Washington, DC.
Counter, D. D., and Houston, J. (**2012**). "Verification of Ares I liftoff acoustic environments via the Ares I scale model acoustic test," NASA Report No. M12-1989, Washington, DC.
Dargaud, J.-B., Troyes, J., Lamet, J.-M., Tessé, L., and Vuillot, F. (**2014**). "Numerical study of solid-rocket motor ignition overpressure wave including infrared radiation," J. Propul. Power **30**(1), 164–174.
Dhamanekar, A., and Srinivasan, K. (**2014**). "Effect of impingement surface roughness on the noise from impinging jets," Phys. Fluids **26**, 036101.
Djojodihardjo, H. (**2015**). "Vibro-acoustic analysis of the acoustic-structure interaction of flexible structure due to acoustic excitation," Acta Astronaut. **108**, 129–145.
Doak, P. E. (**1989**). "Momentum potential theory of energy flux carried by momentum fluctuations," J. Sound Vib. **131**(1), 67–90.
Donn, W., Posmentier, E., Fehr, U., and Balachandran, N. (**1968**). "Infrasound at long-range from Saturn V," Science **162**, 1116–1567.
Dougherty, N. S., and Guest, S. H. (**1984**). "A correlation of scale model and flight aeroacoustic data for the space Shuttle vehicle," AIAA Paper 84-2351.
Dumnov, G., Mel'nikov, D., Karamov, V., and Mepnikov, D. (**2000**). "Acoustic loads on rockets during launching," AIAA Paper 2000-3742.
Edgington-Mitchell, D. (**2019**). "Aeroacoustic resonance and self-excitation in screeching and impinging supersonic jets—A review," Int. J. Aeroacoust. **18**(2–3), 118–188.
Eldred, K. M. (**1959**). "Prediction of sonic exposure histories," Wright Air Development Center TR-59-507, Proc. Fatigue of Aircraft Structures, Wright Air Development Center, 11–13 August, pp. 396–415.
Eldred, K. M. (**1971**). "Acoustic loads generated by the propulsion system," NASA SP-8072, Washington, DC.
Eldred, K. M., Mann, M., White, R. W., and Cottas, M. (**1963**). "Suppression of jet noise with emphasis on the near field," ASD-TDR-62-578, Wright Patterson AFB, OH, February.
Eldred, K. M., Roberts, W. M., and White, R. (**1961**). "Structural vibrations in space vehicles," WADD TR 61-62.
Engblom, W. A. (**2003**). "Numerical simulation of Titan IVB transonic buffet environment," J. Spacecr. Rockets **40**(5), 648–656.
Engblom, W. A., Weaver, M. A., and Ndefo, E. D. (**2001**). "Numerical study of vehicle/pad configuration effects on launch ignition transients," AIAA Paper 2001-0802.
Ericsson, L. E. (**2001**). "Unsteady flow separation can endanger the structural integrity of aerospace launch vehicles," J. Spacecr. Rockets **38**(2), 168–179.
Evans, R. L., and Sparks, O. (**1963**). "Launch deflector design criteria," NASA TN D-1275, Washington, DCMarch.
Ferrara, V., Culla, A., and Preve, A. (**2007**). "High frequency vibroacoustic analyses on VEGA launch vehicle," AIAA Paper 2007-3585.

Ffowcs Williams, J. E. (**1963**). "The noise from turbulence convected at high speed," Philos. Trans. R. Soc., A **255**(1061), 469–503.
Fiévet, R., Tinney, C. E., Baars, W. J., and Hamilton, M. F. (**2016**). "Coalescence in the sound field of a laboratory-scale supersonic jet," AIAA J. **54**, 254–265.
Fujii, K., Nonomura, T., and Tsutsumi, S. (**2010**). "Toward accurate simulation and analysis of strong acoustic wave phenomena—A review from the experience of our study on rocket problems," Int. J. Numer. Methods Fluids **64**(10–12), 1412–1432.
Fukuda, K., Fujii, K., Ui, K., Ishii, T., Oinuma, H., Kazawa, J., and Minesugi, K. (**2009**). "Acoustic measurements and prediction of solid rockets in static firing tests," AIAA Paper 2009-3368.
Gee, K. L. (**2021**). "A tale of two curves and their influence on rocket and supersonic jet noise research," J. Acoust. Soc. Am. **149**, 2159–2162.
Gee, K. L., Akamine, M., Okamoto, K., Neilsen, T. B., Cook, M. R., Tsutsumi, S., Teramoto, S., and Okunuki, T. (**2017**). "Characterization of supersonic laboratory-scale jet noise with vector acoustic intensity," AIAA Paper 2017-3519.
Gee, K. L., Giraud, J., Blotter, J., and Sommerfeldt, S. (**2009**). "Energy-based acoustical measurements of rocket noise," AIAA Paper 2009-3165.
Gee, K. L., Kenny, R. J., Neilsen, T. B., Jerome, T. W., Hobbs, C. M., and James, M. M. (**2013b**). "Spectral and statistical analysis of noise from reusable solid rocket motors," Proc. Mtgs. Acoust. **18**, 040002.
Gee, K. L., Neilsen, T. B., and James, M. M. (**2014**). "Modeling ground reflections for rocket noise," Proc. Mtgs. Acoust. **22**, 040001.
Gee, K. L., Neilsen, T. B., Wall, A. T., Downing, J. M., and James, M. M. (**2013a**). "The 'Sound of Freedom'; characterizing jet noise from high-performance military aircraft," Acoust. Today **9**, 8–21.
Gee, K. L., Neilsen, T. B., Wall, A. T., Downing, J. M., James, M. M., and McKinley, R. L. (**2016a**). "Propagation of crackle-containing jet noise from high-performance engines," Noise Control Eng. J. **64**(1), 1–21.
Gee, K. L., Russavage, P. B., Neilsen, T. B., Swift, S. H., and Vaughn, A. B. (**2018**). "Subjective rating of the jet noise crackle percept," J. Acoust. Soc. Am. **144**(1), EL40–EL45.
Gee, K. L., Sparrow, V. W., James, M. M., Downing, J. M., Hobbs, C. M., Gabrielson, T. B., and Atchley, A. A. (**2008**). "The role of nonlinear effects in the propagation of noise from high-power jet aircraft," J. Acoust. Soc. Am. **123**, 4082–4093.
Gee, K. L., Whiting, E. B., Neilsen, T. B., James, M. M., and Salton, A. R. (**2016b**). "Development of a near-field intensity measurement capability for static rocket firings," Trans. JSASS Aerosp. Tech. Jpn. **14**, Po_2_9–Po_2_15.
Gely, D., Elias, G., Bresson, C., Foulon, H., Radulovic, S., and Roux, P. (**2000**). "Reduction of supersonic jet noise; Application to the Ariane V launch vehicle," AIAA Paper 2000-2026.
Gely, D., Elias, G., Mascanzoni, F., and Foulon, H. (**2005**). "Acoustic environment of the VEGA launch vehicle at lift-off," in *Forum Acusticum 2005*.
Giacomoni, C. (**2013**). "Comparison of a two-source jet noise model to horizontal solid rocket test data," ESSSA-Fy13-1579, July 2013.
Giacomoni, C., and Kenny, R. J. (**2014**). "Comparison of spatial correlation parameters between full and model scale launch vehicles," NASA Report No. M17-5638, Washington, DC.
Giacomoni, C., and Kenny, R. J. (**2016**). "Impact of drift on the vehicle lift-off acoustic environments," NASA Report No. M17-5639, Washington, DC.
Gibson, G. R., Janssen, S. G., Bradford, L. F., and Groom, R. S. (**2004**). "Overview of the development of dynamic environments for Atlas V launch vehicles," J. Spacecr. Rockets **41**(5), 779–786.
Goddard, R. H. (**1920**). "A method of reaching extreme altitudes," Nature **105**, 809–811.
Goldstein, M. E. (**2011**). "Recent developments in the application of the generalized acoustic analogy to jet noise prediction," Int. J. Aeroacoust. **10**(2-3), 89–115.
Goparaju, K., Unnikrishnan, S., and Gaitonde, D. V. (**2018**). "Acoustic characteristics of a supersonic twin-jet configuration," AIAA Paper 2018-3304.
Greska, B. J. (**2005**). "High-speed jet noise reduction using microjet injection," Ph.D. thesis, Florida State University.
Greska, B. J., Krothapalli, A., Horne, W., and Burnside, N. (**2008**). "A near-field study of high temperature supersonic jets," AIAA Paper 2008-3026.
Greska, B. J., Krothapalli, A., Seiner, J. M., Jansen, B., and Ukeiley, L. (**2005**). "The effects of microjet injection on an F404 jet engine," AIAA Paper 2005-3047.
Griffin, S., Lane, S., and Leo, D. (**2000**). "Innovative vibroacoustic control approaches in space launch vehicles," in *29th International Congress and Exhibition on Noise Control Engineering*, Nice, France.
Guest, S. H. (**1964**). "Acoustic efficiency trends for high thrust boosters," NASA TN D-1999, MSFC, Huntsville, AL, July.
Guest, S. H., and Jones, J. H. (**1967**). "Far-field acoustic environmental predictions for launch of Saturn V and Saturn V MLV Configuration," NASA TN D-4117, Washington, DC.
Guest, S. H., and Jones, J. H. (**1976**). "Space Shuttle noise suppression concepts for the Eastern test range," in *Proceedings 13th Space Congress*, April, Cocoa Beach, FL.
Gupta, S. C., Suresh, B. N., and Sivan, K. (**2007**). "Evolution of Indian launch vehicle technologies," Curr. Sci. **93**(12), 1697–1714.
Gurbatov, S. N., and Rudenko, O. V. (**1998**). "Statistical phenomena," in *Nonlinear Acoustics*, edited by M. F. Hamilton and D. T. Blackstock (Academic, San Diego), Chap. 13, pp. 377–398.
Harker, B. M. (**2017**). "Characterization of military aircraft jet noise using wavepacket analysis and other array processing methods," Ph.D. thesis, Brigham Young University.
Harker, B. M., Gee, K. L., Neilsen, T. B., Wall, A. T., and James, M. M. (**2017**). "Beamforming-based wavepacket model for noise environment predictions of tactical aircraft," AIAA Paper 2017-4048.
Harker, B. M., Gee, K. L., Neilsen, T. B., Wall, A. T., McInerny, S. A., and James, M. M. (**2013**). "On autocorrelation analysis of jet noise," J. Acoust. Soc. Am. **133**, EL458– EL464.
Harris, R. E., Collins, E. M., Luke, E. A., and Sescu, A. (**2016**). "Coupled overset unstructured discontinuous Galerkin method for launch environment acoustics prediction," AIAA J. **54**, 1932–1952.
Harris, R. E., Collins, E. M., Luke, E. A., Sescu, A., Strutzenberg, L. L., and West, J. S. (**2015**). "Hybrid discontinuous Galerkin and finite volume method for launch environment acoustics prediction," AIAA J. **53**(11), 3430–3447.
Haynes, J., and Kenny, R. J. (**2009**). "Modifications to the NASA SP-8072 distributed source method II for Ares I lift-off environment predictions," AIAA Paper 2009-3160.
Henderson, B. (**2002**). "The connection between sound production and jet structure of the supersonic impinging jet," J. Acoust. Soc. Am. **111**(2), 735–747.
Henderson, B. (**2010**). "Fifty years of fluidic injection for jet noise reduction," Int. J. Aeroacoust. **9**(1-2), 91–122.
Henderson, B., Bridges, J., and Wernet, M. (**2005**). "An experimental study of the oscillatory flow structure of tone-producing supersonic impinging jets," J. Fluid Mech. **542**, 115–137.
Henderson, B., Gerhart, C., Jensen, E., Griffin, S., and Lazzaro, A. (**2003**). "Vibro-acoustic launch protection experiment (VALPE)," J. Acoust. Soc. Am. **114**(4), 2384.
Himelblau, H., Fuller, C. M., and Scharton, T. D. (**1970**). "Assessment of space vehicle aeroacoustic-vibration prediction, design, and testing," NASA CR-1596, No. July, Washington, DC.
Himelblau, H., Kern, D. L., Manning, J. E., Piersol, A. G., and Rubi, S. (**2001**). "NASA handbook 7005: Dynamics environmental criteria," NASA-HDBK7005, Washington, DC.
Hipol, P. J. (**1989**). "Finite element prediction of vibro-acoustic environments," J. Aeros. **98**(1), 1881–1889.
Houston, J., Counter, D., and Giacomoni, C. (**2015**). "SLS scale model acoustic test liftoff results and comparisons," in *29th Aerospace Testing Seminar*, NASA Report No. M15-4862, Washington, DC.
Houston, J. D. (**2016**). "Liftoff and time equivalent duration data evaluation of exploration flight test 1 Orion multi-purpose crew vehicle," J. Acoust. Soc. Am. **140**, 3096.
Humphrey, A. J. (**1957**). "Rocket noise environments," Shock and Vibration Bulletin No. 25, Pt. II, Department of Defense, Washington, DC, December.
Ignatius, J. K., Sankaran, S., Kumar, R. A., and Satyanarayana, T. N. V. (**2008**). "Suppression of jet noise by staged water injection during launch vehicle lift-off," Int. J. Aeroacoust. **7**(3-4), 223–242.
Ignatius, J. K., Sathiyavageeswaran, S., and Chakravarthy, S. R. (**2015**). "Hot-flow simulation of acoustics and suppression by water injection during rocket liftoff," AIAA J. **53**(1), 235–245.

Ikawa, H., and Laspesat, F. S. (**1985**). "Ignition/duct overpressure induced by Space Shuttle solid rocket motor ignition," J. Spacecr. Rockets **22**(4), 481–488.
Ishii, T., Tsutsumi, S., Ui, K., Tokudome, S., Ishii, Y., Wada, K., and Nakamura, S. (**2012**). "Acoustic measurement of 1:42 scale booster and launch pad," Proc. Mtgs. Acoust. **18**(1), 040009.
Ishii, Y., Ishii, T., Hald, J., Oinuma, H., Tsutsumi, S., and Ui, K. (**2016**). "Application of beam-forming using deconvolution method to the development of the new launch pad of Epsilon," in *Berlin Beamforming Conference*, BeBeC-2016-D13.
Jaeger, S. M., and Allen, C. S. (**1993**). "Two-dimensional sound intensity analysis of jet noise," AIAA Paper 93-4342.
James, M. M., and Gee, K. L. (**2012**). "Advanced acoustic measurement system for rocket noise source characterization," in *Proceedings of Internoise 2012*, Paper in12_1127.
James, M. M., and Salton, A. R. (**2017**). "Modeling community noise impacts from launch vehicle propulsion noise," J. Acoust. Soc. Am. **142**, 2490.
James, M. M., Salton, A. R., Calton, M. F., Downing, M., Gee, K. L., and McInerny, S. A. (**2020**). "Commercial space operations noise and sonic boom measurements," ACRP Project 02-81 Report, Transportation Research Board, Washington, DC.
James, M. M., Salton, A. R., Downing, J. M., Gee, K. L., Neilsen, T. B., Reichman, B. O., McKinley, R. L., Wall, A. T., and Gallagher, H. L. (**2015**). "Acoustic emissions from F-35 aircraft during ground run-up," AIAA Paper 2015-2375.
James, M. M., Salton, A. R., Gee, K. L., and Neilsen, T. B. (**2016**). "Comparative analysis of NASA SP-8072's core length with full-scale rocket data," Trans. JSASS Aerosp. Tech, Jpn. **14**(3), 17–24.
James, M. M., Salton, A. R., Gee, K. L., Neilsen, T. B., and McInerny, S. A. (**2014a**). "Full-scale rocket motor acoustic tests and comparisons with empirical source models," Proc. Mtgs. Acoust. **18**, 040007.
James, M. M., Salton, A. R., Gee, K. L., Neilsen, T. B., McInerny, S. A., and Kenny, R. J. (**2014b**). "Modification of directivity curves for a rocket noise model," Proc. Mtgs. Acoust. **18**, 040008.
Jeun, J., Nichols, J. W., and Jovanovic, M. R. (**2016**). "Input-output analysis of high-speed axisymmetric isothermal jet noise," Phys. Fluids **28**, 047101.
Jiang, C., Han, T., Gao, Z., and Lee, C. H. (**2019**). "A review of impinging jets during rocket launching," Prog. Aerosp. Sci. **109**, 100547.
Jones, H. W. (**2018**). "The recent large reduction in space launch cost," in *18th International Conference on Environmental Systems, ICES-2018-81*.
Jordan, P., and Colonius, T. (**2013**). "Wave packets and turbulent jet noise," Ann. Rev. Fluid Mech. **45**, 173–195.
Kandula, M. (**2006**). "An experimental and numerical study of sound propagation from a supersonic jet passing through a rigid-walled duct with a J-deflector," Int. J. Acoust. Vib. **11**(2), 125–131.
Kandula, M. (**2008a**). "Nearfield acoustics of clustered rocket engines," J. Sound Vib. **309**, 852–857.
Kandula, M. (**2008b**). "On the scaling laws and similarity spectra for jet noise in subsonic and supersonic flow," Int. J. Acoust. Vib. **13**(1), 3–16.
Kandula, M. (**2008c**). "Prediction of turbulent jet mixing noise reduction by water injection," AIAA J. **46**(11), 2714–2722.
Kandula, M. (**2011**). "Sound radiation from a supersonic jet passing through a partially open exhaust duct," J. Vib. Acoust. **133**(6), 1–5.
Kandula, M., and Vu, B. T. (**2003**). "Scale model experiments on sound propagation from a Mach 2.5 cold nitrogen jet flowing through a rigid-walled duct with a J-deflector," NASA TM-2003-211186, Washington, DC.
Kandula, M., and Vu, B. T. (**2013**). "On the scaling laws for jet noise in subsonic and supersonic flow," in *9th AIAA/CEAS Aeroacoustics Conference and Exhibit*, Hilton Head, SC.
Kang, S. H., Joo, H. S., Shin, S. J., Park, T., Ohm, W.-S., and Park, J. W. (**2020**). "Acoustic experiment and numerical simulation on unheated supersonic jet flow for a small-scale nozzle," AIAA Paper 2020-0002.
Kantola, R. A. (**1981**). "Acoustic properties of heated twin jets," J. Sound Vib. **79**(1), 79–106.
Karabasov, S. (**2010**). "Understanding jet noise," Philos. Trans. R. Soc. A **368**, 3593–3608.
Karthikeyan, N., and Venkatakrishnan, L. (**2017**). "Acoustic characterization of jet interaction with launch structures during lift-off," J. Spacecr. Rockets **54**(2), 356–367.
Kaschak, G., Donn, W., and Fehr, U. (**1970**). "Long-range infrasound from rockets," J. Acoust. Soc. Am. **48**(1), 12–20.
Kenny, R. J., and Giacomoni, C. (**2014**). "Prediction of acoustic environments from horizontal rocket firings," NASA Report No. M15-4167, Washington, DC.
Kenny, R. J., Hobbs, C., Plotkin, K. J., and Pilkey, D. (**2009**). "Measurement and characterization of Space Shuttle solid rocket motor plume acoustics," AIAA Paper 2009-3161.
Kiris, C., Chan, W., Kwak, D., and Housman, J. (**2008**). "Time-accurate computational analysis of the flame trench," Compt. Fluid Dyn. **2008**, 261–267.
Kiris, C. C., Housman, J. A., Barad, M. F., Brehm, C., Sozer, E., and Moini-Yekta, S. (**2016**). "Computational framework for launch, ascent, and vehicle aerodynamics (LAVA)," Aerosp. Sci. Technol. **55**, 189–219.
Kobayashi, M. H. (**1999**). "On a class of Padé finite volume methods," J. Comp. Phys. **156**(1), 137–180.
Koudriavtsev, V. (**2000**). "Acoustic environment at jet interaction with a plate," in *29th International Congress and Exhibition on Noise Control Engineering*, Nice, France.
Koudriavtsev, V., Varnier, J., and Safronov, A. (**2004**). "A simplified model of jet aerodynamics and acoustics," AIAA Paper 2004-2877.
Krothapalli, A., Rajkuperan, E., Alvi, F., and Lourenco, L. (**1999**). "Flow field and noise characteristics of a supersonic impinging jet," J. Fluid Mech. **392**, 155–181.
Krothapalli, A., Venkatakrishnan, L., Lourenco, L., Greska, B., and Elavarasan, R. (**2003**). "Turbulence and noise suppression of a high-speed jet by water injection," J. Fluid Mech. **491**, 131–159.
Kumar, S. A., and Karthikeyan, N. (**2013**). "Prediction of launch vehicle noise during lift-off using a modified Eldred's method," in *14th Asian Congress of Fluid Mechanics*, Hanoi and Halong, Vietnam.
Kuo, C. W., McLaughlin, D. K., Morris, P. J., and Viswanathan, K. (**2015**). "Effects of jet temperature on broadband shock-associated noise," AIAA J. **53**(6), 1515–1530.
Kurbatskii, K. A., Guenthoer, B. F., Golubev, V. V., Lyrintzis, A. S., Mankbadi, R. R., and Osman, H. (**2014**). "Effect of inclination angle on mean flow and noise radiation from impinging rocket plume," AIAA Paper 2014-3308.
Kurokawa, M., Teramoto, S., and Okamoto, K. (**2020**). "Acoustic wave generation from two-dimensional supersonic inviscid jet impinging on inclined plate," AIAA J. **58**(8), 3436–3445.
Lambaré, H. (**2016**). "Acoustical design of the ELA4 launch pad for the Ariane 6 launcher," J. Acoust. Soc. Am. **140**, 3422.
Lane, S. A., Kennedy, S., and Richard, R. (**2007**). "Noise transmission studies of an advanced grid-stiffened composite fairing," J. Spacecr. Rockets **44**(5), 1131–1139.
Langenais, A., Vuillot, F., Peyret, C., Chaineray, G., and Bailly, C. (**2018**). "Assessment of a two-way coupling methodology between a flow and a high-order nonlinear acoustic unstructured solvers," Flow, Turbul. Combust. **101**(3), 681–703.
Langenais, A., Vuillot, F., Troyes, J., and Bailly, C. (**2019**). "Accurate simulation of the noise generated by a hot supersonic jet including turbulence tripping and nonlinear acoustic propagation," Phys. Fluids **31**(1), 016105.
Langenais, A., Vuillot, F., Troyes, J., and Lambaré, H. (**2021**). "Computation of the noise radiated by a hot supersonic jet deflected in a flame trench," J. Acoust. Soc. Am. **149**, 1989–2003.
Leete, K. M., Gee, K. L., Liu, J., and Wall, A. T. (**2020**). "Coherence analysis of the noise from a simulated highly heated laboratory-scale jet," AIAA J. **58**, 3426–3435.
Leete, K. M., Vaughn, A. B., Bassett, M. S., Rasband, R. D., Novakovich, D. J., Gee, K. L., Campbell, S. C., Mobley, F. S., and Wall, A. T. (**2021b**). "Jet noise measurements of an installed GE F404 engine," AIAA Paper 2021-1638.
Leete, K. M., Wall, A. T., Gee, K. L., Neilsen, T. B., Downing, J. M., and James, M. M. (**2021a**). "Acoustical holography-based analysis of spatio-spectral lobes in high-performance aircraft jet noise," AIAA J. **59**, 4166–4178.
Leib, S. J., and Goldstein, M. E. (**2011**). "Hybrid source model for predicting high-speed jet noise," AIAA J. **49**(7), 1324–1335.
Li, A. (**2012**). "Semi-empirical methods prediction noise from free supersonic jets," Adv. Mater. Res. **433–440**, 281–284.
Liever, P. A., West, J. S., and Harris, R. E. (**2017**). "Validation of high-fidelity CFD/CAA framework for launch vehicle acoustic environment

simulation against scale model test data," in *JANNAF Conference*, NASA Report M17-5678, Washington, DC.
Lighthill, M. J. (**1952**). "On sound generated aerodynamically. I. General theory," Proc. R. Soc. **211**, 564–587.
Lighthill, M. J. (**1954**). "On sound generated aerodynamically. II. Turbulence as a source of sound," Proc. R. Soc. **222**(1148), 1–32.
Lighthill, M. J. (**1962**). "The Bakerian Lecture, 1961, Sound generated aerodynamically," Proc. R. Soc. (London) **A267**, 147–182.
Lighthill, M. J. (**1963**). "Jet noise," in *Wright Brothers Memorial Lecture*, Institute of Space Science, New York, January 21.
Lipnitskiy, Y. M., and Safronov, A. V. (**2014**). "Ground testing of the launch vehicle acoustics," TsAGI Sci. J. **45**, 237–254.
Liu, J., Corrigan, A., Kailasanath, K., and Gutmark, E. (**2015**). "Impact of chevrons on noise source characteristics in imperfectly expanded jet flows," AIAA Paper 2015-2835.
Liu, J., Corrigan, A. T., Kailasanath, K., and Taylor, B. D. (**2016**). "Impact of the specific heat ratio on the noise generation in a high-temperature supersonic jet," AIAA Paper 2016-2125.
Long, D. F. (**2008**). "Jet noise source location via acoustic holography and shadowgraph imagery," AIAA Paper 2008-2888.
Long, D. F., and Arndt, R. E. A. (**1984**). "The role of Helmholtz number in jet noise," AIAA Paper 84-0403.
Lonzaga, J. B. (**2019**). "Recent enhancements to NASA's PCBoom sonic boom propagation code," AIAA Paper 2019-3386.
Lu, C., Zhou, Z., Shi, Y., Bao, Y., and Le, G. (**2021**). "Numerical simulations of water spray on launch pad during rocket launching," Spacecr. Rockets **58**(2), 566–574.
Lubert, C. P. (**2018**). "From Sputnik to SpaceX: 60 years of rocket launch acoustics," Acoust. Today **14**(4), 38–46.
Lyrintzis, A. S., and Coderoni, M. (**2020**). "Overview of the use of large-eddy simulations in jet aeroacoustics," AIAA J. **58**(4), 1620–1638.
Malbequi, P., Davy, R., and Bresson, C. (**2017**). "Experimental characterization of the acoustics of the future Ariane 6 launch pad," in *7th European Conference for Aeroacoustics and Space Science (EUCASS)*.
Manhart, J. K., Ailman, C. M., Lane, S. R., and Marsh, A. H. (**1966**). "An acoustical study of the KIWI B nuclear rocket," NASA CR-370, Washington, DC.
Margasahayam, R., and Caimi, R. E. (**1997**). "Random vibration response of a cantilever beam to acoustic forcing by supersonic rocket exhausts during a Space Shuttle launch," in *5th International Congress on Sound and Vibration*, Adelaide, Australia, December.
Margasahayam, R., Caimi, R. E., and Hauss, S. (**2002**). "Rocket launch trajectory simulation mechanism," in *Proceedings of the 9th International Congress on Sound and Vibration*, July 8–11, Orlando, FL.
Mathews, L. T., Gee, K. L., and Hart, G. W. (**2021**). "Characterization of Falcon 9 launch vehicle noise from far-field measurements," J. Acoust. Soc. Am. **150**, 620–633.
Mathews, L. T., Gee, K. L., Hart, G. W., Rasband, R. D., Novakovich, D. J., Irarrazabal, F. I., Vaughn, A. B., and Nelson, P. (**2020**). "Comparative analysis of noise from three Falcon 9 launches," J. Acoust. Soc. Korea **39**, 322–330.
Mayes, W. H., Lanford, W. E., and Hubbard, H. H. (**1959**). "Near-field and far-field noise surveys of solid-fuel rocket engines for a range of nozzle exit pressures," NASA TN D-21, Washington, DC.
McInerny, S. A. (**1990**). "Rocket noise—A review," AIAA Paper 90-3981.
McInerny, S. A. (**1992a**). "The broadband noise generated by very high temperature, high velocity exhausts," in *2nd International Congress on Recent Developments in Air- and Structure- Borne Sound and Vibration*, March 6–8, Auburn University.
McInerny, S. A. (**1992b**). "Characteristics and predictions of far-field rocket noise," Noise Control Eng. J. **38**(1), 5–16.
McInerny, S. A. (**1996a**). "Launch vehicle acoustics Part 1: Overall levels and spectral characteristics," J. Aircraft **33**(3), 51–517.
McInerny, S. A. (**1996b**). "Launch vehicle acoustics Part 2: Statistics of the time domain data," J. Aircraft **33**(3), 518–523.
McInerny, S. A. (**2010**). "Perspective on launch noise: Measurement, prediction and characterization," J. Acoust. Soc. Am. **127**, 1742.
McInerny, S. A., and Ölçmen, S. (**2005**). "High-intensity rocket noise: Nonlinear propagation, atmospheric absorption, and characterization," J. Acoust. Soc. Am. **117**(2), 578–591.
McInerny, S. A., Wickiser, J. K., and Mellen, R. H. (**1997**). "Rocket noise propagation," ASME Noise Control Acoust. **24**, 37–50.
McKeon, B. J., and Sharma, A. S. (**2010**). "A critical-layer framework for turbulent pipe flow," J. Fluid Mech. **658**, 336–382.
Menter, F. R., and Egorov, Y. (**2010**). "The scale-adaptive simulation method for unsteady turbulent flow predictions. Part 1: Theory and model description," Flow, Turbul. Combust. **85**(1), 113–138.
Meyer, R., Kuo, C.-W., and McLaughlin, D. K. (**2013**). "Reduction of subsonic jet noise by passive flow control devices," AIAA Paper 2013-2147.
Michel, U., and Ahuja, K. K. (**2014**). "On the scaling of jet noise with Helmholtz number close to the jet axis," in *20th AIAA/CEAS Conference*, June, Atlanta, GA, pp. 1–32.
Miller, S. A. E. (**2015**). "The scaling of broadband shock-associated noise with increasing temperature," Int. J. Aeroacoust **14**(1-2), 305–326.
Mora, P. A., Kastner, J. F., Gutmark, E. J., and Kailasanath, K. (**2015**). "Investigation of a heated supersonic jet chevrons nozzle," AIAA Paper 2015-0233.
Morfey, C. L. (**1984**). "Aperiodic signal propagation at finite amplitudes: Some practical applications," in *Proceedings of the 10th International Symposium on Nonlinear Acoustics*, pp. 199–206.
Morgan, W. V., and Young, K. J. (**1963**). "Studies of rocket noise simulation with substitute gas jets and the effect of vehicle motion on jet noise," Wright Patterson Air Force Base, Report ASD-TDR-62-787, Washington, DC.
Morris, P. J. (**2009**). "A note on noise generation by large scale turbulent structures in subsonic and supersonic jets," Int. J. Aeroacoust. **8**, 301–315.
Morris, P. J., and Farassat, F. (**2002**). "Acoustic analogy and alternative theories for jet noise prediction," AIAA J.. **40**(4), 671–680.
Morris, P. J., and Lilley, J. M. (**2007**). *Handbook of Noise and Vibration Control—Aerodynamic Noise: Theory and Applications* (Wiley, Hoboken, NJ), Chap. 9, 128–158.
Mortain, F., Cléro, F., and Palmieri, D. (**2019**). "Full scale acoustic source identification on VEGA launch pad at lift-off," in *Proceedings of the 26th International Congress on Sound Vibration (ICSV26)*, Montreal, Canada.
Muhlestein, M., Gee, K. L., Neilsen, T. B., and Thomas, D. C. (**2012**). "Prediction of nonlinear propagation of noise from a solid rocket motor," Proc. Mtgs. Acoust. **18**, 1–8.
Nagamatsu, H., and Horvay, G. (**1970**). "Supersonic jet noise," AIAA Paper 70-0237.
Nagamatsu, H. T., Sheer, R. E., and Horvay, G. (**1969**). "Supersonic jet noise theory and experiments," in *Basic Aerodynamic Research, NASA SP-207*.
Nance, D. K., and Liever, P. A. (**2015**). "Space Launch System scale model acoustic test ignition overpressure testing," in *Aerospace Testing Seminar 2015, NASA Report M15-4899*.
Neilsen, T. B., Gee, K. L., Wall, A. T., and James, M. M. (**2013**). "Similarity spectra analysis of high performance supersonic jet aircraft noise," J. Acoust. Soc. Am. **133**, 2116–2125.
Neilsen, T. B., Vaughn, A. B., Gee, K. L., Akamine, M., Okamoto, K., Teramoto, S., and Tsutsumi, S. (**2019b**). "Data-educed broadband equivalent acoustic source model for supersonic jet noise," J. Acoust. Soc. Am. **146**, 3409–3424.
Neilsen, T. B., Vaughn, A. B., Gee, K. L., Swift, S. H., Wall, A. T., Downing, J. M., and James, M. M. (**2019a**). "Three-way spectral decompositions of high-performance military aircraft noise," AIAA J. **57**(12), 1–13.
Nesman, T. (**2017**). "Acoustic model testing chronology," Spacecraft and Launch Vehicle Dynamic Environments Workshop," June 20–22, NASA Report M17-6086.
Nguyen, A. T., Deniau, H., Girard, S., and Alziary De Roquefort, T. (**2003**). "Unsteadiness of flow separation and end-effects regime in a thrust-optimized contour rocket nozzle," Flow, Turbul. Combust. **71**(1–4), 161–181.
Nonomura, T., and Fujii, K. (**2010**). "POD of aeroacoustic fields of a jet impinging on an inclined plate," AIAA Paper 2010-4019.
Nonomura, T., Goto, Y., and Fujii, K. (**2011**). "Aeroacoustic waves generated from a supersonic jet impinging on an inclined flat plate," Int. J. Aeroacoust. **10**(4), 401–426.
Nonomura, T., Honda, H., Nagata, Y., Yamamoto, M., Morizawa, S., Obayashi, S., and Fujii, K. (**2016**). "Plate-angle effects on acoustic waves from supersonic jets impinging on inclined plates," AIAA J. **54**(3), 816–827.

Norum, T. D. (**2004**). "Reductions in multi-component jet noise by water injection," in *10th AIAA/CEAS Aeroacoustics Conference*, 10–12 May, Manchester, United Kingdom.
Oertel, H. (**1982**). "Measured velocity fluctuations inside the mixing layer of a supersonic jet," in *Recent Contributions to Fluid Mechanics* (Springer, Berlin), pp. 170–179.
Olson, J. (**2012**). "Infrasound rocket signatures," in *Advanced Maui Optical and Space Surveillance Technologies Conference*, pp. 1, 82–89.
Onoda, J., and Minesugi, K. (**1997**). "Estimation of mechanical environment of M-V satellite launcher," in *JSASS/JSME Structures Conference*, pp. 229–232 (in Japanese).
Osipov, V., Khasin, M., Hafiychuk, H., Muratov, C., Watson, M., and Smelyanskiy, V. (**2015**). "Mitigation of solid booster ignition over pressure by water aerosol sprays," J. Spacecr. Rockets **52**(3), 928–943.
Pain, R., Weiss, P.-E., and Deck, S. (**2014**). "Zonal detached eddy simulation of the flow around a simplified launcher afterbody," AIAA J. **52**(9), 1967–1979.
Palmieri, D., Nicolini, D., Neri, A., Barbagallo, D., Spina, S., Roviera, P. M., Barad, M. F., Kiris, C., Vu, B., and Chesnutt, D. (**2017**). "Design and validation of VEGA launch pad modifications to reduce payload acoustic environment at lift-off," in *Proceedings of the International Astronautical Congress (IAC)*, September, Vol. 15, pp. 9771–9776.
Panda, J., Garbeff, T., Burnside, N., and Ross, J. (**2018**). "Unsteady pressure fluctuations measured on a hammerhead space vehicle and comparison with Coe and Nute's 1962 data," Int. J. Aeroacoust. **17**(1–2), 70–87.
Panda, J., and Mosher, R. N. (**2011**). "Use of a microphone phased array to determine noise sources in a rocket plume," AIAA Paper 2011-974.
Panda, J., and Mosher, R. N. (**2013**). "Microphone phased array to identify liftoff noise sources in model-scale tests," J. Spacecr. Rockets **50**(5), 1002–1012.
Panda, J., Mosher, R. N., and Porter, B. J. (**2014**). "Noise source identification during rocket engine test firings and a rocket launch," J. Spacecr. Rockets **51**(6), 1761–1772.
Panda, J., Seasholtz, R. G., and Elam, K. A. (**2005**). "Investigation of noise sources in high-speed jets via correlation measurements," J. Fluid Mech. **537**, 349–385.
Park, S. (**2019**). "Multi-objective optimal design of low noise launch pad using empirical method with genetic algorithm," Ph.D. thesis, Seoul National University.
Park, S., Han, D., and Lee, S. (**2018**). "Multi-objective optimal design of launch pad by empirical prediction method combined with NURBS modelling and genetic algorithm," in *INCE Conference Proceedings, InterNoise18*, pp. 6052–6067.
Park, S., Jin-hyeong, K., Shin, S., and Lee, S. (**2017**). "Improved empirical prediction method for impinging acoustic sources distributed around interactive structures," Noise Control Eng. J. **65**(5), 374–385.
Pearsons, K. S., White, P. H., and Wilby, J. F. (**1980**). "An evaluation of the noise impact of satellite power system vehicles on the community and ecology at the launch site," Bolt, Beranek and Newman (BBN) Report 4210, Canoga Park, CA.
Pedersen, M. T., Murray, N. E., and Baars, W. J. (**2020**). "Modeling supersonic jet noise exposure using a data-informed wave packet approach," AIAA Paper 2020-2605.
Petitjean, B. P., Viswanathan, K., and McLaughlin, D. K. (**2006**). "Acoustic pressure waveforms measured in high speed jet noise experiencing nonlinear propagation," Int. J. Aeroacoust. **5**(2), 193–215.
Piatak, D. J., Sekula, M. K., and Rausch, R. D. (**2012**). "Ares launch vehicle transonic buffet testing and analysis techniques," J. Spacecr. Rockets **49**(5), 798–807.
Piatak, D. J., Sekula, M. K., Rausch, R. D., Florance, J. R., and Ivanco, T. G. (**2015**). "Overview of the Space Launch System transonic buffet environment test program," AIAA Paper 2015-0557.
Pickering, E., Rigas, G., Schmidt, O. T., Sipp, D., and Colonius, T. (**2021**). "Optimal eddy viscosity for resolvent-based models of coherent structures in turbulent jets," J. Fluid Mech. **917**, A29, 1–34.
Pineau, P., and Bogey, C. (**2021a**). "Numerical investigation of wave steepening and shock coalescence near a cold Mach 3 jet," J. Acoust. Soc. Am. **149**, 357–370.
Pineau, P., and Bogey, C. (**2021b**). "Acoustic shielding and interaction effects for strongly heated supersonic twin jets," AIP Adv. **11**, 075114.
Pirk, R., and Souto, C. D. (**2015**). "Deterministic, hybrid and statistical vibro-acoustic models—A methodology to determine the Vls payload fairing acoustic behavior," J. Aerosp. Technol. Manage. **7**(1), 101–109.
Plotkin, K. J., Sutherland, L., and Vu, B. T. (**2009**). "Liftoff acoustics predictions for the Ares I launch pad," AIAA Paper 2009-3163.
Potter, R. C. (**1968**). "An investigation to locate the acoustic sources in a high speed jet exhaust stream," NASA-CR-101105, Washington, DC.
Potter, R. C., and Crocker, M. J. (**1966**). "Acoustic prediction methods for rocket engines, including the effects of clustered engines and deflected exhaust flow," NASA-CR-566, Washington, DC.
Ragaller, P. A., Annaswamy, A. M., Gustavsson, J. P. R., and Alvi, F. S. (**2011**). "Impinging jet noise suppression using water microjets," AIAA Paper 2011-913.
Rainey, A. G. (**1965**). "Progress on the launch-vehicle buffeting problem," J. Spacecr. Rockets **2**(3), 289–299.
Raman, G., Panickar, P., and Chelliah, K. (**2012**). "Aeroacoustics of twin supersonic jets: A review," Int. J. Aeroacoust. **11**, 957–984.
Ranow, F. (**2021**). "Acoustic prediction methods for rocket flame deflector design," Dissertation for Mechanical Engineering degree, Swedish Space Corporation (SSC) and KTH, Stockholm, Sweden.
Ravish, D. L., Pavish, D. L., and Deese, J. E. (**2000**). "CFD analysis of unsteady ignition overpressure effects on Delta II and Delta III launch vehicles," AIAA Paper 2000-3922.
Reba, R., Narayanan, S., and Colonius, T. (**2010**). "Wave-packet models for largescale mixing noise," Int. J. Aeroacoust. **9**, 533–558.
Reichman, B. O., Neilsen, T. B., Gee, K. L., and Ohm, W. S. (**2016**). "Acoustic measurements in the far field during QM-2 solid rocket motor static firing," Proc. Mtgs. Acoust. **29**, 045008.
Requena-Plens, J. M., Jiménez, N., Cebrecos, A., Picó, R., and Sánchez-Morcillo, V. J. (**2020**). "Acoustic field prediction during the launch of rockets," in *Acústica 2020*.
Rojo, R., Tinney, C. E., and Ruf, J. H. (**2016**). "Effect of stagger on the vibroacoustic loads from clustered rockets," AIAA J. **54**(11), 3588–3597.
Roth, D. J. (**1984**). "Sound intensity techniques for identifying locations of scale model jet noise sources," J. Acoust. Soc. Am. **75**, S80.
Salehian, S., and Mankbadi, R. R. (**2020**). "Simulations of rocket launch noise suppression with water injection from impingement pad," Int. J. Aeroacoust. **19**(3–5), 207–239.
Samimy, M., Zamant, K. B. M. Q., and Reederj, M. F. (**1993**). "Effect of tabs on the flow and noise field of an axisymmetric jet," AIAA J. **31**(4), 609–619.
Sankaran, S., Ignatius, J. K., Ramkumar, R., Satyanarayana, T. N. V., Chakravarthy, R., and Panchapakesan, N. R. (**2009**). "Suppression of high Mach number rocket jet noise by water injection," J. Spacecr. Rockets **46**(6), 1164–1170.
Sarae, W., Sawada, A., Terashima, K., Haga, T., Tsutsumi, S., and Hiraiwa, T. (**2016**). "Results of scale model acoustic tests using supersonic cold jets for H3 launch vehicle," J. Acoust. Soc. Am. **140**, 3043.
Schlinker, R., Liljenberg, S., Polak, D., Post, K., Chipman, C., and Stern, A. (**2007**). "Supersonic jet noise source characteristics and propagation: Engine and model scale," AIAA Paper 2007-3623.
Schmidt, O. T., Towne, A., Rigas, G., Colonius, T., and Brès, G. A. (**2018**). "Spectral analysis of jet turbulence," J. Fluid Mech. **855**, 953–982.
Seiner, J. M., Ponton, M. K., Jansen, B. J., and Lagen, N. T. (**1992**). "The effects of temperature on supersonic jet noise emission," AIAA Paper 92-2046.
Shimizu, T., Hirai, M., Tsutsumi, S., Takaki, R., and Arita, M. (**2009**). "Study on attenuation of sound by droplets," J. Jpn. Soc. Aero. Space Sci. **57**(661), 71–76 (in Japanese).
Sinha, A., Rodrıguez, D., Bres, G. A., and Colonius, T. (**2014**). "Wavepacket models for supersonic jet noise," J. Fluid Mech. **742**, 71–95.
Smith, W. O., III (**2013**). "An empirical and computational investigation into the acoustical environment at the launch of a space vehicle," Ph.D. thesis, Auburn University.
Soderman, P. T. (**1990**). "The prediction of STOVL noise—Current semi-empirical methods and comparisons with jet noise data," SAE Trans. **99**(1), 307–335.
Stout, T. A., Gee, K. L., Neilsen, T. B., Wall, A. T., and James, M. M. (**2015a**). "Source characterization of full-scale jet noise using acoustic intensity," Noise Control Eng. J. **63**, 522–536.
Stout, T. A., Gee, K. L., Neilsen, T. B., Wall, A. T., and James, M. M. (**2015b**). "Acoustic intensity near a high-powered military jet aircraft," J. Acoust. Soc. Am. **138**, EL1–EL7.

Sutherland, L. C. (**1968**). "Sonic and vibration environments for ground facilities…a design manual," Wyle Lab. Report number WR 68-2.
Sutherland, L. C. (**1993**). "Progress and problems in rocket noise prediction for ground facilities," AIAA Paper 93-4383.
Sutton, G. P., and Biblarz, O. (**2000**). *Rocket Propulsion Elements*, 7th ed. (Wiley, Hoboken, NJ), Chap. 5, pp. 160–196.
Suzuki, T. (**2013**). "Coherent noise sources of a subsonic round jet investigated using hydrodynamics and acoustic phased-array microphones," J. Fluid Mech. **730**, 659–698.
Swift, S. H., Gee, K. L., Neilsen, T. B., Wall, A. T., Downing, J. M., and James, M. M. (**2018**). "Spatiotemporal-correlation analysis of jet noise from a round nozzle high-performance aircraft," AIAA Paper 2018-3938.
Taira, K., Brunton, S. L., Dawson, S. T. M., Rowley, C. W., Colonius, T., McKeon, B. J., Schmidt, O. T., Gordeyev, S., Theofilis, V., and Ukeiley, L. S. (**2017**). "Modal analysis of fluid flows: An overview," AIAA J. **55**(12), 4013–4041.
Taira, K., Hemati, M. S., Brunton, S. L., Sun, Y., Duraisamy, K., Bagheri, S., Dawson, S. T. M., and Yeh, C. (**2020**). "Modal analysis of fluid flows: Applications and outlook," AIAA J. **58**(3), 998–1022.
Tam, C. K. W. (**1972**). "On the noise of a nearly ideally expanded supersonic jet," J. Fluid Mech. **51**(1), 69–95.
Tam, C. K. W. (**1995**). "Supersonic jet noise," Annu. Rev. Fluid Mech. **27**, 17–43.
Tam, C. K. W. (**2009**). "Mach wave radiation from high-speed jets," AIAA J. **47**(10), 2440–2448.
Tam, C. K. W., Aubert, A. C., Spyropoulos, J. T., and Powers, R. W. (**2018**). "On the dominant noise components of tactical aircraft: Laboratory to full scale," J. Sound Vib. **422**, 92–111.
Tam, C. K. W., and Burton, D. E. (**1984a**). "Sound generated by instability waves of supersponic flows. Part 1. Two-dimensional mixing layers," J. Fluid. Mech. **138**, 249–271.
Tam, C. K. W., and Burton, D. E. (**1984b**). "Sound generated by instability waves of supersponic flows. Part 2. Axisymmetric jets," J. Fluid. Mech. **138**, 273–295.
Tam, C. K. W., Golebiowski, M., and Seiner, J. M. (**1996**). "On the two components of turbulent mixing noise from supersonic jets," AIAA Paper 96-1716.
Tam, C. K. W., Horne, W. C., Burnside, N. J., and Panda, J. (**2017**). "Spectral analysis of the acoustic near field of a solid-propellant rocket," AIAA Paper 2017-4193.
Tam, C. K. W., and Hu, F. Q. (**1989**). "On the three families of instability waves of high-speed jets," J. Fluid Mech. **201**, 447–483.
Tam, C. K. W., and Parrish, S. A. (**2015**). "Noise of high-performance aircraft at afterburner," J. Sound Vib. **352**, 103–128.
Tam, C. K. W., Viswanathan, K., Ahuja, K. K., and Panda, J. (**2008**). "The sources of jet noise: Experimental evidence," J. Fluid Mech. **615**, 253–292.
Tatsukawa, T., Nonomura, T., Oyama, A., and Fujii, K. (**2016**). "Multi-objective aeroacoustic design exploration of launch-pad flame deflector using large-eddy simulation," J. Spacecr. Rockets **53**(4), 751–758.
Tedrick, R. M. (**1964**). "Acoustical measurements of static tests of clustered and single-nozzled rocket engines," J. Acoust. Soc. Am. **36**(11), 2027–2032.
Towne, A., Schmidt, O. T., and Colonius, T. (**2018**). "Spectral proper orthogonal decomposition and its relationship to dynamic mode decomposition and resolvent analysis," J. Fluid. Mech. **847**, 821–867.
Tran, K., Lim, D., Min, S., Oh, K., and Mavris, D. (**2018**). "Noise and sonic boom analysis from rocket launches," AIAA Paper 2018-2816.
Troclet, B., Hiverniau, B., Ichchou, M. N., Jezequel, L., Kayvantash, K., Bekkour, T., Mouillet, J. B., and Gallet, A. (**2009**). "FEM/SEA hybrid method for predicting mid and high frequency structure-borne transmission," Open Acoust. J. **2**(1), 45–60.
Troclet, B., Mureaux, L., Alestra, S., Terrasse, I., Jeanjean, S., and Srithammavanh, V. (**2007**). "Identification of overpressure sources at launch vehicle liftoff using an inverse method," J. Spacecr. Rockets **44**(3), 597–606.
Troclet, B., Vanpeperstraete, S., and Schott, M.-O. (**1995**). "Experimental analysis lift-off aerodynamic noise Ariane 5 launch vehicle," AIAA Paper 95-070.
Troyes, J., Vuillot, F., Varnier, J., and Malbéqui, P. (**2009**). "Numerical simulations of rocket solid motor engine ignition and duct overpressure waves at reduced scale," AIAA Paper 2009-4981.
Tsutsumi, S., Fukuda, K., Takaki, R., Shima, E., Fujii, K., and Ui, K. (**2008b**). "Numerical study on acoustic radiation for designing launch-pad of advanced solid rocket," AIAA Paper 2008-5148, July.
Tsutsumi, S., Ishii, T., Ui, K., Tokudome, S., and Wada, K. (**2015b**). "Assessing prediction and reduction technique of lift-off acoustics using Epsilon flight data," AIAA Paper 2015-1007.
Tsutsumi, S., Ishii, T., Ui, K., Wada, K., and Tokudome, S. (**2015a**). "Study on acoustic prediction and reduction of Epsilon launch vehicle at liftoff," J. Spacecr. Rockets **52**(2), 350–361.
Tsutsumi, S., Kato, S., Fukuda, K., Takaki, R., and Ui, K. (**2009**). "Effect of deflector shape on acoustic field of launch vehicle at lift-off," AIAA Paper 2009-328.
Tsutsumi, S., Sarae, W., and Terashima, K. (**2019**). "Effect of rocket engine clustering on acoustic level of H3 launch vehicle at lift-off," in *32nd International Symposium on Space Technology and Science, Japan Society for Aeronautical and Space Sciences (JSASS)*, p. 2019-g-12.
Tsutsumi, S., Takaki, R., Ikaida, H., and Terashima, K. (**2015c**). "Numerical aeroacoustics analysis of a scaled solid jet impinging on flat plate with exhaust hole," in *Proceedings of the 30th International Symposium on Space Technology and Science, Japan Society for Aeronautical and Space Sciences (JSASS)*.
Tsutsumi, S., Takaki, R., Nakanishi, Y., Okamoto, K., and Teramoto, S. (**2014**). "Acoustic generation mechanism of a supersonic jet impinging on deflectors," AIAA Paper 2014-0882.
Tsutsumi, S., Takaki, R., Shima, E., Fujii, K., and Arita, M. (**2008a**). "Generation and propagation of pressure waves from H-IIA launch vehicle at lift-off," AIAA Paper 2008-390.
Unnikrishnan, S., and Gaitonde, D. (**2016**). "Acoustic, hydrodynamic and thermal modes in a supersonic cold jet," J. Fluid Mech. **800**, 387–432.
Unnikrishnan, S., and Gaitonde, D. (**2020**). "A pressure decomposition framework for aeroacoustic analysis of turbulent jets," Eur. J. Mech. B Fluids **81**, 41–61.
Varnier, J. (**2001**). "Experimental study and simulation of rocket engine free jet noise," AIAA J. **39**(10), 1851–1859.
Varnier, J., Piet, J., Gely, D., Elias, G., and Radulovic, S. (**1996**). "Modeling of the acoustic environment on the Ariane 5 fairing using test data," AIAA Paper 96-1721.
Varnier, J., and Raguenet, W. (**2002**). "Experimental characterization of the sound power radiated by impinging supersonic jets," AIAA J. **40**(5), 825–831.
Vaughn, A. B., Neilsen, T. B., Gee, K. L., Okamoto, K., and Akamine, M. (**2016**). "Spatial variation in similarity spectra decompositions of a Mach 1.8 laboratory-scale jet," J. Acoust. Soc. Am. **140**, 3044.
Vaughn, A. B., Neilsen, T. B., Gee, K. L., Wall, A. T., Downing, J. M., and James, M. M. (**2018**). "Broadband shock-associated noise from a high-performance military aircraft," J. Acoust. Soc. Am. **144**, EL242–EL247.
Viswanathan, K. (**2002**). "Analysis of the two similarity components of turbulent mixing noise," AIAA J. **40**(9), 1735–1744.
Viswanathan, K. (**2009**). "Mechanisms of jet noise generation: Classical theories and recent developments," Int. J. Aeroacoust. **8**(4), 355–407.
Viswanathan, K., Underbrink, J. R., and Brusniak, L. (**2011**). "Space-time correlation measurements in near fields of jets," AIAA J. **49**, 1577–1599.
Vu, B. T., Moss, N., and Sampson, Z. (**2014**). "Multi-phase modeling of rainbird water injection," AIAA Paper 2014-3076.
Vu, B. T., and Plotkin, K. J. (**2010**). "Lift-off acoustics predictions of clustered rocket engines in the near field," NASA Technical Report KSC-2010-081, Washington, DC.
Wall, A. T., Gee, K. L., Leete, K. M., Neilsen, T. B., and Stout, T. A. (**2018**). "Partial-field decomposition analysis of full-scale supersonic jet noise using optimized-location virtual references," J. Acoust. Soc. Am. **144**, 1356–1367.
Wall, A. T., Gee, K. L., Neilsen, T. B., Harker, B. M., McInerny, S. A., McKinley, R. L., and James, M. M. (**2015**). "Investigation of multi-lobed fighter jet noise sources using acoustical holography and partial field decomposition methods," AIAA Paper 2015-2379.
Wall, A. T., Gee, K. L., Neilsen, T. B., McKinley, R. L., and James, M. M. (**2016**). "Military jet noise source imaging using multisource statistically optimized near-field acoustical holography," J. Acoust. Soc. Am. **139**(4), 1938–1950.
Wall, A. T., Leete, K. M., Gee, K. L., Neilsen, T. B., James, M. M., and McKinley, R. L. (**2017**). "Preliminary investigation of multilobe fighter jet noise sources using acoustical holography," AIAA Paper 2017-3520.

Walsh, E. J., and Hartt, P. M. (**1982**). "Liftoff ignition overpressure—A correlation," J. Spacecr. Rockets **19**(6), 550–556.
West, J. S., Strutzenberg, L. L., Putnam, G. C., Liever, P. A., and Williams, B. R. (**2012**). "Development of modeling capabilities for launch pad acoustics and ignition transient environment prediction," AIAA Paper 2012-2094.
Westley, R., and Lilley, G. M. (**1952**). "An investigation of the noise field from a small jet and methods for its reduction," "Report no. 53," College of Aeronautics, Cranfield University, UK, January.
Wilby, J. F. (**2007**). "Problems in predicting noise levels on launch vehicles at liftoff," in *NOISE-CON 2007*, October, Reno, NV.
Wilhold, G., Guest, S., and Jones, J. (**1963**). "A technique for predicting far-field acoustic environments due to a moving rocket sound source," in NASA TN D-1832, Washington, DC, August.
Worden, T. J., Shih, C., and Alvi, F. S. (**2017**). "Supersonic jet impingement on a model-scale jet blast deflector," AIAA J. **55**(8), 2522–2536.
Xing, C., Le, G., Shen, L., Zhao, C., and Zheng, H. (**2020**). "Numerical investigations on acoustic environment of multi-nozzle launch vehicle at lift-off," Aerosp. Sci. Technol. **106**, 106140.
Xu, Q. (**2004**). "An analysis of near-field rocket noise involving shock waves," in *Proceedings of the SPIE 5439, Independent Component Analyses, Wavelets, Unsupervised Smart Sensors, and Neural Networks II*, 12 April, Orlando, FL.
Xu, Q. (**2005**). "Study the noise characteristics of a single-chamber two-stage rocket motor," AIAA Paper 2005-2933.
Yeh, C. A., and Taira, K. (**2019**). "Resolvent-analysis- based design of airfoil separation control," J. Fluid Mech. **867**, 572–610.
Yenigelen, E., and Morris, P. J. (**2020**). "Numerical investigation of a noise reduction strategy for rocket launch vehicles," AIAA Paper 2020-2606.
Yunis, I. (**2013**). "Standard deviation of launch vehicle vibration and acoustic environments," J. Spacecr. Rockets **50**(4), 829–837.
Zhou, Z., Lu, C., Zhao, C., and Le, G. (**2020**). "Numerical simulations of water spray on flame deflector during the four-engine rocket launching," Adv Space Res. **65**(4), 1296–1305.
Zoppellari, E., and Juve, D. (**1998**). "Reduction of hot supersonic jet noise by water injection," AIAA Paper 98-2204.